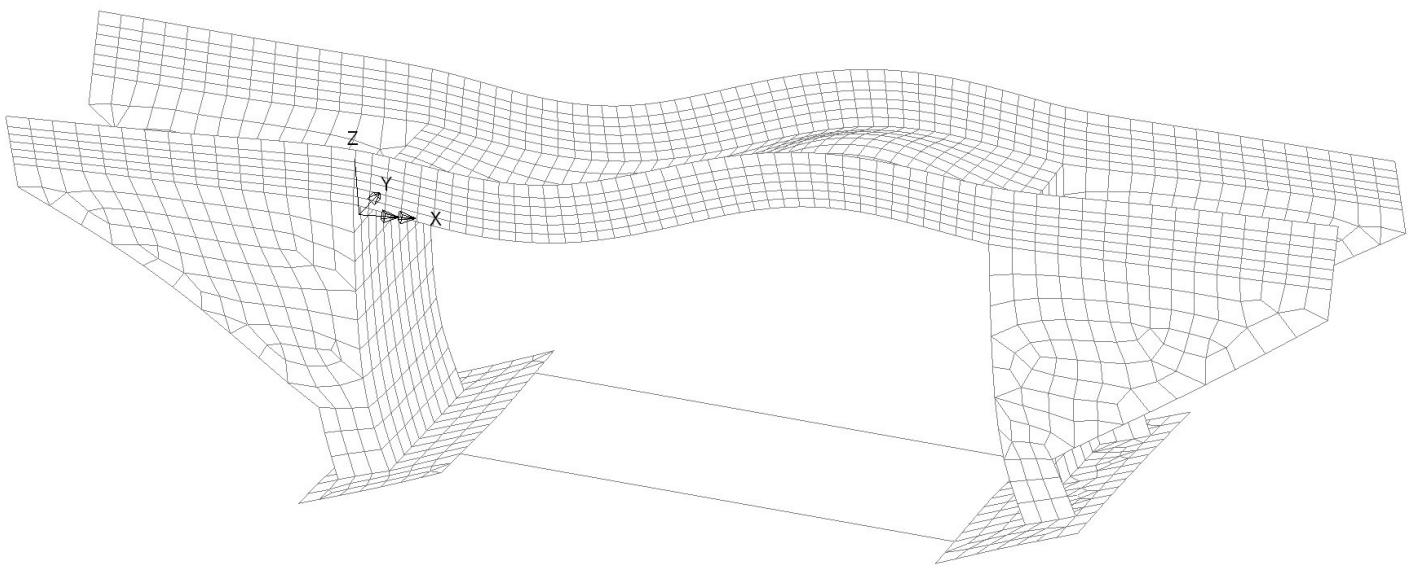


CHALMERS



Dynamic analysis of railway bridges using the mode superposition method

The Mass Participation Factor as convergence criterion

Master's Thesis in the International Master's programme Structural Engineering

ANDREAS KARLSSON AND ANDREAS NILSSON

Department of Civil and Environmental Engineering

Division of Structural Engineering

Concrete Structures

CHALMERS UNIVERSITY OF TECHNOLOGY

Göteborg, Sweden 2007

Master's Thesis 2007:115

MASTER'S THESIS 2007:115

Dynamic analysis of railway bridges using the mode superposition method

The Mass Participation Factor as convergence criterion

Master's Thesis in the *International Master's programme Structural Engineering*

ANDREAS KARLSSON AND ANDREAS NILSSON

Department of Civil and Environmental Engineering
Division of Structural Engineering
Concrete Structures

CHALMERS UNIVERSITY OF TECHNOLOGY

Göteborg, Sweden 2007

Dynamic analysis of railway bridges using the mode superposition method
The Mass Participation Factor as convergence criterion
Master's Thesis in the *International Master's programme Structural Engineering*
ANDREAS KARLSSON AND ANDREAS NILSSON

© ANDREAS KARLSSON AND ANDREAS NILSSON, 2007

Master's Thesis 2007:115
Department of Civil and Environmental Engineering
Division of Structural Engineering
Concrete Structures
Chalmers University of Technology
SE-412 96 Göteborg
Sweden
Telephone: + 46 (0)31-772 1000

Cover:
Eigenmode 21 of the Norra Kungsvägen bridge using original boundary conditions.

Chalmers Reproservice
Göteborg, Sweden, 2007

Dynamic analysis of railway bridges using the mode superposition method

The Mass Participation Factor as convergence criterion

Master's Thesis in the *International Master's programme Structural Engineering*

ANDREAS KARLSSON AND ANDREAS NILSSON

Department of Civil and Environmental Engineering

Division of Structural Engineering

Concrete Structures

Chalmers University of Technology

ABSTRACT

In today's quest of creating more efficient railway transportations, the desire to increase the train velocities arise. The increased speeds will subject railway bridges to dynamic loads far greater than previously considered. In traditional design of railway bridges, static load cases are calculated and amplified to represent the dynamic effects. The limitations to this procedure are obvious due to the resonance peaks not captured in static analysis. The resonant effects are substantial for train velocities greater than 200 km/h and the need for a detailed dynamic analysis is necessary. A dynamic analysis, using the finite element method, can be carried out by applying direct transient integration schemes or by performing a modal analysis using mode superposition. When applying mode superposition, a linear combination of the structure's natural modes is representing the dynamic response. A natural mode is describing a structure's behaviour when subjected to harmonic load. The number of natural modes of large complex bridge structures can be very extensive, making the dynamic analysis time consuming. A reduction of the full system of governing equilibrium equations is therefore desirable. A suggested parameter when determining which modes to exclude is the mass participation factor (MPF). The MPF describes the amount of the structure's mass excited in each mode.

The purpose of this project is to investigate if a high MPF can be considered as a measure of good convergence. A parameter study of a previously analysed railway bridge, showing lack of convergence even though high MPF is provided, is performed. The results of the analysis indicate that MPF is not a suitable parameter to study when determining the cut-off frequency for accelerational response. The accelerational response is greatly influenced by the choice of boundary conditions. The boundary conditions are modelled to represent the soil conditions present at the bridge site. If the soil is modelled with flexible translational springs, the bridge is allowed to have eigenmodes with a significant rigid body component. The rigid body modes will have large contributions to the total MPF without any structural deformations occurring. The MPF will therefore be extremely high for narrow frequency ranges, making the parameter unsuitable as a convergence criterion. On the contrary, if the soil is modelled as too stiff the maximum accelerations will be underestimated, preventing an accurate analysis. However, the results are indicating that MPF may be used as a convergence criterion when analysing section forces.

Key words: dynamics, mode superposition, MPF, high-speed railway bridges

Dynamisk analys av järnvägsbroar med hjälp av modsuperposition

Mass Participation Faktorn som konvergens kriterium

Examensarbete inom Civilingenjörsprogrammet Väg och vattenbyggnad

ANDREAS KARLSSON OCH ANDREAS NILSSON

Institutionen för bygg- och miljöteknik

Avdelningen för Konstruktionsteknik

Betongbyggnad

Chalmers tekniska högskola

SAMMANFATTNING

För att möta samhällets krav på effektivare järnvägstransporter har ett behov av att öka linjehastigheten på svenska broar uppstått. De ökade tåghastigheterna kommer att utsätta brokonstruktionen för större dynamiska laster vilket medför betydligt större påfrestningar än tidigare. I traditionell brokonstruktion har dynamiska laster beaktats genom att förstora det statiska lastfallet med en dynamisk faktor. Begränsningen med denna metod är uppenbar då en statisk analys inte kan fånga resonansfenomen. Risker för resonanseffekter är påtagliga för tåghastigheter över 200 km/h varför en mer detaljerad dynamisk analys blir nödvändig. Den dynamiska analysen kan utföras antingen genom direkt-tidsintegration eller med modsuperposition. När modsuperposition används representerar en linjärkombination av bronns egenmoder den dynamiska responsen, där egenmoderna beskriver strukturens beteende när den blir utsatt för en harmonisk last. En komplex brokonstruktion har ett stort antal moder vilket medför en stor tidsåtgång vid dynamiska analyser. Det är därför önskvärt att reducera det fulla systemet av jämviktsekvationer. En föreslagen parameter för att bestämma vilka moder som ska trunkeras är den så kallade ”mass participation factor” (MPF), vilken kortfattat beskriver andelen massa som är aktiv i en mod.

Målet med projektet är att undersöka om en hög MPF kan anses vara en garant för konvergens. För att undersöka detta har en parameterstudie på en nyligen analyserad bro utförts. Bron visade brist på konvergens för maximal acceleration trots att en hög MPF var uppnådd. Resultaten av studien pekar på att MPF inte är en lämplig parameter för att bestämma vilket frekvensintervall som bör beaktas när den maximala accelerationen ska bestämmas. Accelerationerna är mycket beroende på valet av randvillkor. Randvillkoren är modellerade för att beskriva grundläggningförutsättningarna på den aktuella platsen. Om grunden modelleras med flexibla fjädrar tillåts bron att translatera relativt odeformerat i en så kallad stelkroppsrörelse. Dessa stelkroppsmoder har stor inverkan på den totala MPF:en utan att bron deformeras, detta medför i sin tur att den totala MPF:en kommer att vara extremt hög även om moder med hög frekvens inte beaktas. Om grunden istället modelleras för styv, visar studien att de maximala accelerationerna underskattas, vilket förhindrar en korrekt analys. Resultaten av parameterstudien visar dock att MPF kan användas som ett konvergenskriterium när snittkrafter ska bestämmas.

Nyckelord: dynamik, modsuperposition, MPF, järnvägsbroar för höghastighetståg

Contents

ABSTRACT	I
SAMMANFATTNING	II
CONTENTS	III
PREFACE	VII
NOTATIONS	VIII
1 INTRODUCTION	1
1.1 Background	1
1.2 Aim	1
1.3 Method	1
1.4 Limitations	2
2 DYNAMICS OF SINGLE DEGREE-OF-FREEDOM SYSTEMS	3
2.1 Un-damped mass-spring model	3
2.1.1 Assumptions	3
2.1.2 Equation of motion	4
2.1.3 Free vibration	5
2.1.4 Forced vibration	6
2.1.5 Harmonic excitation	6
2.2 Damped mass-spring model	9
2.2.1 Equation of motion	10
3 MATHEMATICAL MODELS OF MDOF SYSTEMS	13
3.1 Newton's Laws to describe the equation of motion	13
3.1.1 Un-damped MDOF system	13
3.1.2 Damped MDOF system	14
3.2 Vibration of un-damped MDOF system	16
3.2.1 Free vibration of 2-DOF system	16
3.2.2 Procedure to determine natural frequencies and mode shapes	18
4 VIBRATION PROPERTIES OF MDOF SYSTEMS	20
4.1 Properties of stiffness and mass matrices	20
4.2 Normalisation of modes	21
4.3 Orthogonality of natural modes	21
4.4 Generalisation of matrices	22
4.5 Damping in MDOF systems	22
4.5.1 Difficulties of expressing the damping matrix	23
4.5.2 Rayleigh damping	23
4.5.3 Modal damping	24

5	DYNAMICS OF RAILWAY BRIDGES	25
5.1	Theoretical bridge models	25
5.1.1	Beams	25
5.1.2	Plates	27
5.2	Natural frequencies of railway bridges	27
5.3	Resonance of railway bridges	28
5.4	Damping of railway bridges	28
6	METHODS OF DYNAMIC ANALYSIS	30
6.1	Direct integration methods	30
6.1.1	Central difference method	31
6.1.2	Wilson's θ method	31
6.1.3	Newmark's β method	33
6.1.4	Hilber-Hughes-Taylor method	34
6.2	Mode superposition	34
6.2.1	Model reduction	35
6.2.2	Error estimation	36
6.2.3	Mass participation factor	37
6.2.4	Mode superposition method in commercial FE-software	38
7	THE FINITE ELEMENT METHOD AND LUSAS	41
7.1	Modelling procedures in LUSAS	41
7.1.1	Elements	42
7.1.2	Damping	45
7.1.3	Loads	45
7.2	Dynamic analysis	46
7.2.1	Direct integration	46
7.2.2	Eigenvalue analysis	46
7.2.3	Modal analysis	49
7.3	Moving load analysis	49
7.3.1	IMDPlus assumptions	49
7.3.2	Definition of required input	50
7.3.3	Running moving load analysis	50
8	CODE REQUIREMENTS IN BV BRO	52
8.1	High-speed load models	52
8.2	Damping	54
8.3	Speed increment	54
8.4	Vertical accelerations	55
8.5	Choice of model	55
9	THE NORRA KUNGSVÄGEN BRIDGE	56

9.1	Bridge description	56
9.2	Previous analyses	57
9.3	Finite element model	61
9.3.1	Geometry	61
9.3.2	Element types and mesh	62
9.3.3	Boundary conditions	64
9.3.4	Loading	65
9.3.5	Material properties	67
10	RESULT OF ANALYSES	70
10.1	Static analysis	70
10.2	Parameter study	71
10.2.1	Load step increment	72
10.2.2	Time-step increment	72
10.2.3	Mesh density	73
10.2.4	Truncation of modes	74
10.3	Patch load	75
10.4	Modelling of ballast and track	77
10.5	Modelled soil pressure	78
10.6	Different boundary conditions	81
10.6.1	Fixed vertical translation	81
10.6.2	Increased spring stiffness	82
10.6.3	Fixed translations	87
11	CONCLUSIONS	89
11.1	General	89
11.2	Further investigations	90
12	REFERENCES	91

Preface

In this Master's Thesis, an investigation to determine the effectiveness of utilising the mass participation factor as a cut-off criterion for the mode superposition method was performed. The project was introduced when convergence issues were experienced during the dynamic analysis of the Norra Kungsvägen bridge. The required analyses have been performed at ELU Konsult, Göteborg under the supervision of Erik Hollunger MSc, Costin Pacoste PhD and Susanne Åderman MSc. The project was initiated in June 2007 and completed in October 2007.

We would like to express our sincerest regards to our supervisors, and examiner Professor Mario Plos, at Chalmers University of Technology, for their guidance and support.

We would also express our appreciation to our opponents David Lehtonen and Anna Hallberg for their continuous assistance.

Göteborg, October 2007

Andreas Karlsson and Andreas Nilsson

Notations

Roman upper case letters

A	Amplitude [m]
A	Area [m ²]
C	Amplitude [m]
C	Damping matrix
D	Dimensions
D	Bending stiffness [Nm]
D	Coach length [m]
D	Dynamic magnification factor, total
D_s	Dynamic magnification factor, steady state
DOF	Degree-of-freedom
E	Modulus of elasticity [N/m ²]
EOM	Equation of motion
F	External force [N]
F_x	External force in x-direction [N]
F_x^*	Force including inertia [N]
F_D	Damping force vector
F_E	Elastic force vector
F_I	Inertia force vector
HHT	Hilber-Hughes-Taylor
HSLM	High-speed load model
I	Moment of inertia [m ⁴]
I	Identity matrix
K	Modal stiffness
K	Stiffness matrix
L	Length [m]
M	Modal mass
M	Mass [kg]
M	Mass matrix
MDOF	Multi degree-of-freedom
MPF	Mass participation factor
N	Number of axles
P	Participation factor
Q	Equivalent load [kN/m]
R	Load vector
\bar{R}	Wilson's load vector
RBM	Rigid body mode
SDOF	Single degree-of-freedom
SMPF	Sum of MPF
T	Kinetic energy [J]
T	Rigid body response vector
T_n	Natural period [s]
U	Translational degree-of-freedom
U	Amplitude [m]

U	Scaled mode
U_0	Static displacement [m]
V	Translational degree-of-freedom
V	Strain energy [J]
W	Translational degree-of-freedom
X	Arbitrary matrix
X	Rigid body response vector

Roman lower case letters

a	Coefficient
a_x	Acceleration in x-direction [m/s ²]
c	Viscous damping coefficient [Ns/m]
c	Constant
d	Boogie axle spacing [m]
f	Force [N]
f	Frequency [Hz]
f_D	Damping force [N]
f_s	Spring force [N]
g	Gravity [m/s ²]
h	Plate thickness [m]
k	Stiffness [N/m]
l	Span length [m]
m	Mass [kg]
m	Truncated number of eigenvalues
n	Total number of eigenvalues
p	Load [N]
p	Pressure [N/m ²]
p	External load vector
p_0	Force amplitude [N]
q	Load [kN/m ³]
r	Frequency ratio
t	Time [s]
u	Vertical deflection [m]
u	Displacement [m]
u	Degree-of-freedom
u	Displacement vector
u_0	Initial displacement [m]
u_c	Complementary solution
u_p	Particular solution
u_x	Displacement in x-direction [m]
\dot{u}	Velocity [m/s]
\dot{u}	Velocity vector
\ddot{u}	Acceleration [m/s ²]
\ddot{u}	Acceleration vector
\hat{u}	Truncated displacement vector

$\tilde{\mathbf{u}}$	Displacement approximation vector
v_0	Initial velocity [m/s]
v_x	Velocity in x-direction [m/s]
w	Vertical deflection [m]
x	Space coordinate
y	Space coordinate
z	Space coordinate
z	Depth [m]

Greek lower case letters

α	Arbitrary out of phase angle [rad]
α	Hilber-Hughes-Taylor parameter
β	Mode shape ratio
β	Displacement to height ratio
β	Newmark's parameter
γ	Density [kg/m^3]
γ	Newmark's parameter
δ	Displacement [m]
ε^m	Truncation error
ζ	Modal damping factor
η	Modal displacement
$\boldsymbol{\eta}$	Modal coordinates
$\dot{\eta}$	Modal velocity
$\ddot{\eta}$	Modal acceleration
$\hat{\boldsymbol{\eta}}$	Truncated modal displacements
θ	Wilson's parameter
θ	Rotational degree-of-freedom
λ	Eigenvalue
μ	Mass per unit length [kg/m]
μ	Mass per unit area [kg/m^2]
μ	Shift parameter
ν	Poisson's number
ξ	Damping parameter
ρ	Density [kg/m^3]
τ	Time [s]
φ	Mode shape
ϕ	Mode shape element
ω_n	Un-damped natural frequency [rad/s]
ω_b	Circular frequency of viscous damping [rad/s]
ω^2	Eigenvalue

Greek upper case letters

Γ	Participation factor
----------	----------------------

Λ	Eigenvalue matrix
Φ	Modal matrix
$\hat{\Phi}$	Truncated modal matrix
Ω	Driving frequency [rad/s]

1 Introduction

1.1 Background

In today's quest of creating more efficient railway transportations the desire to increase the train velocities arises. The moving train will subject the bridge to dynamic loads which are amplified by increasing velocities. In traditional design of railway bridges static load cases are calculated and amplified to represent the dynamic effects. The limitations to this procedure are obvious due to the resonance peaks not captured in static analysis. The resonant effects are substantial for train velocities greater than 200 km/h and the need for a detailed dynamic analysis arises.

A dynamic analysis, using the finite element method (FEM), can be carried out by applying direct transient integration schemes or by performing a modal analysis using mode superposition. When applying the mode superposition method, a linear combination of the structure's natural modes is representing the dynamic response. A natural mode is describing a structure's behaviour when subjected to harmonic load. The number of natural modes of large complex bridge structures can be very extensive making the dynamic analysis time consuming. A reduction of the full system of governing equilibrium equations is therefore desirable to minimise the computational effort. A suggested parameter to study when determining which modes to exclude, without substantial effect of the accuracy, is the mass participation factor (MPF). The MPF describes the amount of the structure's mass that is active in each mode. The translation or deformation of the associated mass is thus enabled to be represented by a linear combination of the structural response. A frequently used praxis is to include the modes, with the lowest natural frequencies, until 90 % of the total mass can be excited.

The Swedish consultant company ELU Konsult has recently experienced lack of accelerational convergence of an analysed bridge, even though high total mass participation is ensured. Doubts have therefore been expressed concerning the correlation between high total MPF (SMPF) and good accuracy.

1.2 Aim

The aim of this project is to determine if the MPF is a reliable criterion when choosing a cut-off frequency for the modal superposition method. If concluded that the use of MPF as a convergence criterion is limited, the goal is to identify the problematic situations to allow further use of the parameter. Furthermore, the objective is to identify, if possible, additional parameters indicating good accuracy.

1.3 Method

The effectiveness of applying MPF as a frequency cut-off criterion will be studied by performing a parameter study of a bridge model, provided by ELU Konsult. The bridge is modelled as a three-dimensional (3-D) structure accompanied by appropriate

boundary conditions, using the general finite element software LUSAS. The objective of the parameter study is to identify the critical values of the input parameters, i.e. mesh density, load step increment, time-step increment and truncation of modes.

A literature study of the MPF and the fundamental of dynamics is performed to obtain deeper knowledge of their theoretical formulations. The theoretical knowledge will create a better understanding of the physical behaviour of the bridge structure.

1.4 Limitations

Due to the extensive computational time needed to perform the dynamic analyses, a few limitations are needed:

- The parameter study will be limited to the bridge model previously developed by ELU Konsult.
- Only one train model will be included, i.e. the load model that generates the greatest dynamic response.
- Only the vertical accelerations will initially be studied. The accelerations are very sensitive to the magnitude of the natural frequencies corresponding to the modes included in the dynamic analysis.
- Track irregularities and interaction between rail and train wheels will, in accordance to specification acknowledged in the Swedish railway bridge code BV BRO, Banverket (2006), not be considered.
- Idealised material behaviour is assumed, i.e. linear and viscoelastic materials.

2 Dynamics of single degree-of-freedom systems

The behaviour of a complex multi-degree-of-freedom (MDOF) system can be described as a system of coupled single-degree-of-freedom (SDOF) systems. To achieve better understanding of the dynamic response of a structure, a SDOF system will be studied and the knowledge will be generalised to a MDOF system.

2.1 Un-damped mass-spring model

The mass-spring system is the simplest structure that can be analysed dynamically. The structure must have an elastic component which can store and release potential energy and a mass able to store and release kinetic energy. The structure will be subjected to the simplest forms of vibrations, creating a mass-spring oscillator illustrated in Figure 2.1.

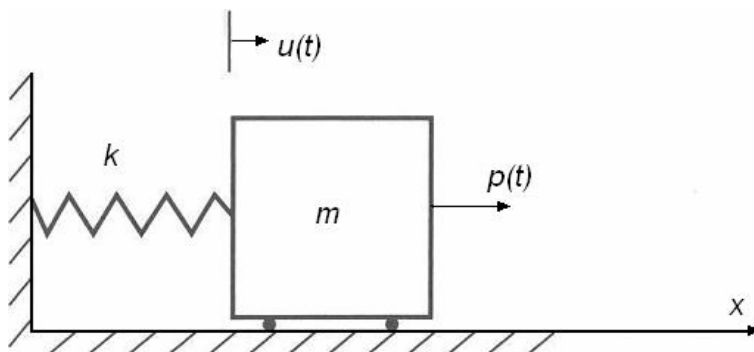


Figure 2.1 Mass-spring oscillator.

The potential energy stored in the linear spring is called strain energy, which is defined as:

$$V = \frac{1}{2}ku^2 \quad (2.1)$$

where u is the relative elongation/contraction of the spring.

The kinetic energy due to inertia forces is given by:

$$T = \frac{1}{2}m\dot{u}^2 \quad (2.2)$$

where m is the mass and \dot{u} is the velocity of the mass.

2.1.1 Assumptions

To simplify the prototype model a few assumptions are made:

1. No friction will affect the point mass when moving in the horizontal direction. The displacement of the mass in the studied direction is designated the variable $u(t)$. The initial position of the mass is defined where the spring is undeformed.
2. The connection between the fixed base and the mass consist of an idealised massless linear spring. Figure 2.2 describes the linear relationship between elongation and contraction of the spring and the force $f_s(t)$ acting on the mass. Tension of the spring will result in a positive value of f_s and compression of the spring to a negative value of f_s .
3. An external force $p(t)$ acts on the mass according to Figure 2.1.

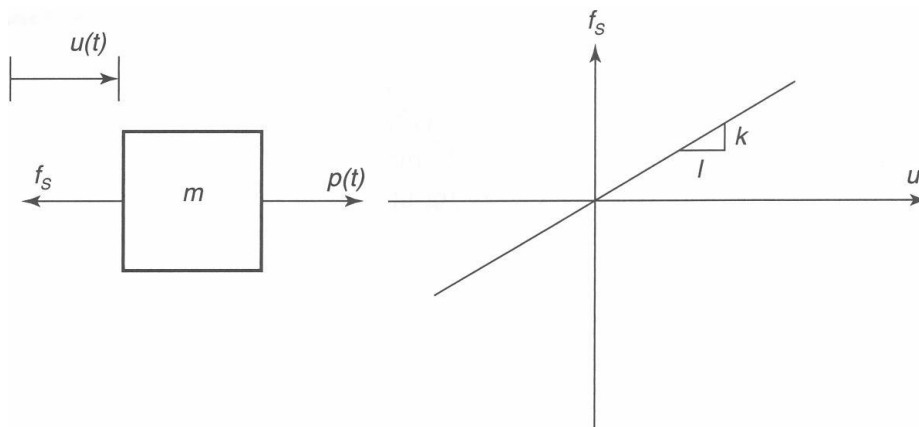


Figure 2.2 Free-body diagram of the oscillator and the linear relation between force and elongation of a spring.

The instantaneous position of the mass can be described with one variable, $u(t)$, and is therefore called a single degree-of-freedom system.

2.1.2 Equation of motion

To obtain a mathematical model able to describe the behaviour of the mass-spring oscillator, the system is studied by drawing a free-body diagram of the mass (Figure 2.2) and applying Newton's second law:

$$\sum F_x = ma_x \quad (2.3)$$

where m is the mass, a_x is the acceleration and F_x is the external forces acting on the mass. The acceleration a_x is given by the second time derivative of the displacement, $a_x = \ddot{u}(t)$. The velocity is similarly defined by the first time derivative of the displacements, $v_x = \dot{u}(t)$. By assuming that the mass is displaced in positive u_x direction the spring will be in tension, producing a spring force acting on the left side of the mass (Figure 2.2). Equation (2.3) can now be rewritten as:

$$-f_s + p(t) = m\ddot{u} \quad (2.4)$$

The relation between the force in the spring and the displacement can be rewritten as:

$$f_s = ku \quad (2.5)$$

where k is the stiffness of the spring.

By combining equations (2.4) and (2.5) the equation of motion (EOM) for the un-damped SDOF model is obtained:

$$m\ddot{u} + ku = p(t) \quad (2.6)$$

The equation is a second order ordinary differential equation that governs the SDOF mass-spring oscillator's behaviour. To determine the response of the system, initial conditions of the displacement and velocity at $t = 0$ are required.

$$u(0) = u_0 = \text{initial displacement} \quad \dot{u}(0) = v_0 = \text{initial velocity} \quad (2.7)$$

2.1.3 Free vibration

If the external force acting on the mass-spring oscillator is equal to zero, i.e. $p(t) = 0$, and at least one of the initial conditions stated in equation (2.7) is non-zero, the system will be at free vibration. This will enable the equation of motion to be rewritten as a homogenous second-order differential equation:

$$m\ddot{u} + ku = 0 \quad (2.8)$$

The general solution to this equation is:

$$u(t) = A_1 \cos \omega_n t + A_2 \sin \omega_n t \quad (2.9)$$

where ω_n is the un-damped circular natural frequency defined as:

$$\omega_n = \sqrt{\frac{k}{m}} \quad (2.10)$$

The natural frequency is of the unit radians per second (rad/s).

The constants A_1 and A_2 are chosen so that the initial conditions in equations (2.7) are satisfied. The time dependent displacement of a free vibrating un-damped mass-spring oscillator is characterised by:

$$u(t) = u_0 \cos \omega_n t + \frac{v_0}{\omega_n} \sin \omega_n t \quad (2.11)$$

The response of the mass-spring oscillator released from a resting state, $v_0 = 0$, with an initial displacement of $u_0 = 1$ is depicted in Figure 2.3. The motion of the response is given by:

$$u(t) = \cos \omega_n t = \cos \frac{2\pi t}{T_n} \quad (2.12)$$

The free vibration presented in Figure 2.3 consists of harmonic motion that repeats itself with a period given by:

$$T_n = \frac{2\pi}{\omega_n} \quad (2.13)$$

The amplitude of the vibration is defined as the maximum displacement experienced by the mass. For an un-damped free vibration system the amplitude is equal to u_0 .

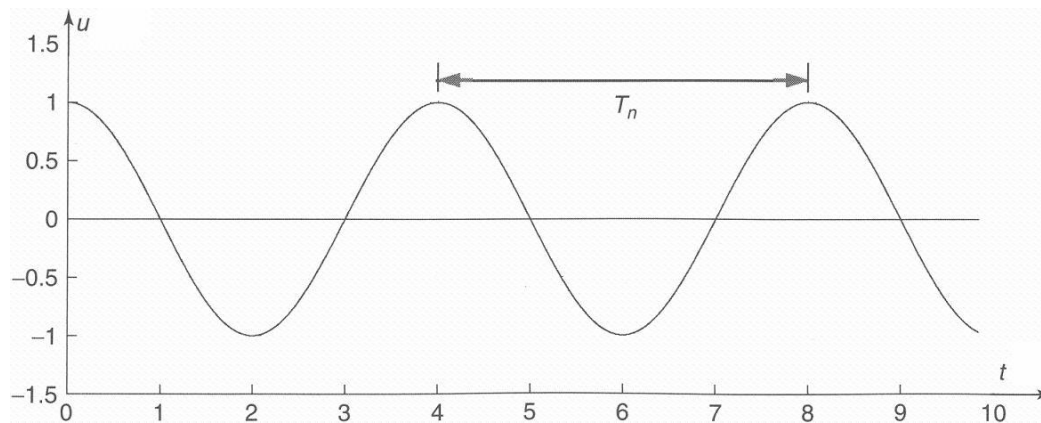


Figure 2.3 Free vibration of mass-spring oscillator, $u_0 = 1$ and $T = 4s$.

2.1.4 Forced vibration

If the excitation force is non-zero, i.e. $p(t) \neq 0$, the system is considered to undergo forced vibration. The solution of the differential equation of motion (2.6) consists of a complementary and a particular solution. The displacement is thus defined as:

$$u(t) = u_c(t) + u_p(t) \quad (2.14)$$

2.1.5 Harmonic excitation

As noted in Section 2.1.4 the total response of a linear system consists of a forced motion, u_p , and a natural motion u_c . The forced motion occurring in case of harmonic excitation is referred to as the steady-state response. The un-damped mass-spring SDOF system illustrated in Figure 2.4 is assumed to be linear and the excitation force amplitude p_0 and the driving frequency Ω are constants. The equation of motion for the described system is:

$$m\ddot{u} + ku = p_0 \cos \Omega t \quad (2.15)$$

Due to the fact that only even-order derivatives appear on the left hand side, the steady-state response has the following form:

$$u_p = U \cos \Omega t \quad (2.16)$$

where U is the amplitude of the steady-state response. Equation (2.16) is substituted into the equation of motion in (2.15), producing the following expression:

$$U = \frac{p_0}{k - m\Omega^2} \quad (2.17)$$

provided that $k - m\Omega^2 \neq 0$.

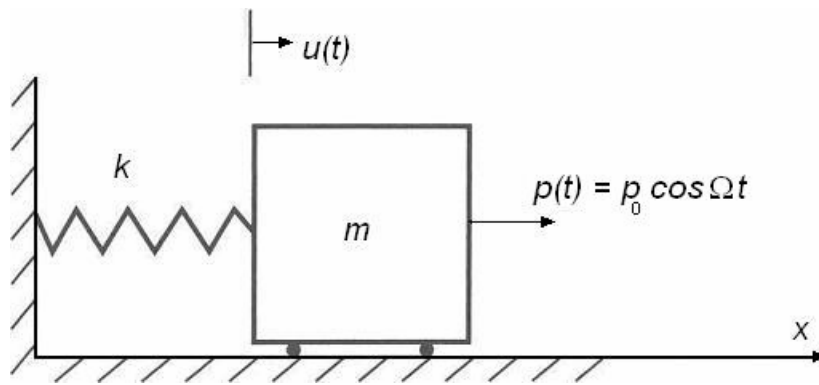


Figure 2.4 Harmonic excitation of an un-damped SDOF system.

The static displacement is the displacement that the mass will sustain if a force with a magnitude p_0 is applied statically and is defined as:

$$U_0 = \frac{p_0}{k} \quad (2.18)$$

allowing equation (2.17) to be reformulated as:

$$\frac{U}{U_0} = \frac{1}{1 - r^2}, \quad r \neq 1 \quad (2.19)$$

where r is the frequency ratio between the forcing frequency and the un-damped natural frequency. The steady-state magnification factor provides the magnitude and sign of the steady-state motion as a function of the frequency ratio r and is defined:

$$D_s(r) \equiv \left| \frac{U}{U_0} \right| \quad (2.20)$$

The variation of the magnification factor is plotted in Figure 2.5.

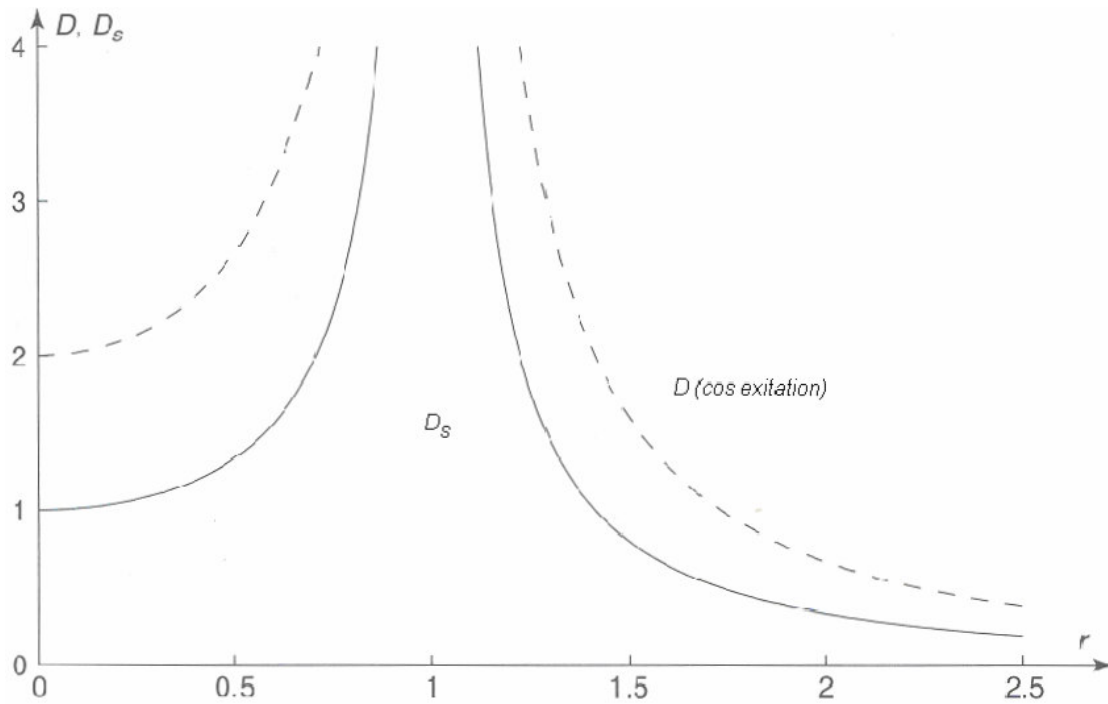


Figure 2.5 Dynamic magnification factors of an un-damped SDOF system: D_s (steady-state) and D (total magnification).

The presented equations are combined to formulate the steady-state response:

$$u_p = \frac{U_0}{1-r^2} \cos \Omega t, \quad r \neq 1 \quad (2.21)$$

The total response due to the harmonic excitation $p(t) = p_0 \cos \Omega t$ is given by:

$$u(t) = \frac{U_0}{1-r^2} \cos \Omega t + A_1 \cos \omega_n t + A_2 \sin \omega_n t \quad (2.22)$$

where A_1 and A_2 are constants determined by the initial conditions. Equation (2.22) is not valid when $r = 1$. When $r = 1$, the forcing frequency and the natural frequency are equal, i.e. $\Omega = \omega_n$. When studying Figure 2.6 it should be noticed that the response when the excitation frequency is close to the natural frequency becomes very large. This phenomenon is called resonance, and it is of great importance to control the response of the structure in order to avoid the resonance condition, where large amplitude motion may occur. When the forcing frequency is equal to the un-damped natural frequency it is necessary to replace equation (2.16) with the assumed particular solution:

$$u_p = Ct \sin \omega_n t \quad (2.23)$$

By substituting equation (2.23) into equation (2.15) the following expression of C is obtained:

$$C = \frac{p_0}{2m\omega_n} \quad (2.24)$$

producing the particular solution for the cosine-type excitation at resonance:

$$u_p(t) = \frac{U_0}{2}(\omega_n t) \sin \omega_n t \quad (2.25)$$

Figure 2.6 illustrates the response plotted with time. The amplitude of the particular solution increases constantly with each period.

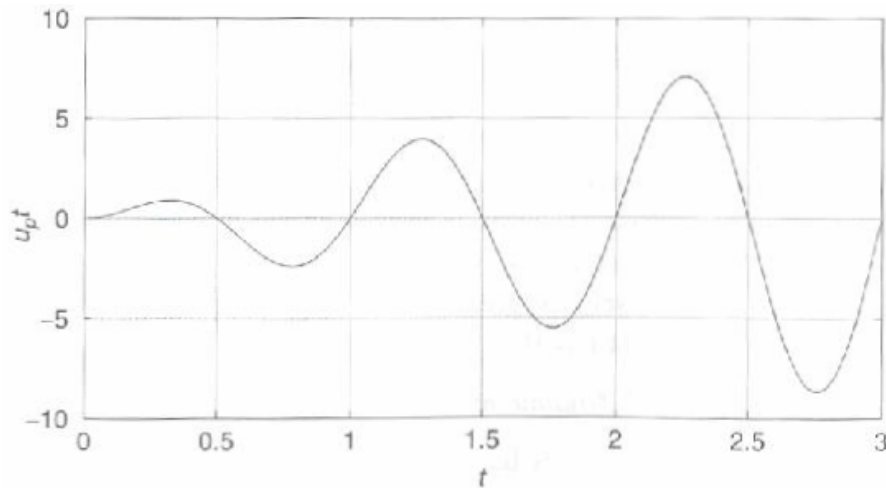


Figure 2.6 Response $u_p(t)$ at resonance: $p(t) = p_0 \cos(\omega_n t)$.

2.2 Damped mass-spring model

A viscous damping element serves as an additional energy storage device when introduced to a system. The energy is dissipated from the vibrating SDOF system. Previous researches, e.g. Bathe (1996), have proposed several techniques to describe material damping mathematically, but due to the complicated nature of damping it is usually impossible to determine it for a real structure. Figure 2.7 illustrates the simplest analytical model of damping used in structural dynamic analyses. The damping force is for this model a linear function of the relative velocity between the two ends of the damper:

$$f_D = c(\dot{u}_2 - \dot{u}_1) \quad (2.26)$$

The constant c is called the coefficient of viscous damping and is of the unit Newton seconds per metre (Ns/m).

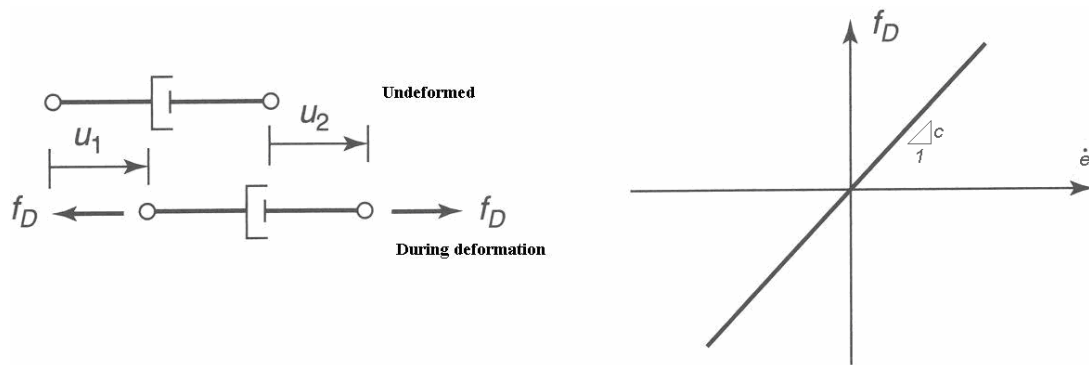


Figure 2.7 Un-deformed and deformed viscous dashpot with a force versus elongation rate.

2.2.1 Equation of motion

The equation of motion for this simple mass-spring-dashpot system can be derived using several different methods. In this section, the equilibrium equation for the example illustrated in Figure 2.8 will be determined in two ways independently, by using Newton's Laws and d'Alembert Force Method, respectively.

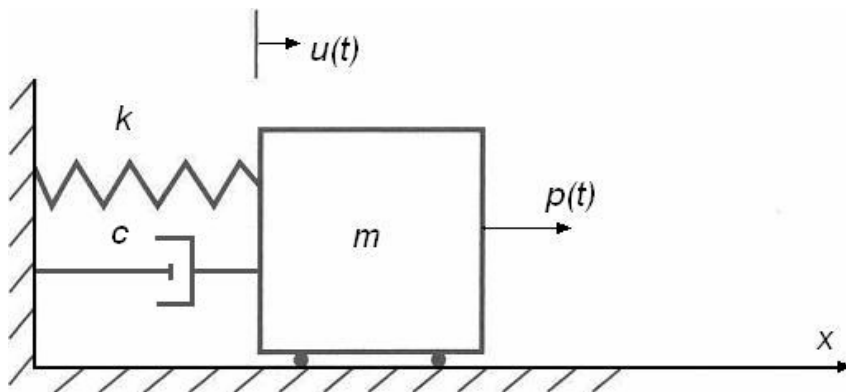


Figure 2.8 Mass-spring-dashpot SDOF system.

In the example, the spring and dashpot are assumed to be linear with a spring constant k and a damping coefficient c . The system is set up in such a way that only horizontal motion is allowed with the relative displacement to a fixed surface, denoted $u(t)$. When u is equal to zero the spring and damping forces are zero.

2.2.1.1 Newton's Laws

To determine the equation of motion of the mass m a free-body diagram is used (Figure 2.9).



Figure 2.9 Free-body diagram of SDOF system (Newton's Laws).

The free-body diagram of the mass includes the external forces acting on the mass. Newton's second Law is applied generating the following horizontal equilibrium equation:

$$\sum F_x = m\ddot{u} \quad (2.27)$$

The forces acting on the mass can be determined by studying Figure 2.9, which enables equation (2.27) to be rewritten:

$$p(t) - f_S - f_D = m\ddot{u} \quad (2.28)$$

The forces in equation (2.28) can be related to the motion variables as:

$$\begin{aligned} f_S &= ku \\ f_D &= c\dot{u} \end{aligned} \quad (2.29)$$

Combining and simplifying equations (2.28) and (2.29) generates the second order differential equation known as the fundamental equation in structural dynamics and linear vibration theory:

$$m\ddot{u} + c\dot{u} + ku = p(t) \quad (2.30)$$

2.2.1.2 d'Alembert force method

The d'Alembert force method includes inertia forces along with all real forces acting on the mass. The free-body diagram will therefore have a different appearance (Figure 2.10).

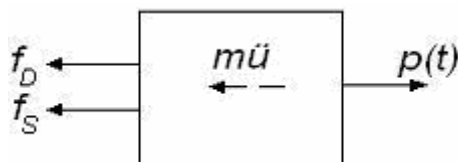


Figure 2.10 Free-body diagram of SDOF system (d'Alembert force method).

By studying the free-body diagram and considering the dynamic horizontal equilibrium equation the following expressions can be derived:

$$\sum F_x^* = 0 \quad (2.31)$$

$$p(t) - f_s - f_D - m\ddot{u} = 0 \quad (2.32)$$

Equation (2.32) combined with the motion variables stated in equations (2.29) enables the following definition of the equation of motion:

$$m\ddot{u} + c\dot{u} + ku = p(t) \quad (2.33)$$

The equation is identical to equation (2.30) indicating that the choice of method is arbitrary.

The d'Alembert force method is especially useful when describing support excitation by including the use of inertia forces.

3 Mathematical models of MDOF systems

Although SDOF models are able to describe the dynamical behaviour of some systems, it is in most cases necessary to expand the model to more complex MDOF models. The theory on which MDOF systems are based on is very similar to the theory presented in the previous chapter concerning SDOF systems.

3.1 Newton's Laws to describe the equation of motion

To derive the general form of the governing equations of motion for a linear MDOF system a lumped parameter model consisting of a mass-spring and a mass-spring-dashpot will be studied respectively. The lumped parameter model is a system of connected rigid bodies in general motion.

3.1.1 Un-damped MDOF system

Figure 3.1 illustrates a 3-DOF un-damped system of rigid bodies, each subjected to an external load $p_i(t)$.

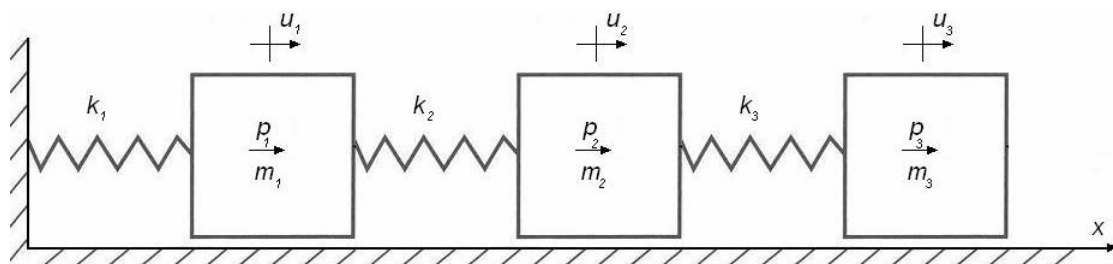


Figure 3.1 Mass-spring model.

The displacements, u_i , of the rigid bodies are defined relative the position where the forces in the springs are zero, i.e. the springs are neither in contraction nor elongation. The spring stiffnesses are denoted k and the masses are denoted m . Free-body diagrams of each individual mass are drawn according to Figure 3.2.

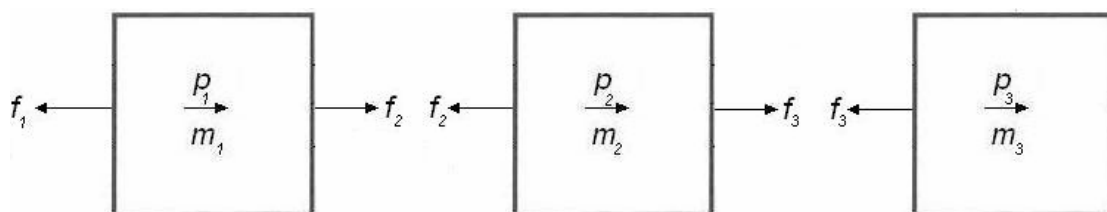


Figure 3.2 Free-body diagrams of the masses.

By applying Newton's second law for each mass the following equilibrium equations are obtained:

$$\begin{aligned}
\sum F_1 &= m_1 \ddot{u}_1 = p_1 + f_2 - f_1 \\
\sum F_2 &= m_2 \ddot{u}_2 = p_2 + f_3 - f_2 \\
\sum F_3 &= m_3 \ddot{u}_3 = p_3 - f_3
\end{aligned} \tag{3.1}$$

The linear elastic forces in the springs are related to the relative deformation of the springs, i.e. the difference between two adjacent masses.

$$\begin{aligned}
f_1 &= k_1 u_1 \\
f_2 &= k_2 (u_2 - u_1) \\
f_3 &= k_3 (u_3 - u_2)
\end{aligned} \tag{3.2}$$

The equations (3.1) and (3.2) are combined and simplified to create three differential equations:

$$\begin{aligned}
m_1 \ddot{u}_1 + (k_1 + k_2) u_1 - k_2 u_2 &= p_1(t) \\
m_2 \ddot{u}_2 - k_2 u_1 + (k_2 + k_3) u_2 - k_3 u_3 &= p_2(t) \\
m_3 \ddot{u}_3 - k_3 u_2 + k_3 u_3 &= p_3(t)
\end{aligned} \tag{3.3}$$

The equations (3.3) can be written in matrix form according to:

$$\begin{bmatrix} m_1 & 0 & 0 \\ 0 & m_2 & 0 \\ 0 & 0 & m_3 \end{bmatrix} \begin{bmatrix} \ddot{u}_1 \\ \ddot{u}_2 \\ \ddot{u}_3 \end{bmatrix} + \begin{bmatrix} k_1 + k_2 & -k_2 & 0 \\ -k_2 & k_2 + k_3 & -k_3 \\ 0 & -k_3 & k_3 \end{bmatrix} \begin{bmatrix} u_1 \\ u_2 \\ u_3 \end{bmatrix} = \begin{bmatrix} p_1(t) \\ p_2(t) \\ p_3(t) \end{bmatrix} \tag{3.4}$$

which in symbolic matrix notation is represented by:

$$\mathbf{M}\ddot{\mathbf{u}} + \mathbf{K}\mathbf{u} = \mathbf{p}(t) \tag{3.5}$$

The set of coupled ordinary differential equations represent the 3-DOF mathematical model of the lumped mass system.

The matrices notated \mathbf{M} and \mathbf{K} are the system's mass and stiffness matrices, while \mathbf{p} is the external load vector.

3.1.2 Damped MDOF system

Also for the MDOF model the system can be expanded to include dampers. Figure 3.3 illustrates a 2-DOF mass-spring-dashpot system. The equations of motion can be derived similarly to previous examples.

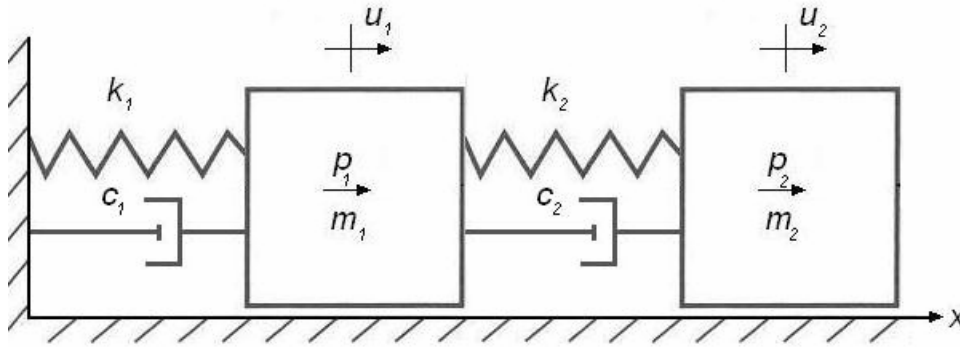


Figure 3.3 2-DOF mass-spring-dashpot system.

The notation of spring stiffnesses and masses is analogous to the example presented in Figure 3.2, with the addition of the damping coefficients c .

A free-body diagram for each mass in Figure 3.3 is drawn, where the internal and external forces are identified.

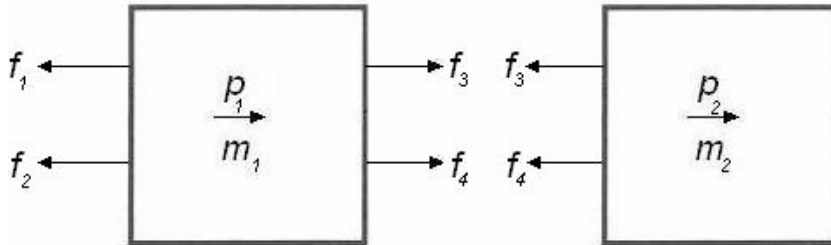


Figure 3.4 Free-body diagrams of the masses.

Newton's second law is applied to generate the equations of motion:

$$\begin{aligned} \sum F_1 &= m_1 \ddot{u}_1 = -f_1 - f_2 + f_3 + f_4 + p_1 \\ \sum F_2 &= m_2 \ddot{u}_2 = -f_3 - f_4 + p_2 \end{aligned} \quad (3.6)$$

The linear elastic spring forces (f_1 and f_3) are related to the displacements, and the damping forces (f_2 and f_4) are related to the velocities.

$$\begin{aligned} f_1 &= k_1 u_1 \\ f_2 &= c_1 \dot{u}_1 \\ f_3 &= k_2 (u_2 - u_1) \\ f_4 &= c_2 (\dot{u}_2 - \dot{u}_1) \end{aligned} \quad (3.7)$$

The equations (3.6) and (3.7) can be simplified and combined into a set of equations of motion:

$$\begin{bmatrix} m_1 & 0 \\ 0 & m_2 \end{bmatrix} \begin{bmatrix} \ddot{u}_1 \\ \ddot{u}_2 \end{bmatrix} + \begin{bmatrix} c_1 + c_2 & -c_2 \\ -c_2 & c_2 \end{bmatrix} \begin{bmatrix} \dot{u}_1 \\ \dot{u}_2 \end{bmatrix} + \begin{bmatrix} k_1 + k_2 & -k_2 \\ -k_2 & k_2 \end{bmatrix} \begin{bmatrix} u_1 \\ u_2 \end{bmatrix} = \begin{bmatrix} p_1(t) \\ p_2(t) \end{bmatrix} \quad (3.8)$$

Equation (3.8) can be written in symbolic matrix notation as:

$$\mathbf{M}\ddot{\mathbf{u}} + \mathbf{C}\dot{\mathbf{u}} + \mathbf{K}\mathbf{u} = \mathbf{p}(t) \quad (3.9)$$

where \mathbf{C} is the damping matrix. The stated expression is the generalised fundamental equation of motion using matrix notation.

3.2 Vibration of un-damped MDOF system

The most important dynamic parameter of a structure is its natural frequency. The natural frequency determines the level of vibration for a given excitation, and is defined as the number of oscillations per second during harmonic motion. Each natural frequency oscillates with a specific configuration that describes the deformation of the structure. The deformation configuration corresponding to a natural frequency is called natural mode.

To present the derivation of the natural frequency and natural modes, an un-damped 2-DOF system is the most instructive example. The equations of motion for an un-damped 2-DOF system are of the form:

$$\begin{bmatrix} m_{11} & m_{12} \\ m_{21} & m_{22} \end{bmatrix} \begin{bmatrix} \ddot{u}_1 \\ \ddot{u}_2 \end{bmatrix} + \begin{bmatrix} k_{11} & k_{12} \\ k_{21} & k_{22} \end{bmatrix} \begin{bmatrix} u_1 \\ u_2 \end{bmatrix} = \begin{bmatrix} p_1(t) \\ p_2(t) \end{bmatrix} \quad (3.10)$$

where u_i may be physical displacement or generalised coordinates. The solution to equation (3.10) will consist of a complementary and particular solution. The complementary solution is obtained by setting the external load vector to zero and involves the system's dynamical properties; natural modes and natural frequencies. By examining the response of the system subjected to harmonic excitation an important analysis method in structural dynamics is made possible, namely the mode superposition method (Section 6.2).

3.2.1 Free vibration of 2-DOF system

To solve the equations of motion for a system that is at free vibration the applied loads p_i are set to zero:

$$\begin{bmatrix} m_{11} & m_{12} \\ m_{21} & m_{22} \end{bmatrix} \begin{bmatrix} \ddot{u}_1 \\ \ddot{u}_2 \end{bmatrix} + \begin{bmatrix} k_{11} & k_{12} \\ k_{21} & k_{22} \end{bmatrix} \begin{bmatrix} u_1 \\ u_2 \end{bmatrix} = \begin{bmatrix} 0 \\ 0 \end{bmatrix} \quad (3.11)$$

assuming that the system undergoes harmonic motion of the form:

$$\begin{aligned} u_1(t) &= U_1 \cos(\omega t - \alpha) \\ u_2(t) &= U_2 \cos(\omega t - \alpha) \end{aligned} \quad (3.12)$$

where U_i are the amplitudes of the sinusoidal motions. The assumed solutions in equation (3.12) are substituted into the equations of motion (3.11) forming the algebraic eigenvalue problem:

$$\left[\begin{bmatrix} k_{11} & k_{12} \\ k_{21} & k_{22} \end{bmatrix} - \omega_i^2 \begin{bmatrix} m_{11} & m_{12} \\ m_{21} & m_{22} \end{bmatrix} \right] \begin{bmatrix} U_1 \\ U_2 \end{bmatrix} = \begin{bmatrix} 0 \\ 0 \end{bmatrix} \quad (3.13)$$

The set of homogenous linear algebraic equations only has one non-trivial solution corresponding to the values of ω^2 that satisfy the characteristic equation:

$$\left[\begin{bmatrix} k_{11} & k_{12} \\ k_{21} & k_{22} \end{bmatrix} - \omega_i^2 \begin{bmatrix} m_{11} & m_{12} \\ m_{21} & m_{22} \end{bmatrix} \right] = 0 \quad (3.14)$$

The polynomial equation is of the second order in the unknown parameter ω^2 indicating that the characteristic equation (3.14) has two roots labelled ω_1^2 and ω_2^2 . In mathematical terminology the roots are called eigenvalues and are organised in an increasing order such that $\omega_1^2 < \omega_2^2$. In structural dynamics the parameters are called circular natural frequencies and describe the rate of oscillation in harmonic motion. The parameters are sometimes modified and referred to as natural frequencies (f_i) of the system, expressed in Hertz:

$$f_i = \frac{\omega_i}{2\pi} \quad (3.15)$$

The eigenvalue ω_1^2 is substituted into the first of the equations in (3.13) to obtain the ratio $\beta_1 = (U_2/U_1)^{(1)}$, defining the mode shape corresponding to the first natural frequency. In literature the mode shape is sometimes referred to as the natural mode. The procedure is repeated for the second eigenvalue enabling $\beta_2 = (U_2/U_1)^{(2)}$ to be determined. The mode shapes, or eigenvectors, are often notated as Φ_r and are written as:

$$\Phi_r \equiv \begin{bmatrix} \phi_1 \\ \phi_2 \end{bmatrix} = \begin{bmatrix} 1 \\ \beta_r \end{bmatrix}, \quad r = 1, 2 \quad (3.16)$$

where r indicates the identity of each mode shape. The procedure using β to determine the mode shapes is only applicable for 2-DOF systems. For larger MDOF systems the governing equations are solved simultaneously. Using the presented expression of the mode shapes and the natural frequencies the general un-damped algebraic eigenvalue problem can be satisfied by the following equation, expressed with matrix notation:

$$[\mathbf{K} - \omega_r^2 \mathbf{M}] \Phi_r = 0 \quad (3.17)$$

Free vibration will only occur at the frequencies corresponding to ω_1 and ω_2 . The general solution of equation (3.11) is a linear combination of the two expressions:

$$\begin{aligned} u_1(t) &= A_1 \cos(\omega_1 t - \alpha_1) + A_2 \cos(\omega_2 t - \alpha_2) \\ u_2(t) &= \beta_1 A_1 \cos(\omega_1 t - \alpha_1) + \beta_2 A_2 \cos(\omega_2 t - \alpha_2) \end{aligned} \quad (3.18)$$

where A_1, A_2, α_1 and α_2 are constants determined from initial conditions.

3.2.2 Procedure to determine natural frequencies and mode shapes

The derivation of the natural frequencies and mode shapes of a vibrating structure is the most important procedure in structural dynamic analysis. As an example, the procedure is demonstrated for the 2-DOF system illustrated in Figure 3.5. The equations of motion for free vibration are:

$$\begin{aligned} m\ddot{u}_1 + 2ku_1 - ku_2 &= 0 \\ m\ddot{u}_2 - ku_1 + 2ku_2 &= 0 \end{aligned} \quad (3.19)$$

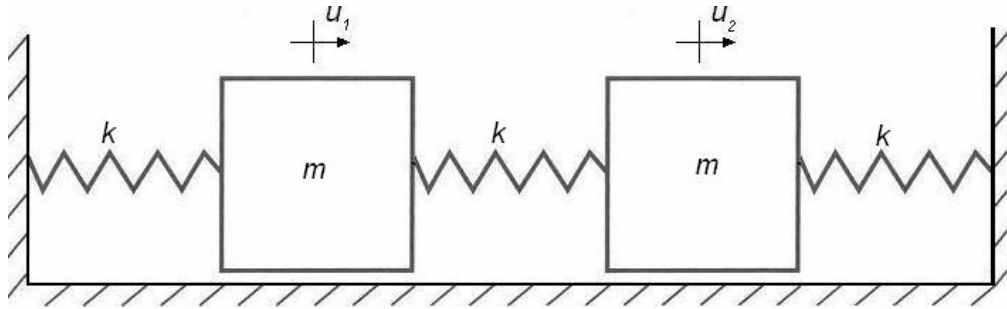


Figure 3.5 Symmetric 2-DOF mass-spring system.

The harmonic solution can be assumed to be identical to equation (3.12). This means that when the 2-DOF system vibrates at a natural frequency, u_1 and u_2 have the same time dependence, i.e. constant amplitude ratio.

The algebraic eigenvalue problem is obtained by substituting the harmonic solution into the equation of motion:

$$\begin{bmatrix} 2k - m\omega_i^2 & -k \\ -k & 2k - m\omega_i^2 \end{bmatrix} \begin{bmatrix} U_1 \\ U_2 \end{bmatrix} = \begin{bmatrix} 0 \\ 0 \end{bmatrix} \quad (3.20)$$

The characteristic equations are obtained by the determinant of the coefficient matrix in equation (3.20):

$$\begin{vmatrix} 2k - m\omega_i^2 & -k \\ -k & 2k - m\omega_i^2 \end{vmatrix} = 0 \Leftrightarrow (2k - m\omega_i^2)^2 - k^2 = 0 \quad (3.21)$$

where the roots are solved using factorisation.

$$\begin{aligned} \omega_1^2 = \frac{k}{m} &\Rightarrow \omega_1 = \sqrt{\frac{k}{m}} \\ \omega_2^2 = \frac{3k}{m} &\Rightarrow \omega_2 = \sqrt{\frac{3k}{m}} \end{aligned} \quad (3.22)$$

The eigenvalues are substituted into (3.20), generating the mode shape ratios:

$$\beta_i \equiv \left(\frac{U_2}{U_1} \right)^{(i)} = \frac{2k - m\omega_i^2}{k} = 2 - \frac{m\omega_i^2}{k} \quad (3.23)$$

For the studied example the mode shape ratios are:

$$\beta_1 = 2 - 1 = 1$$

$$\beta_2 = 2 - 3 = -1$$

giving the following appearance to the mode shapes with corresponding eigenvectors:

a) Mode 1 (symmetric)



b) Mode 2 (asymmetric)

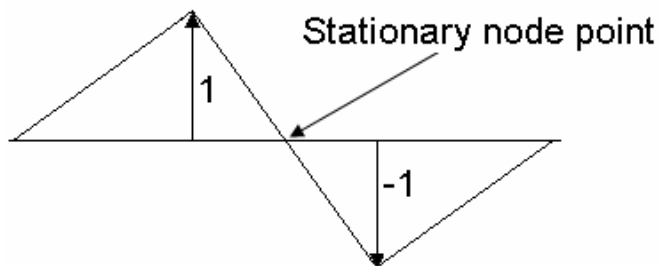


Figure 3.6 Mode shapes of the 2-DOF system.

$$\Phi_1 = \begin{bmatrix} 1 \\ 1 \end{bmatrix} \quad \Phi_2 = \begin{bmatrix} 1 \\ -1 \end{bmatrix}$$

It should be noticed that the system is symmetric about the centre of the middle spring, resulting in mode shapes with both symmetric (mode 1) and asymmetric (mode 2) configurations. This is an important result since many structures possess such a physical symmetry, e.g. many railway bridges.

The derivation of mode shapes for a general MDOF system is analogous to the described example. The expansion of the system is relatively uncomplicated, but involves more unknown variables needed to be solved simultaneously.

4 Vibration properties of MDOF systems

As mentioned in Section 3.2 the natural modes and natural frequencies are two very important dynamic parameters. This chapter will be focused on describing the properties of these dynamic parameters and the coefficient matrices encountered in structural dynamics.

4.1 Properties of stiffness and mass matrices

The stiffness matrix \mathbf{K} and the mass matrix \mathbf{M} can be related to the strain and kinetic energy similarly as for the SDOF system described in Section 2.1. The quadratic potential and kinetic energy formulations using matrix notation are:

$$\begin{aligned} V &= \frac{1}{2} \mathbf{u}^T \mathbf{K} \mathbf{u} \\ T &= \frac{1}{2} \dot{\mathbf{u}}^T \mathbf{M} \dot{\mathbf{u}} \end{aligned} \quad (4.1)$$

where $\mathbf{u}(t)$ is the displacement vector, \mathbf{K} is the symmetric stiffness matrix and \mathbf{M} is the symmetric mass matrix. Due to the symmetry of the coefficient matrices they possess the property $\mathbf{X}^T = \mathbf{X}$. For most structures, \mathbf{M} and \mathbf{K} are positive definite resulting in positive values of V and T using arbitrary displacement vectors.

If a system has rigid body freedom an exception from the positive definiteness of \mathbf{K} occurs, allowing rigid body displacement vectors. The stiffness matrix is in this case considered semi-definite, permitting the strain energy to be zero for rigid body displacement. A semi-definite matrix has a determinant equal to zero and is called singular. The singularity of the stiffness matrix is avoided by introducing proper boundary conditions. Also the mass matrix can diverge from the positive definiteness. Examples of this are when degrees-of-freedom (DOF) are not associated with inertia (Figure 4.1).

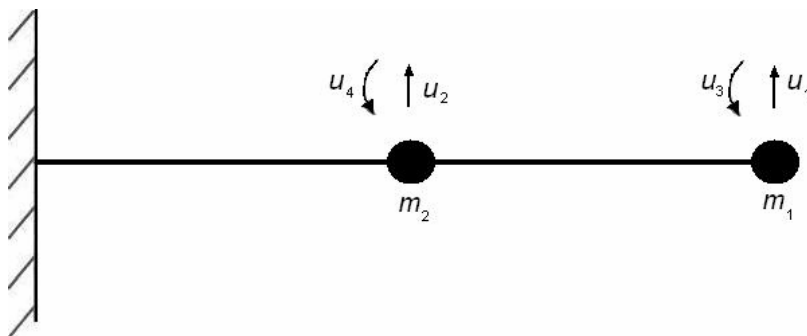


Figure 4.1 Beam with a positive semi-definite mass matrix.

In Figure 4.1, no mass is associated with the rotational degrees of freedom (u_3 and u_4) making \mathbf{M} a positive semi-definite matrix.

4.2 Normalisation of modes

The system's natural modes are describing the deformation shapes with a specific ratio between the individual nodal points. The modes can be multiplied with any constant, keeping the ratio intact. Due to this property, a normalisation of the modes is possible and is commonly utilised to reduce extreme magnitudes of the nodal elements:

$$\mathbf{U}_r = c_r \boldsymbol{\phi}_r \quad (4.2)$$

where \mathbf{U}_r is the scaled r :th normal mode and $\boldsymbol{\phi}_r$ is the corresponding arbitrary modal vector.

The three most commonly employed normalisation procedures of modes are:

1. Scale the r :th mode such that the i :th nodal element of the vector is unity, i.e. $(\phi_i)_r = 1$.
2. Scale the r :th mode such that the length of the vector is unity, i.e. $\|\boldsymbol{\phi}_r\| = 1$.
3. Scale the r :th mode so that its generalised mass, or modal mass, defined by:

$$M_r = \boldsymbol{\phi}_r^T \mathbf{M} \boldsymbol{\phi}_r \quad (4.3)$$

is assigned a specific value, commonly $M_r = 1$. The generalised stiffness, or modal stiffness, is similarly defined according to the following expression:

$$K_r = \boldsymbol{\phi}_r^T \mathbf{K} \boldsymbol{\phi}_r \quad (4.4)$$

This normalisation is convenient when the solution to the algebraic eigenvalue problem is sought. The natural frequency is related to the modal stiffness and modal mass by:

$$\omega_r = \sqrt{\frac{K_r}{M_r}} \quad (4.5)$$

4.3 Orthogonality of natural modes

One of the most important properties of the natural modes is the orthogonality between arbitrary vectors. By pre-multiplying the algebraic eigenvalue problem and evaluating the results it can be proven that two arbitrary eigenmodes, $\boldsymbol{\phi}_r$ and $\boldsymbol{\phi}_s$ are orthogonal with respect to the stiffness matrix and mass matrix:

$$\begin{aligned} \boldsymbol{\phi}_s^T \mathbf{M} \boldsymbol{\phi}_r &= 0 \\ \boldsymbol{\phi}_s^T \mathbf{K} \boldsymbol{\phi}_r &= 0 \end{aligned} \quad \text{for } s \neq r \quad (4.6)$$

4.4 Generalisation of matrices

Generalised matrices are often used to simplify the computation by decreasing the number of non-zero elements included in the calculations. To enable these simplifications the modal and eigenvalue matrices are introduced. The modal matrix Φ is a matrix consisting of the natural modes sorted in increasing order, $\Phi \equiv [\varphi_1 \varphi_2 \dots \varphi_N]$. The eigenvalue matrix Λ is a diagonal matrix of eigenvalues, $\Lambda \equiv \text{diag}(\omega_1^2 \omega_2^2 \dots \omega_N^2)$. The variable N is determined by the number of degrees-of-freedom assumed to represent the system.

By utilising the definitions of the modal mass and modal stiffness matrices together with the orthogonality property, the diagonal modal mass matrix and modal stiffness matrix are obtained.

$$\begin{aligned} \mathbf{M} &= \Phi^T \mathbf{M} \Phi = \text{diag}(M_1, M_2, \dots, M_N) \\ \mathbf{K} &= \Phi^T \mathbf{K} \Phi = \text{diag}(K_1, K_2, \dots, K_N) = \text{diag}(\omega_1^2 M_1, \omega_2^2 M_2, \dots, \omega_N^2 M_N) \end{aligned} \quad (4.7)$$

If the natural modes are normalised so that $M_r = 1$ the modal mass matrix becomes a $N \times N$ unit matrix:

$$\Phi^T \mathbf{M} \Phi = \mathbf{I} \quad (4.8)$$

with the corresponding modal stiffness matrix equal to the eigenvalue matrix:

$$\Phi^T \mathbf{K} \Phi = \Lambda \quad (4.9)$$

4.5 Damping in MDOF systems

Determining a structure's true physical damping is very complex. To obtain a simplified model it is therefore often assumed that the damping of a structure can be represented by viscous damping. This assumption enables the following representation of the MDOF system's equations of motion to be stated:

$$\mathbf{M}\ddot{\mathbf{u}} + \mathbf{C}\dot{\mathbf{u}} + \mathbf{K}\mathbf{u} = \mathbf{p}(t) \quad (4.10)$$

where \mathbf{C} is the systems viscous damping matrix in physical or generalised coordinates \mathbf{u} . By utilising a mode superposition solution based on free vibrational modes of an un-damped structure the equations of motion can be expressed in principal coordinates as:

$$\mathbf{M}\ddot{\boldsymbol{\eta}} + \mathbf{C}\dot{\boldsymbol{\eta}} + \mathbf{K}\boldsymbol{\eta} = \Phi^T \mathbf{p}(t) \quad (4.11)$$

where $\boldsymbol{\eta}$ are called the modal or principal coordinates, and \mathbf{M} and \mathbf{K} are normalised according to equation (4.7). Typically, the generalised damping matrix:

$$\mathbf{C} = \Phi^T \mathbf{C} \Phi \quad (4.12)$$

is not diagonal. Material damping properties are normally not defined well enough to permit a derivation analogous to the finite element procedures used to obtain the stiffness and mass matrices. Damping of a structure is therefore usually defined at system level rather than employing individual element properties. In the following sections, procedures leading to a diagonal arrangement of the generalised damping matrix are presented.

4.5.1 Difficulties of expressing the damping matrix

As previously mentioned there are a number of situations in which damping can not be properly represented by an un-coupled modal damping model. An example of this is a structure and its surrounding soil. The damping level of the structure's rigid foundation is far less than the level possessed by the soil, leading to off-diagonal coupling terms in the combined soil and structure model. There are two methods to solve systems with this type of general viscous damping; mode superposition using complex modes of the damped systems and direct integration of the coupled equations of motion. Both procedures are presented in Chapter 6.

4.5.2 Rayleigh damping

A method to define the viscous damping matrix in terms of the diagonal generalised damping matrix \mathbf{C} is to employ Rayleigh or proportional damping, defined by:

$$\mathbf{C} = a_0\mathbf{M} + a_1\mathbf{K} \quad (4.13)$$

The damping matrix is proportional to a linear combination of the mass and stiffness matrices. The constant coefficients a_0 and a_1 are usually chosen to produce specified modal damping factors for two critical modes. By combining the equations in (4.7) with the definition presented in (4.13) the following result is obtained:

$$\mathbf{C} = \mathbf{\Phi}^T \mathbf{C} \mathbf{\Phi} = \text{diag}(C_r) = \text{diag}(a_0 + a_1\omega_r^2)M_r = \text{diag}(2\zeta_r\omega_r M_r) \quad (4.14)$$

where the modal damping factor ζ_r is defined as:

$$\zeta_r = \frac{1}{2} \left(\frac{a_0}{\omega_r} + a_1\omega_r \right) \quad (4.15)$$

By using this definition it is easy to describe the Rayleigh damping by choosing ζ_r for two modes and solving the corresponding damping coefficient a_0 and a_1 .

4.5.3 Modal damping

The type of damping most frequently used in structural dynamic computations is modal damping. Modal damping is assumed to satisfy orthogonality, allowing the following formulation of equation (4.14):

$$\mathbf{C} = \mathbf{\Phi}^T \mathbf{C} \mathbf{\Phi} = \text{diag}(C_r) = \text{diag}(2\zeta_r \omega_r M_r) \quad (4.16)$$

By utilising this diagonalised form of the modal damping, the set of coupled equations of motion (4.10) are transformed into N un-coupled equations of motion in modal coordinates:

$$M_r \ddot{\eta}_r + 2M_r \omega_r \zeta_r \dot{\eta}_r + \omega_r^2 M_r \eta_r = \phi_r^T p(t) \quad r = 1, 2, \dots, N \quad (4.17)$$

Unlike Rayleigh damping, the modal damping allows all N damping factors to be assigned individual values. The values of the modal damping factors ζ_r are assumed on the basis of providing damping that is characteristic for the type of structure considered. Typical values of ζ_r are in the range of 1 % to 10 %.

5 Dynamics of railway bridges

A railway bridge can be represented with a MDOF system consisting of an immense amount of degrees-of-freedom. The choice of model should be determined by the complexity of the actual structure and the desired accuracy of the results. The equations of motion which governs the bridge's dynamic behaviour can in theory be derived similarly as described in Chapter 4.

The solution to a dynamic analysis is influenced by a dynamic load with magnitude, direction and position varying with time. Therefore, also the structural response will be time dependent, which introduces a higher level of complexity compared to the static analysis. The dynamic analysis will, in contrary to the static analysis, not have one single solution but rather a succession of solutions established to correspond to all time instances of interest.

A dynamic load introduces an addition of inertia and damping to the elastic resistance force, generated to resist the accelerations of the structure. The structure will therefore not only equilibrate to the externally applied loads but also with the internal forces. If the internal forces are negligible compared to the total load, the solution can be considered similar to the static response, using a dynamic amplification factor to represent the maximum structural response. Studies are indicating that trains travelling with a velocity greater than 200 km/h will generate internal stresses great enough to produce problems of dynamic character, requiring more detailed analyses.

5.1 Theoretical bridge models

The theoretical models can be divided into two categories; models with continuously distributed mass and those with mass concentrated in the modelled nodal points. The choice of model should be made to suit the specific structure and the purpose of the analysis.

5.1.1 Beams

The most frequently utilised model applied on railway bridges is the beam model which often can characterise the structure in a simple way due to the small transverse dimension compared to the total length.

5.1.1.1 Beam with continuously distributed mass

The mass of medium span and large span bridge structures are generally greater or similar to the mass of the vehicle travelling on the structure and can therefore not be neglected. To model these bridges, the use of beams with continuously distributed mass is required. The equation of motion for the beam expresses the force equilibrium per unit length:

$$EI \frac{\partial^4 u(x,t)}{\partial x^4} + \mu \frac{\partial^2 u(x,t)}{\partial t^2} + 2\mu\omega_b \frac{\partial u(x,t)}{\partial t} = f(x,t) \quad (5.1)$$

where the cross section is assumed to be constant and the damping is considered to be proportional to the velocity of the vibration. The notation used is:

- $u(x,t)$ vertical deflection of the beam at the point x and time instance t
- E modulus of elasticity
- I moment of inertia
- μ mass per unit length of the beam
- ω_b circular frequency of viscous damping
- $f(x,t)$ load at point x and time t per unit length of the beam

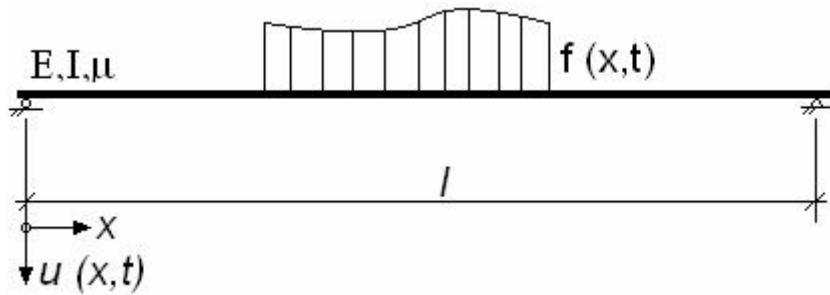


Figure 5.1 Beam with continuously distributed mass and a span length l .

The differential equation (5.1) applies to Bernoulli-Euler beams and is derived assuming the theory of small deformations, Hooke's law, Navier's hypothesis and the Saint-Venant principle. The formulation presented in equation (5.1) is utilised in all analytical and numerical methods of applied mathematics.

5.1.1.2 Massless beams

The alternative to the beam with distributed continuous mass is the massless beam which is possible to employ when the mass of the bridge structure is substantially lower than the vehicle's mass. This idealisation is commonly used for bridges with short spans and longitudinal or transverse girders, fulfilling the stated conditions. The equation of motion is derived by letting $\mu \rightarrow 0$ in equation (5.1) generating the following expression:

$$EI \frac{\partial^4 u(x,t)}{\partial x^4} = f(x,t) \quad (5.2)$$

with analogous notation. The load $f(x,t)$ is in this case considered to include both the external load and inertia effects making the solution more difficult to obtain.

5.1.2 Plates

Railway bridges are often consisting of reinforced or pre-stressed concrete plates. The governing differential equation of plates can be derived by applying the same assumptions made for equation (5.1):

$$D \left[\frac{\partial^4 w(x, y, t)}{\partial x^4} + 2 \frac{\partial^4 w(x, y, t)}{\partial x^2 \partial y^2} + \frac{\partial^4 w(x, y, t)}{\partial y^4} \right] + \mu \frac{\partial^2 w(x, y, t)}{\partial t^2} = f(x, y, t) \quad (5.3)$$

where,

$w(x, y, t)$	vertical deflection of the plate at the point (x, y) and time instance t
$D = \frac{Eh^3}{12(1-\nu^2)}$	bending stiffness of the plate
E	modulus of elasticity
h	plate thickness
μ	mass per unit area of the plate
ν	Poisson's number
$f(x, y, t)$	load per unit area of the plate

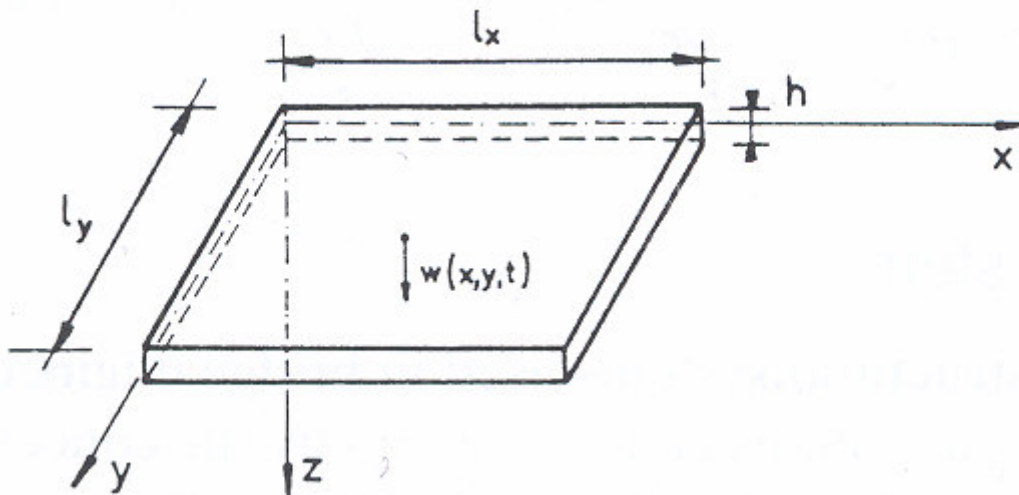


Figure 5.2 Geometrical properties of plate. Adapted from Frýba (1996).

Even though plates are commonly used when constructing railway bridges, the use of plates while modelling the bridges is limited.

5.2 Natural frequencies of railway bridges

The most important dynamic characteristic of a railway bridge trafficked by trains with velocities exceeding 200 km/h is the natural frequency, characterising the extent of the bridge's sensitivity to dynamic loads. A mechanical system with continuously

distributed mass has an infinite number of natural frequencies, all determined using previously presented methods. In practical application, only the lowest frequencies will influence the structural response. The external excitation generated by the moving train is commonly applied to the system over a wide spectrum of frequencies. The structure will react stronger to the dynamic loads with a driving frequency near the natural frequencies of the bridge, enhancing its influence on the total response.

5.3 Resonance of railway bridges

Resonance of a railway bridge may occur when a train with equally spaced axle groups is travelling over the bridge at high speeds. Resonance is a precarious phenomenon endangering the structural stability. The risk of resonance occurring arises when the excitation frequency, or a multiple of it, coincides with the natural frequency of the structure. Resonance will generate a rapid increase of the structure's response and may cause the maximum allowed stress levels to be exceeded. The main factors influencing the occurrence and magnitude of the resonant peaks are; load duration, damping of the structure and characteristic properties of the load and structure. The magnitudes of the resonant peaks are highly dependent on the level of structural damping. A low structural damping generates high resonant peaks that may compromise the safety of the bridge. Figure 5.3 illustrates the dynamic amplification effects for different damping ratios.

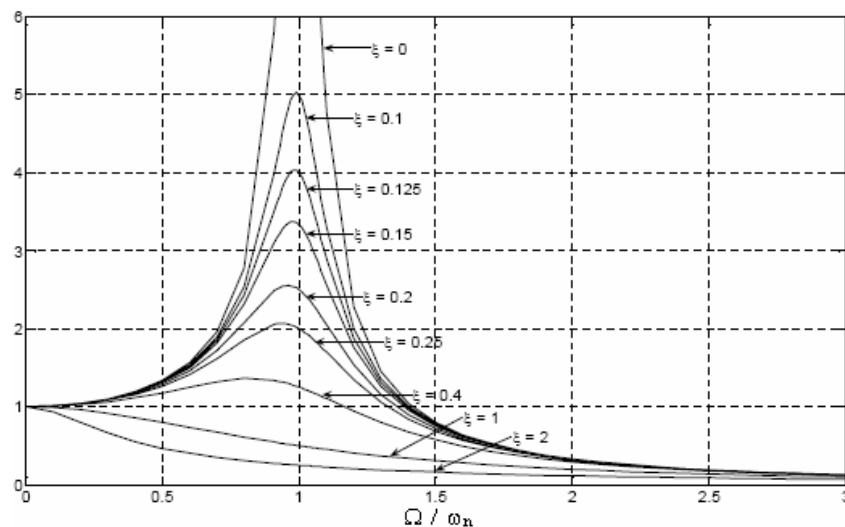


Figure 5.3 Relation between dynamic amplification and driving frequency of the load for different damping ratios.

5.4 Damping of railway bridges

Damping is, as previously described, a key parameter governing the total response of a structure. During the vibration phase, a part of the energy is converted between potential and kinetic energy, while another part is utilised to sustain irreversible plastic deformation or is lost to friction and dissipates into the surrounding environment.

There are two types of damping present in a bridge structure; internal and external damping. The internal damping occurs during the deformation of the building material, producing viscous internal friction due to non-homogenous properties and cracks. The external sources include friction at the supports, bearings, ballast material, joints of the structure and viscoelastic properties of the soil in contact with the bridge and abutments.

It is obvious that the number of sources influencing the damping makes it virtually impossible to determine the actual level of damping for a structure. The damping depends on material parameters and the state of the structure, but is also influenced by the amplitude of the vibrations.

Damping is a desirable property of a structure, able to reduce the dynamic response and cause a bridge to reach equilibrium faster.

6 Methods of dynamic analysis

The equilibrium equations, stated in Section 4.5, governing the response of a linear dynamic system of finite elements are:

$$\mathbf{M}\ddot{\mathbf{u}} + \mathbf{C}\dot{\mathbf{u}} + \mathbf{K}\mathbf{u} = \mathbf{p}(t) \quad (6.1)$$

where \mathbf{M} , \mathbf{C} and \mathbf{K} are the mass, damping and stiffness matrices. The externally applied loads are incorporated in the vector \mathbf{p} , while \mathbf{u} , $\dot{\mathbf{u}}$ and $\ddot{\mathbf{u}}$ represent displacements, velocities and accelerations. The externally applied loads will give rise to internal forces which can be described as:

$$\mathbf{F}_I(t) + \mathbf{F}_D(t) + \mathbf{F}_E(t) = \mathbf{p}(t) \quad (6.2)$$

The reaction forces are time dependent. Therefore, the dynamic analysis is in principle static equilibriums at an arbitrary time t , which includes the effects of acceleration dependent inertia forces $\mathbf{F}_I(t) = \mathbf{M}\ddot{\mathbf{u}}$, velocity dependent damping forces $\mathbf{F}_D(t) = \mathbf{C}\dot{\mathbf{u}}$ and elastic forces $\mathbf{F}_E(t) = \mathbf{K}\mathbf{u}$.

Mathematically, equation (6.1) represents a system of linear differential equations of second order with a solution that can be obtained using standard procedures of solving differential equations. For large structural systems the coefficient matrices \mathbf{M} , \mathbf{C} and \mathbf{K} contains an extensive number of differential equations, leading to a time consuming analysis to obtain the exact solutions. In finite element analysis, the two mainly utilised integration techniques are; direct integration and mode superposition.

6.1 Direct integration methods

By applying a direct integration scheme, equation (6.1) is integrated using a numerical step-by-step procedure. The methods do not require any transformations of the equations into different forms and are therefore considered as direct. Direct numerical integration is based on fulfilling two fundamental conditions, (1) instead of satisfying equation (6.1) at any time t the aim is to satisfy it only at discrete time intervals separated by an increment Δt . The result of this is that static equilibrium, which includes the effect of inertia and damping forces, is sought at discrete time instances within the studied time interval. The second condition (2) is that the variation of displacements, velocities and accelerations within each time interval Δt is assumed. These assumptions will determine the accuracy and stability of the solution procedure.

In linear analysis, it is common to apply a constant time-step, but it is fairly easy to extend the complexity of the analysis by introducing varying time-steps. Direct integration must be applied to solve non-linear problems.

There are numerous methods for direct integration, all based on the presented essential conditions. The derivations of a selection of algorithms are presented in the following sections.

6.1.1 Central difference method

The central difference method is an explicit integration method, meaning that it does not require any factorisation of the stiffness matrix in the step-by-step solution. The integration scheme considers the equilibrium equations as a system of ordinary differential equations with constant coefficients. The method assumes the following acceleration at time-step t :

$${}^t\ddot{\mathbf{u}} = \frac{1}{\Delta t^2} ({}^{t-\Delta t}\mathbf{u} - 2{}^t\mathbf{u} + {}^{t+\Delta t}\mathbf{u}) \quad (6.3)$$

To have the same order of error on the velocity and the acceleration the following expression is used:

$${}^t\dot{\mathbf{u}} = \frac{1}{2\Delta t} (-{}^{t-\Delta t}\mathbf{u} + {}^{t+\Delta t}\mathbf{u}) \quad (6.4)$$

By inserting equations (6.3) and (6.4) into the equilibrium equations (6.1), the displacement solution for time $t+\Delta t$ is obtained.

$$\left(\frac{1}{\Delta t^2} \mathbf{M} + \frac{1}{2\Delta t} \mathbf{C} \right) {}^{t+\Delta t}\mathbf{u} = {}^t\mathbf{p} - \left(\mathbf{K} - \frac{2}{\Delta t^2} \mathbf{M} \right) {}^t\mathbf{u} - \left(\frac{1}{\Delta t^2} \mathbf{M} - \frac{1}{2\Delta t} \mathbf{C} \right) {}^{t-\Delta t}\mathbf{u} \quad (6.5)$$

Due to the fact that the algorithm involves ${}^{t-\Delta t}\mathbf{u}$ to determine the displacement at the sought time-step, ${}^t\mathbf{u}$, a special initiation procedure must be utilised. The initial conditions ${}^0\mathbf{u}$, ${}^0\dot{\mathbf{u}}$ and ${}^0\ddot{\mathbf{u}}$ can be derived using equation (6.1). The results from the derivations, combined with equations (6.3) and (6.4) will produce an expression for the displacement ${}^{-\Delta t}\mathbf{u}$:

$${}^{-\Delta t}u_i = {}^0u_i - \Delta t {}^0\dot{u}_i + \frac{\Delta t^2}{2} {}^0\ddot{u}_i \quad (6.6)$$

where i denotes the i :th element of the considered vector.

The central difference method is very effective since each time-step solution can be performed efficiently, i.e. a small time-step will require a larger number of time-steps to be analysed. For this reason, the method should only be applied when a lumped mass matrix can be assumed and the velocity dependent damping can be neglected.

6.1.2 Wilson's θ method

The theory supporting the formulation of the Wilson θ method is essentially the same as the Newmark method, described in Section 6.1.3, assuming a linear variation of acceleration between the time-steps. In order to obtain an unconditionally stable result θ needs to be assigned a value of 1.37 or higher.

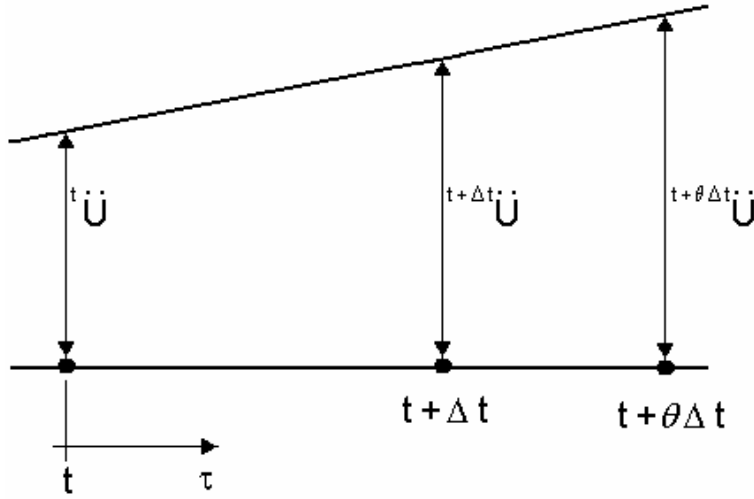


Figure 6.1 Linear acceleration assumption of the Wilson θ method.

With τ denoting the time increase, $0 \leq \tau \leq \theta\Delta t$, it is assumed that for the time interval from t to $t+\theta\Delta t$, the following variation occurs (Figure 6.1):

$${}^{t+\tau}\ddot{\mathbf{u}} = {}^t\ddot{\mathbf{u}} + \frac{\tau}{\theta\Delta t} ({}^{t+\theta\Delta t}\ddot{\mathbf{u}} - {}^t\ddot{\mathbf{u}}) \quad (6.7)$$

By integrating equation (6.7), the velocities and the displacements are obtained.

$${}^{t+\tau}\dot{\mathbf{u}} = {}^t\dot{\mathbf{u}} + {}^t\ddot{\mathbf{u}} \tau + \frac{\tau^2}{2\theta\Delta t} ({}^{t+\theta\Delta t}\ddot{\mathbf{u}} - {}^t\ddot{\mathbf{u}}) \quad (6.8)$$

$${}^{t+\tau}\mathbf{u} = {}^t\mathbf{u} + {}^t\dot{\mathbf{u}} \tau + \frac{1}{2} {}^t\ddot{\mathbf{u}} \tau^2 + \frac{1}{6\theta\Delta t} \tau^3 ({}^{t+\theta\Delta t}\ddot{\mathbf{u}} - {}^t\ddot{\mathbf{u}}) \quad (6.9)$$

By combining equations (6.8) and (6.9) the velocities and displacements at $t+\theta\Delta t$ can be expressed as:

$${}^{t+\theta\Delta t}\dot{\mathbf{u}} = {}^t\dot{\mathbf{u}} + \frac{\theta\Delta t}{2} ({}^{t+\theta\Delta t}\ddot{\mathbf{u}} - {}^t\ddot{\mathbf{u}}) \quad (6.10)$$

$${}^{t+\theta\Delta t}\mathbf{u} = {}^t\mathbf{u} + \theta\Delta t {}^t\dot{\mathbf{u}} + \frac{\theta^2\Delta t^2}{6} ({}^{t+\theta\Delta t}\ddot{\mathbf{u}} - 2{}^t\ddot{\mathbf{u}}) \quad (6.11)$$

Equations (6.10) and (6.11) can be used to express the velocities and accelerations in terms of the displacements.

$${}^{t+\theta\Delta t}\ddot{\mathbf{u}} = \frac{6}{\theta^2\Delta t^2} ({}^{t+\theta\Delta t}\mathbf{u} - {}^t\mathbf{u}) - \frac{6}{\theta\Delta t} {}^t\dot{\mathbf{u}} - 2{}^t\ddot{\mathbf{u}} \quad (6.12)$$

$${}^{t+\theta\Delta t}\dot{\mathbf{u}} = \frac{3}{\theta\Delta t} ({}^{t+\theta\Delta t}\mathbf{u} - {}^t\mathbf{u}) - 2{}^t\dot{\mathbf{u}} - \frac{\theta\Delta t}{2} {}^t\ddot{\mathbf{u}} \quad (6.13)$$

To obtain the displacements, velocities and accelerations at $t+\Delta t$ the equations of motion are used. Since the accelerations are assumed to vary linearly, a linear load vector is extrapolated.

$$\mathbf{M}^{t+\theta\Delta t}\ddot{\mathbf{u}} + \mathbf{C}^{t+\theta\Delta t}\dot{\mathbf{u}} + \mathbf{K}^{t+\theta\Delta t}\mathbf{u} = {}^{t+\theta\Delta t}\bar{\mathbf{R}} \quad (6.14)$$

where ${}^{t+\theta\Delta t}\bar{\mathbf{R}} = {}^t\mathbf{R} + \theta({}^{t+\theta\Delta t}\mathbf{R} - {}^t\mathbf{R})$

By inserting equations (6.12) and (6.13) into equation (6.14), the displacements at $t+\theta\Delta t$ can be solved. Knowing the displacements will enable equation (6.12) to solve the accelerations. By setting the evaluated time τ equal to the time-step Δt the accelerations, velocities and displacements at the sought time $t+\Delta t$ are obtained.

It should be noticed that the Wilson θ method is an implicit integration method, with the stiffness matrix \mathbf{K} acting as a coefficient matrix to the unknown displacement vector.

6.1.3 Newmark's β method

The Newmark integration scheme is an extension of the linear acceleration method and showcase obvious similarities to the Wilson θ method. The following assumptions are made:

$${}^{t+\Delta t}\dot{\mathbf{u}} = {}^t\dot{\mathbf{u}} + [(1-\gamma){}^t\ddot{\mathbf{u}} + \gamma{}^{t+\Delta t}\ddot{\mathbf{u}}]\Delta t \quad (6.15)$$

$${}^{t+\Delta t}\mathbf{u} = {}^t\mathbf{u} + {}^t\dot{\mathbf{u}}\Delta t + \left[\left(\frac{1}{2} - \beta \right) {}^t\ddot{\mathbf{u}} + \beta{}^{t+\Delta t}\ddot{\mathbf{u}} \right] \Delta t^2 \quad (6.16)$$

where β and γ are parameters that can be determined to obtain integration accuracy and stability. The Newmark method is an unconditionally stable implicit integration scheme, with an assumed accelerational variation illustrated in Figure (6.2).

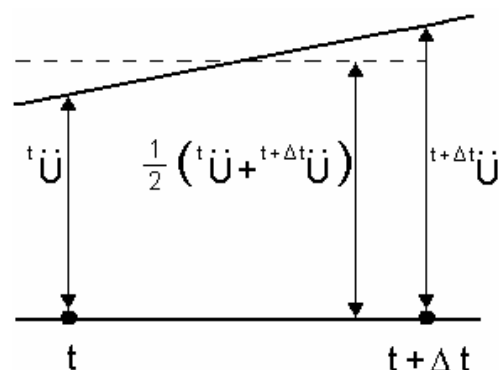


Figure 6.2 Newmark's constant-average acceleration scheme.

If the parameters β and γ is set to 0.25 and 0.5 respectively, the Newmark's method will be identical to the trapezoidal method.

6.1.4 Hilber-Hughes-Taylor method

The Hilber-Hughes-Taylor (HHT) method, Hilber, Hughes, Taylor (1977), is an implicit continuation of the Newmark β method and is widely used in structural dynamics for the numerical integration of the equations of motion presented in equation (6.1). One of the limitations with the trapezoidal formula, used in the Newmark method, is that it does not introduce any numerical damping in the solution. This makes the method impractical for problems that have high frequency oscillations that are of no interest. Thus, the major disadvantage possessed by the Newmark method is that it can not provide a formula that is stable and display a desired level of numerical damping. The HHT method is providing a stable solution and allows an introduction of numerical damping by reformulating the Newmark method. The second order ordinary differential equations introduced by the HHT method are:

$$\mathbf{M}^{t+\Delta t}\ddot{\mathbf{u}} + (1+\alpha)\mathbf{C}^{t+\Delta t}\dot{\mathbf{u}} - \alpha\mathbf{C}^t\dot{\mathbf{u}} + (1+\alpha)\mathbf{K}^{t+\Delta t}\mathbf{u} - \alpha\mathbf{K}^t\mathbf{u} = \mathbf{p}(t + \Delta t(1+\alpha)) \quad (6.17)$$

in which equations (6.15) and (6.16) are substituted into. The HHT method possesses the advertised stability if α belongs to the interval $[-1/3, 0]$ and:

$$\gamma = \frac{1-2\alpha}{2} \quad \beta = \frac{(1-\alpha)^2}{4} \quad (6.18)$$

A small value of α provides greater numerical damping. It should be noticed that the limit case where $\alpha = 0$ provides the trapezoidal method.

6.2 Mode superposition

This section will show how it is possible to express and approximate the displacements using a linear combination of a system's natural modes. The mode superposition method is commonly utilised when a reduction of large MDOF systems is needed. The approximated displacements are obtained using only a few modes to approximate the true solution. A reduced system is often pursued to minimise the usage of computer capacity and thus enabling more simulations to be performed. Due to the properties of the method it is not possible to integrate non-linear behaviour or un-coupled damping into the model.

If the coefficient matrices in the equations of motion for MDOF systems are assumed to be of the dimensions $n \times n$ with non-zero coupling terms, it requires a simultaneous solution of n equations. The analysed MDOF system will have n natural frequencies with corresponding natural modes. The natural eigenmodes for an un-damped system are obtained by solving equation (3.17). The basic procedure of mode superposition is to introduce a coordinate transformation into principle coordinates:

$$\mathbf{u}(t) = \mathbf{\Phi}\boldsymbol{\eta}(t) = \sum_{r=1}^n \phi_r \eta_r(t) \quad (6.19)$$

By substituting the displacement in equation (3.5) with equation (6.19) and multiplying the expression by Φ^T the equations of motion in principle coordinates are obtained according to equation (4.11) as:

$$\mathbf{M}\ddot{\boldsymbol{\eta}} + \mathbf{C}\dot{\boldsymbol{\eta}} + \mathbf{K}\boldsymbol{\eta} = \Phi^T \mathbf{p}(t) \quad (6.20)$$

where \mathbf{M} and \mathbf{K} are the diagonal modal mass and modal stiffness matrices, indicating that equation (6.20) only is coupled through non-zero off-diagonal coefficients in the generalised damping matrix. By applying modal damping according to Section 4.5.3 the coupled equations of motion are reduced to a set of n un-coupled modal equations.

6.2.1 Model reduction

The coordinate transformation relating the physical coordinates \mathbf{u} and the modal coordinates $\boldsymbol{\eta}$ stated in equation (6.19) includes all n modes of the system. As previously stated, this analysis is very time consuming for large finite element models and a truncation of modes is often desired. The reduced analysis will only include a fraction of the modes and will therefore provide an approximation of the original MDOF system's solution. The choice of the number of modes to include in the analysis is crucial. Factors ensuring that acceptable accuracy is provided are discussed in Section 6.2.3.

If instead a truncated form of equation (6.19) is used, a solution that completely ignores the contribution of the excluded modes is obtained:

$$\hat{\mathbf{u}}(t) = \hat{\Phi}\hat{\boldsymbol{\eta}}(t) = \sum_{r=1}^m \boldsymbol{\varphi}_r \eta_r(t) \quad (6.21)$$

where m is a constant representing the number of modes considered ($m < n$). The truncated modal matrix is given by:

$$\hat{\Phi} = [\boldsymbol{\varphi}_1, \boldsymbol{\varphi}_2, \dots, \boldsymbol{\varphi}_m] \quad (6.22)$$

This method of limiting the number of equations included is called the mode displacement method. The choice of modes is not limited to only include the lowest frequency modes but allows any selection of mode shapes considered to be of importance.

A similar method providing a more accurate solution called the mode acceleration method, can be utilised to solve systems with viscous damping. The solution is obtained by rearranging equation (6.1):

$$\mathbf{u} = \mathbf{K}^{-1} [\mathbf{p}(t) - \mathbf{C}\dot{\mathbf{u}} - \mathbf{M}\ddot{\mathbf{u}}] \quad (6.23)$$

and incorporating the coordinate transformation in equation (6.19):

$$\mathbf{u} = \mathbf{K}^{-1} [\mathbf{p}(t) - \mathbf{C}\Phi\dot{\boldsymbol{\eta}} - \mathbf{M}\Phi\ddot{\boldsymbol{\eta}}] \quad (6.24)$$

If the conditions for modal damping are satisfied by \mathbf{C} , the two right most terms in equation (6.24) can be simplified. The final mode acceleration approximation is obtained by letting the velocity and acceleration be approximated by m mode displacement approximations:

$$\tilde{\mathbf{u}}(\mathbf{t}) = \mathbf{K}^{-1}\mathbf{p}(\mathbf{t}) - \sum_{r=1}^m \frac{2\zeta_r}{\omega_r} \phi_r \dot{\eta}_r(t) - \sum_{r=1}^m \frac{1}{\omega_r^2} \phi_r \ddot{\eta}_r(t) \quad (6.25)$$

The mode displacement method may in some cases fail to provide an accurate solution. A result of this is that convergence is relatively slow due to the extensive modes needed to ensure sufficient accuracy. A solution to this problem is to extend the analysis to the mode acceleration method with superior convergence properties. The improved convergence rate is proven by studying the two right most terms of equation (6.25) where ω is present in the denominator.

A level of good engineering judgement is required when determining which modes to include in the analysis. However, it is especially important to incorporate natural modes with a frequency in the vicinity of the driving load frequency, as they will have a greater impact on the total response.

6.2.2 Error estimation

Due to the reduced number of equations of motion included in the simplified analysis and numerical errors there will be a deviation from the exact solution, obtained when all natural modes are included. Generally, the following errors are considered to have a substantial effect on the result, Dutta and Ramakrishnan (1995):

- Domain discretisation errors
- Modal truncation errors
- Numerical errors in eigenmodes and eigenvalues
- Truncation errors in numerical integration

The magnitude of the error is mainly influenced by the extent of the modal truncation made and the accuracy of the orthogonal eigenmodes used. The level of approximation made and which modes relevant for the particular model are highly case specific, but in general they depend on the size of the original model and the type of excitation acting on the structure. Generally, a linear variation of stresses and displacements are assumed within the elements, but a greater accuracy can be obtained by introducing a higher order of the interpolating polynomial at element level.

A finite element analysis is normally carried out by dividing the domain into a number of subdomains, each of which is further subdivided into elements. The division of the structure creates a mesh on which the variation of displacements and stresses are calculated. To find an optimal mesh density is therefore a key factor for a successful analysis. A too coarse mesh will generate large errors as the variation of

the stresses and displacements between the nodal points cannot be properly described. However, if the applied mesh is too dense the time needed to perform the analysis will be very extensive. An error criterion which considers the error variation as a function of time may therefore be introduced. By using an error measurement, an adaptive mesh refinement strategy enabling good control of the discretisation errors in transient dynamic analysis using modal superposition is obtained.

Since the dynamic equilibrium in the equations of motion (6.1) will not be fully satisfied an approximation of the modal truncation error can be estimated by the following equation:

$$\boldsymbol{\varepsilon}^m(\mathbf{t}) = \frac{\|\mathbf{p}(\mathbf{t}) - [\mathbf{M}\ddot{\mathbf{u}}^m(\mathbf{t}) + \mathbf{K}\mathbf{u}^m(\mathbf{t})]\|}{\|\mathbf{p}(\mathbf{t})\|} \quad (6.26)$$

where m denotes the number of included modes and \mathbf{u}^m is the predicted response using mode superposition with m modes in consideration. The error measure $\boldsymbol{\varepsilon}^m$ determines how well equilibrium, including inertia forces, can be satisfied by a linear combination of the included modes. Modal truncation errors are a serious problem for the modal superposition method that can only be studied after obtaining an optimal mesh. Using a large number of modes to control truncation errors without using an optimal mesh can lead to incorrect results due to discretisation errors.

An improper choice of time increment leads to truncation errors during the numerical integration, producing a misrepresentation of modes. Numerical integration errors of eigenmodes and eigenvalues, as well as numerical truncation errors can be avoided by a proper choice of the time-step and an effective control of tolerances.

6.2.3 Mass participation factor

A parameter often studied when trying to determine which modes to include in modal analysis is the mass participation factor. The MPF provides an indication of how large the fraction of the total mass that is active in a specific direction for a given mode is. Modes with a large MPF are assumed to have a greater influence on describing the structure's response to a dynamic load. In some commercial FE software, e.g. LUSAS, MPF is defined as:

$$MPF_{i,j} = \frac{P_i^2}{\mathbf{X}^T \mathbf{M} \mathbf{X}}; \quad P_i = \boldsymbol{\phi}_i^T \mathbf{M} \mathbf{X}; \quad j = x, y, z \quad (6.27)$$

where $\boldsymbol{\phi}_i$ is the i :th eigenvector and \mathbf{X} is a vector defining the magnitude of the rigid body response of a DOF in the model to imposed rigid body motion in each direction. The vector is generated by letting the components of \mathbf{X} , associated with translation in a specific direction, to be equal to 1 with the remaining components set to 0. Many national building codes, e.g. Uniform Building Codes (UBC), Seismological Committee of the Structural Association of California (SEAOC) and Chile Seismic Code (CHSC), require that all significant modes until the total sum of MPF is greater than 90 % are included in the analysis, López O.A., Cruz M. (1996):

$$SMPF_j = \sum_{i=1}^m MPF_{i,j} \geq 0.90; \quad j = x, y, z \quad (6.28)$$

Equation (6.28) is stating that the total translational mass of the considered modes must be greater than 90 %. A disadvantage relating the MPF to a converging result is that the contribution to the response generated by asymmetric modes is disregarded. The MPF for the asymmetric modes are infinitesimal and will thus not contribute to the SMPF. By studying the definition presented in equation (6.27), the active mass of the asymmetric modes is cancelled out by the equal deformations in positive and negative direction. Figure 6.3 illustrates an asymmetric mode of a 3-DOF system. The positive mass contribution active in the mode is approximately equal to the negative mass contribution and the MPF for the mode is thus infinitesimal.

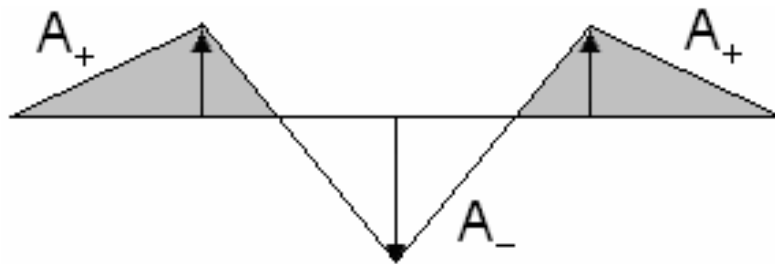


Figure 6.3 Example of asymmetric mode of a 3-DOF system.

6.2.4 Mode superposition method in commercial FE-software

6.2.4.1 LUSAS

LUSAS is using the mode superposition method in the IMDPlus module. The recommendation is to include enough modes so that the SMPF is greater than 90 %. The MPF is defined according to equation (6.27). However, a LUSAS representative admits that MPF is not always an appropriate criterion to ensure that enough modes have been included in the analysis if the asymmetric modes are contributing to an increased acceleration of the structure. In these situations a convergence study based on the number of modes analysed is advised.

6.2.4.2 TDV

The Austrian software developer TDV is using the mode superposition method for earthquake analysis, advanced wind buffeting and analysis of forced vibrations. However, in case of dynamic analysis of railway bridges they rely on direct time integration. TDV's opinion is that mode superposition is not suitable for train passage problems due to the different load effects on the superstructure depending on the position of the loads. The benefits of applying time integration is increased quality of the results and the possibility to solve non-linear problems. To reduce the increased amount of computer capacity required, numerous matrix reduction methods are utilised for faster data processing.

6.2.4.3 Scanscot Technology

Swedish software developer Scanscot Technology is offering the mode superposition method in the Brigade Plus module. The general advice is to consider all modes so that 90 % of the total mass is excited. The participation factor of the α :th mode is defined as:

$$\Gamma_{\alpha i} = \frac{1}{m_{\alpha}} \boldsymbol{\varphi}_{\alpha}^T \mathbf{M} \mathbf{T}_i \quad (6.29)$$

where \mathbf{T}_i defines the magnitude of the rigid body response of a degree-of-freedom in the model to imposed rigid body motion in the i -direction.

6.2.4.4 ADINA

ADINA is an American software, initially developed by Klaus-Jürgen Bathe. Their recommendation is to only apply the mode superposition method when very long time histories, or special demands on the damping, are present. If the use of proportional or Rayleigh damping is desired it is a necessity to utilise mode superposition. ADINA is using the Lanczos method to solve the eigenvalue problem. MPF is available in the software, but is not suggested as a convergence criterion. ADINA recommends that a Fourier analysis of the loading is performed and modes with a natural frequency up to three times the dominating frequencies are included in the modal analysis.

6.2.4.5 Risa Technologies

Risa's FEM software is currently not capable of performing transient analysis or time history analysis.

6.2.4.6 GTS Cadbuild

GTS Cadbuild is offering STRAP to perform dynamic analyses. The mode superposition method is utilised in the DYNAM2 module, while time history analysis is used in the DYNAM3 module. DYNAM2 is advised to use for seismic loading while DYNAM3 is applicable to any generalised dynamic loading, e.g. train loading.

STRAP is using a mathematical procedure called missing mass correlation (MMC) to include a correction mode, representing the contribution of higher order mode shapes and thus providing greater accuracy with reduced calculation time. The program solves a set of equations for the missing mass mode shape such that its modal mass will be equal to the difference between the structures total mass and the sum of the mass included in known mode shapes. This provides a unique solution called the missing mass mode shape which represents an approximation of all modes that were not computed.

6.2.4.7 TNO Diana

TNO Diana's software MIDAS is able to perform a dynamic analysis by applying either the mode superposition method or a transient direct integration algorithm. Representatives from TNO Diana are claiming that their software is so memory efficient that an exact direct integration is preferred for dynamic analyses. If a longer time history is desired the modal superposition method may be applied. The MPF is defined as "The fraction of the mass that is active for a given mode with a given distribution of dynamic loads". However, TNO Diana insists that, due to their memory management, more modes can be included while keeping the duration of the analysis relatively short. The use of MPF as cut-off criterion is therefore excessive since the large amount of modes included always ensures that most of the mass can be excited.

7 The finite element method and LUSAS

The finite element method is a numerical methodology to approximately solve general differential equations, which often are too cumbersome to solve in a classical analytical fashion. This is an important method since basically all physical phenomena encountered in structural engineering are described by differential equations.

A characteristic feature of the FEM is that the analysed structure is divided into smaller parts, i.e. elements, for which a relatively simple approximation is implemented. So, instead of seeking approximations that holds directly for the entire structure the approximations are carried out over each element. The collection of all elements is called a mesh, the mesh size is arbitrary but it can, as described in section 6.2.2, effect the accuracy of the final results.

The approximations for each element are in fact an interpolation over the element, requiring known variables at certain points in the element, nodal points. The nodal points are often located at the boundaries of each element and consist of a number of degrees-of-freedom, which states the way in which the nodes are free to displace.

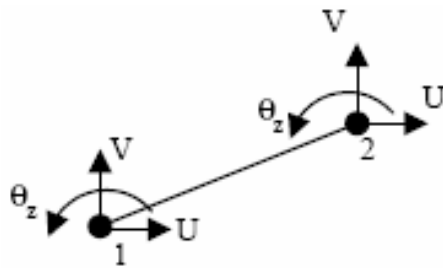


Figure 7.1 Beam element with denoted nodal degrees-of-freedom.

The next step is to determine the corresponding behaviour of each element and then merge them together to form the whole structure.

While studying the results produced by the finite element analysis it is important to remember that the output data is only an approximation reflecting the predetermined geometry and boundary conditions. To determine the quality of the results obtained a convergence study and a certain level of engineering judgement are required.

7.1 Modelling procedures in LUSAS

The finite element software LUSAS was used to perform the dynamic analyses in this project. This section describes how the modelling procedures are performed for both static and dynamic analysis.

7.1.1 Elements

The LUSAS element library contains several different element types, classified into groups according to their function. The available element groups in LUSAS are; bar elements, beam elements, continuum elements (2-D and 3-D), plate elements, shell elements, membrane elements, joint elements, field elements and interface elements. This section is providing a brief description of the element types important for bridge modelling. A more detailed element description can be studied in the LUSAS Theory Manual and in the LUSAS Element Reference Manual.

7.1.1.1 Beam elements

There are numerous types of beam elements available in the beam section of the LUSAS element library. The beam elements are commonly used to model plane and space frame structures, both in 2-D and 3-D. In addition to the standard thin and thick beam elements, LUSAS offers specialised elements for modelling of grillage and eccentrically ribbed plate structures. The beam elements are able to transfer axial, bending and torsional forces. The beam elements can be modelled as either straight or curved. The force variation along the beam is assumed to be constant for axial and torsional forces, linear for shear forces and quadratic for moments. The corresponding displacements will thus vary linearly for axial and rotational displacements while the transverse displacement varies cubically. The formulation of the beam elements are based on a 3-D thick beam element which can conveniently be used to model 3-D frame structures or stiffeners. The geometrical properties are assumed to be constant along the length of the beam, preventing the strains to be obtained within the element. Beam elements are not able to described non-linear behaviour, but can if combined with other elements be included in a non-linear analysis. The beam elements are advantageous while performing linear, eigenvalue or dynamic analyses.

7.1.1.2 Shell elements

Shell elements can be used to model 3-D structures, capturing both flexural and membrane effects. The element can either be thick or thin, flat or curved, with a triangular or quadrilateral shape, illustrated in Figure (7.2). The elements, on which the formulation is based on, are 3-D thick shell elements that can be used to analyse flat and curved 3-D shell structures. Shell elements are especially good to describe structures where transverse shear deformations have a considerable influence on the response. The elements may be used for modelling intersecting shells or branched shell junctions as well as stiffened shell structures, where shells are connected to beam elements.

The elements can be equipped with an arbitrary thickness and composite non-linear material properties. A common shell element is often modelled with two rotational degrees-of-freedom and a common nodal normal degree-of-freedom associated with each node. However, if higher flexibility is desired additional rotational degrees-of-freedom may be incorporated.

The element formulation relies on an isoparametric approach with consideration to membrane, shear and flexural deformations. Quadrilateral shell elements assume a strain field to define transverse shear and provides a good representation of bending deformations. Thick shell elements offer a consistent formulation of the tangent stiffness, enabling the elements to be effective in geometrically non-linear application.

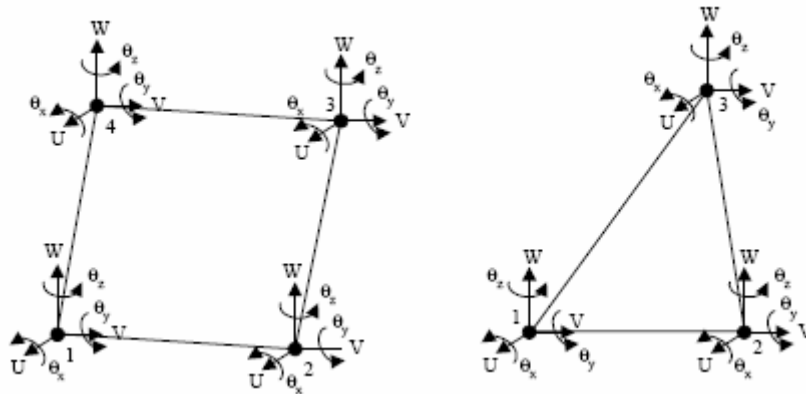


Figure 7.2 Quadrilateral and triangular shell elements with denoted degrees-of-freedom.

7.1.1.3 Joint elements

Joint elements may be used to connect nodes of different element with elastic springs. The springs can be given any desired configuration concerning translational and rotational stiffness. The joint elements will, via an interface mesh, connect nodes of different elements. An initial gap between the nodes is allowed, but to maximise the efficiency of the joint element and capture the time variation the gap should be minimised.

The stiffness matrix corresponding to the joint element does not rely on engineering beam theory, implying that joint elements are independent of both shear forces and joint length. Even though the joint elements remain geometrically linear, they are able to be included in non-linear analyses due to assumed infinitesimal strains and the neglecting large deformations effects.

Joint elements are valid for both 2-D and 3-D modelling. The connection is represented by a line joint in 2-D while modelling in 3-D requires a surface joint mesh to be generated. There are two methods of applying the surface joint mesh, either by a single joint where the joint mesh is assigned to a single line or by connecting the elements with multiple nodes by means of a joint mesh interface. The method using a single line is more suitable when only a few joints are desired due to the required definition of each joint.

The joint mesh interface utilise a master and slave connection to tie the desired lines or surfaces together. The joint properties are applied by assigning them to the selected master feature, describing the behaviour of the joint. To create a joint with rotational degrees-of-freedom, the geometric properties of the joint are required to be assigned

due to the eccentricity present. Additionally, the joint mesh requires that material properties are defined.

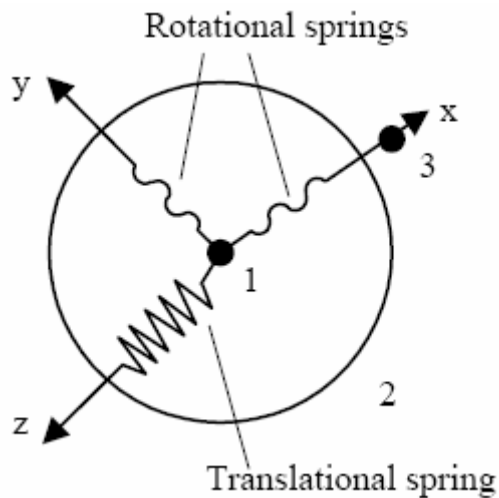


Figure 7.3 Joint three-dimensional element for plate bending elements. The joint element consists of rotational springs in x- and y-direction and a translational spring in z-direction.

7.1.1.4 Slidelines

Slidelines are attributes that may be utilised to model contact or impact problems, or to tie dissimilar meshes together. Slidelines are a useful alternative to joint elements and are advantageous when there is no prior knowledge of the contact point. The user is allowed to define the important properties of the slidelines, such as stiffness scale factor, friction coefficient and pre-contact behaviour. When applying slidelines between multiple features of the model, one feature is assigned master while the others are assigned slave. To increase the convergence rate and reduce the solution time, the general advice is to set the feature with the greater stiffness as master.

There are several different types of slidelines:

- Null – Utilised to perform linear analysis while ignoring the slide definition.
- No friction – Used for contact analyses with ignored friction between the surfaces.
- Friction – Used for constant or intermittent contact and impact problems.
- Tied – Used to tie dissimilar meshes together.
- Sliding – Used for problem where surfaces are kept in contact, allowing sliding without friction.

The tied slideline option eliminates the requirement of a transition zone in the mesh discretisation. This feature is extremely useful while creating localised meshes in regions of high stress gradients.

7.1.2 Damping

LUSAS enables the application of both viscous damping and structural modal damping ratios when defining the bridge structure's total damping. A combination of the two types of damping is also allowed. However, structural damping cannot be used in modal response analysis in the time domain. The damping ratio, expressed with a percentage of the critical damping, can either be user specified or automatically calculated by the software. The provided estimation of the modal damping is only available if relevant damping data is included in the eigenvalue analysis. Any arbitrary damping ratio can be individually assigned to each mode. However, a maximum damping ratio of 10 % is commonly regarded for bridge structures in order to efficiently use the modal superposition method and to avoid coupling between modes. For dynamic analysis of structures with a damping greater than the prescribed maximum ratio a direct step-by-step integration is suggested.

7.1.3 Loads

The external loads acting on the model are in LUSAS represented by loading datasets. With the exception of discrete loads all loads available in LUSAS are feature based. Feature based loads are assigned to a specific instance of the model geometry and is thus only effective on the selected areas. The loads can either be assigned to act in local or global element directions. The magnitude of the load will by default be defined as constant for all the nodes in the feature, unless a variation is specified. Variations can be applied to all feature type loads except for beam distributed loads, where a variation is present in the definition. The feature based loads includes:

- Structural loads, e.g. body force, distributed, face, concentrated, temperature, stress/strain and beam loads.
- Prescribed loads, used to specify initial conditions on displacement, velocity or acceleration of a specific node.
- Thermal loads, used to describe temperature or heat input to a thermal analysis.

The discrete, or general, loads are assigned to points in the finite element model. The points do not have to belong to the surface on which it is applied, as the patch is projected onto the surface in a normal direction to the patch definition. The main difference between discrete and structural loads is that the discrete loads are not limited to application on the structure and are thus independent of the model geometry. The two types of general loads available are:

- Patch Load, where in general 2 or 3 points are used to define a straight or curved continuous line load in space. It is also possible to express the geometry of a straight sided or curved patch by increasing the number of selected points.
- Point Load, assigned to a single or general set of discrete points. Each individual point can have separate load values.

For a more detailed description of the loads and their applicability, the LUSAS Modeller User Manual can be referred.

7.2 Dynamic analysis

When the loading cannot be considered instantaneous or where inertia and damping forces are significant a dynamic analysis is required. Generally, the dynamic solution is obtained by performing numerical step-by-step integration in the time domain. A variation of the displacements and the velocities are assumed as the solution progresses with each time increment. The simultaneously solved set of equations within each time-step represents the response at discrete time instances when dynamic equilibrium is fulfilled. When the initial conditions are known, successive application of the procedure produces the dynamic response of the structure.

7.2.1 Direct integration

There are several different methods able to solve the dynamic equilibrium equations by using direct integration. The algorithms are further described in Section 6.1. The choice of which integration scheme to apply onto a specific model is highly dependent on the complexity of the structure and the type of analysis required.

An explicit integration scheme will only generate a stable result if the time-step is shorter than the critical length. Explicit algorithms permit de-coupling of the equilibrium equations which implies that an inversion of the stiffness matrix is not needed. This characteristic makes the explicit algorithms more suited for analyses which require small time-steps, irrespective of the stability requirements. When an explicit direct integration is desired, LUSAS applies the central difference integration scheme, described in Section 6.1.1. The central difference method is particularly effective when a uniform discretisation of lower order elements is used.

The implicit algorithms are unconditionally stable allowing the time-step to increase with a retained convergence. The total number of time instances where equilibrium is calculated can therefore be reduced. The computational effort at each time-step is more extensive due to the required inversion of the stiffness matrix. Generally, an implicit integration is preferred for inertial problems where the total response is governed by relatively low frequencies. The main reason for this is that the time-step is commonly set to be greater than the critical length preventing optimal accuracy for the higher modes. The higher modes have less influence on the total response implying that the total accuracy is condensed. The Hilber-Hughes-Taylor implicit integration scheme, described in Section 6.1.4, is the default implicit algorithm of LUSAS.

7.2.2 Eigenvalue analysis

If solving the dynamic problem by means of modal analysis, the extraction of natural frequencies and natural modes are required. The natural frequencies and eigenmodes are determined by an eigenvalue analysis. To solve a moving load problem in LUSAS the first step is to provide the eigenvalues as input data to the dynamic analysis. This procedure is also needed for other dynamic applications, e.g. when determining the

buckling load which estimates the maximum load that can be supported prior to structural instability.

There are different methods available in LUSAS to extract the eigenvalues and eigenvectors from large systems of equations. The algorithms of the methods have several common features. The algorithms initially determine which degrees-of-freedom that will provide the greatest contribution to the structural response. Thereafter, a transformation matrix and a reduced set of equations are assembled. Finally, the eigenvalues and eigenvectors of the reduced system are extracted and are thereafter transformed to represent the complete system.

The solution is completed by calculating error estimations of the precision provided by the eigenvalues and corresponding eigenvectors. A normalisation of the eigenvectors is recommended in order to decrease the duration of the dynamic analysis.

7.2.2.1 Subspace iteration

The subspace iteration procedure is utilised to solve eigenvalue problems of the form:

$$\mathbf{K}\Phi = \Lambda\mathbf{M}\Phi \quad (7.1)$$

where Λ is a diagonal matrix containing the eigenvalues λ_i and Φ contains the corresponding eigenvectors, ϕ_i .

To efficiently obtain the lowest m eigenvalues and corresponding eigenvectors a simultaneous inverse iteration, utilising a set of iterative vectors followed by a subspace projection of the problem matrices, is performed. This procedure generates a reduced eigenvalue problem that is solved using Jacobi iteration. A transformation of the eigenvectors corresponding to the reduced problem is thereafter performed to obtain the full space iteration vectors. This process is repeated until convergence of the lowest m eigenvectors of the full problem is obtained. The procedure can be divided into three principle steps:

1. Establish initial iteration vectors.
2. Extract the optimal eigenvalue and eigenvector approximations by using simultaneous inverse iteration and Ritz analysis.
3. Verify the generated eigenvalues and eigenvectors by utilising the Sturm sequence.

The main advantage of the subspace iteration method is that the iterative vector is improved with each update of the subspace, making the method very stable. Consequently, the method will converge even with a bad selection of master degrees-of-freedom but will require more iteration. The subspace iteration is considered to be the most effective iteration algorithm available.

7.2.2.2 Guyan reduction

When searching a finite element approximation a condensation of the full discrete model to a reduced system is often utilised. A structure subjected to low frequency natural vibrations, often has degrees-of-freedom whose contribution is of a higher significance to the oscillatory structural behaviour. This characteristic allows a significant reduction of the total problem. Such a reduction procedure is often called Guyan reduction or Guyan condensation.

To obtain acceptable accuracy of the Guyan reduction the selection of the significant degrees-of-freedom, denoted master freedoms, is central. In typical Guyan reduced eigenvalue extraction the mass contribution of the degrees-of-freedom whose inertia effect are relatively insignificant to the structural response, denoted slave freedoms, is therefore condensed from the system. It is assumed for the lower frequencies that the inertia forces of the slave degrees-of-freedom are insignificant when compared to the elastic forces transmitted by the master degrees-of-freedom.

The remaining $m \times m$ condensed system is solved by using implicit QL or Jacobian iteration for the master degrees-of-freedom.

7.2.2.3 Inverse iteration with shift

To determine eigenvalues and corresponding eigenvectors within a specific frequency range of interest, it can be useful to employ inverse iteration with shift. The method is especially effective to produce convergence of an eigenvalue other than the fundamental. By letting the shift μ be in the vicinity of the frequency of interest the eigenvalue problem can be modified to locate the eigenvalue closest to the value of the shift:

$$\left[(\mathbf{K} - \mu\mathbf{M}) - (\lambda_i - \mu)\mathbf{M} \right] \boldsymbol{\varphi}_i = \mathbf{0} \quad (7.2)$$

Inverse iteration with spectrum shift is a commonly used procedure to find eigenvectors after the eigenvalues have been determined using a different method. The method can also be utilised to avoid problems associated with the singularity of \mathbf{K} for a system with rigid body modes.

7.2.2.4 Lanczos method

In contrary to the vector iterative methods, i.e. the subspace iteration method and the inverse iteration method, the Lanczos method is considered as a transformation algorithm. The algorithm transforms a given real and symmetric matrix into a tridiagonal matrix. The transformation to the tridiagonal form is achieved by a recurrence relation generating an orthogonal basis for certain Krylov subspaces. Though the method is practical from a mathematical perspective, the recurrence relation is numerically unstable. Still, the Lanczos method has several desirable features making it well suited for treating large sparse matrix eigenvalue problems. The Lanczos method is considered to be one of the fastest and most robust methods.

7.2.3 Modal analysis

There are two types of modal analyses available in LUSAS to solve a linear system of equations, spectral response analysis suitable during e.g. earthquake analysis and harmonic response analysis which is preferred for arbitrary periodic loading. Modal analysis techniques reduce the number of unknowns to represent the global behaviour of a structure rather than solving a full set of n unknown displacement. The results from a modal analysis are highly dependent of the type of problem analysed. The efficiency rate is greatly improved when the problem is dominated by global displacement rather than local displacement.

7.3 Moving load analysis

The module, integrated in LUSAS, able to perform a dynamic analysis of the structural response caused by a moving load is called IMDPlus. The module provides the linear dynamic response of the structure subjected to a passing train load. Prior to the dynamic analysis an eigenvalue analysis is required, as the eigenvalues and eigenvectors are required as input parameters to IMDPlus. To obtain correct results, the eigenvalue analysis must be performed using mass normalised eigenvectors.

The moving load analysis requires that the magnitude and configuration of the load remains constant throughout the analysis to provide the response of the structure. The load is applied to each individual mode separately and the frequency dependent response of the structure is obtained by summarising each modes contribution using superposition techniques. The summation of the modes is made possible due to the assumption of linear structural behaviour.

There are two methods to define the path and the magnitude of a moving load travelling along the structure. The load configuration can either be defined explicit with a discrete load definition in the modeller, or by a composite axle where a single unit axle is defined as a discrete load in the modeller and the axle configuration defined separately. The explicit definition is preferred when only a single passage of a load configuration occurs.

When for example multiple train rolling stock configurations passing a bridge structure is to be analysed the composite axle definition is preferred. The method enables a more rapid analysis where the initial steps do not have to be repeated to obtain the solution. The composite axle definition allows complex loading configurations from a single axle with different spacing and magnitudes to be analysed. The moving load analysis requires that the equivalent modal forces for the moving load path are determined prior to the analysis.

7.3.1 IMDPlus assumptions

The assumptions for the IMDPlus modal dynamics facility are:

- The system is linear in terms of geometry, material properties and boundary conditions.
- No cross-coupling of modes due to the damping matrix is assumed. This assumption is reasonable for most structures with the exception of highly damped structures or applications.
- The lowest modes dominate the response.
- Damping ratios are required to be less than the critical damping due to the solution of the time domain response using Duhamel's integral.

7.3.2 Definition of required input

A moving load generator is used to automatically calculate the structural response of a selected number of static load cases at prescribed locations along a load path, represented by a continuous line or arc. The load cases can thereafter be imported into IMDPlus where modal forces, equivalent to the applied loading are determined.

The load path has to be selected prior to entering the moving load generator and a discrete load representing the load configuration, moving across the structure must be defined. There are different requirements for the discrete load depending on what the input of the moving load used in IMDPlus is. If the entire load configuration is represented by the discrete load, the load is required to contain all the loading associated with the configuration. However, if a composite axle definition is desired the discrete load should represent a subset of the total load configuration. The discrete load will accompany a composite axle definition file to complete the configuration imported into IMDPlus.

If the load path is defined above several planes of the model on which the discrete load could be applied, a definition of search area is required. The search area will determine on which of the planes the static load will act while calculating the desired load cases. The static load cases will be calculated incrementally, separated by a distance sufficiently small to provide an accurate movement of the load.

The discrete loads are required to be converted into equivalent modal forces before they are imported into the module. A modal force calculator is utilised to perform the required conversion from eigenvalues and static load cases into modal forces.

7.3.3 Running moving load analysis

Following the calculation of the modal forces, the moving load analysis can be performed. The analysis uses the modal force history file and the composite axle definition as input parameters. LUSAS enables the number of modes included in the analysis to be restricted to a defined interval, or by a specified subset. The default setting is to include all modes in the analysis. When deselecting modes the total mass

participation factor decreases. LUSAS advice is that the total mass participation factor should exceed 90 % in any given direction to guarantee sufficient accuracy.

The damping ratio of the modes can be defined by selecting a default value applying to all modes using the damping control feature. By applying viscous damping in the eigenvalue analysis it is also possible to ignore or limit the influence of overdamped modes by assigning mode specific damping ratios.

Before the input data is submitted for analysis the speed and time-stepping information are defined. The speed input consists of a range in which the speed varies and a speed increment length. If the aim of the analysis is to study the decay of the structural vibration a quiet time can be added after the passage of the load. The length of the time-step can either be defined by the user or calculated by the Nyquist time-step, which is dependent of the maximum frequency included in the analysis.

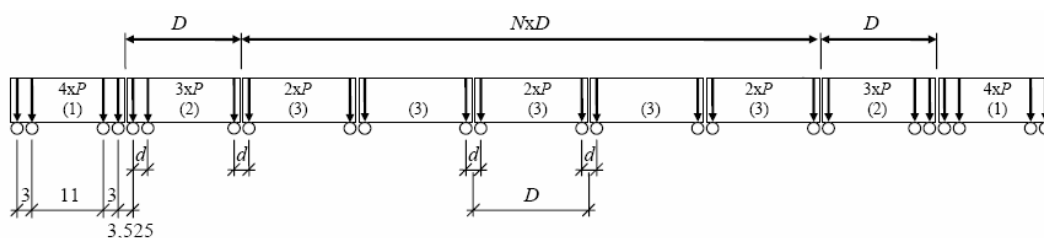
8 Code requirements in BV BRO

The design procedure for any type of structure is regulated by national and international building codes. The building codes describe both limit values and design procedures required to consider. The codes are provided to ensure that quality and safety requirements are obtained. The Swedish railway bridge code, regulating the dynamic analyses of railway bridges, BV BRO is almost identical to the European standard code Eurocode. The content of BV BRO will therefore be the only code presented in this chapter.

The Swedish railway bridge code, BV BRO, is issued by the Swedish Rail Administration. The code requires that dynamic analyses of bridges with train velocities exceeding 200 km/h are performed at the design stage. The considered interval of velocities should range from 100 km/h to 120 % of the theoretical maximum velocity expected on the bridge.

8.1 High-speed load models

The code provides different load models that should be applied when performing the dynamic control. The high-speed load models HSLM-A and HSLM-B are representing the loads generated by the wheel axels of the train in contact with the rail. The most commonly used load model is HSLM-A which contains 10 load cases representing theoretical idealisations of real trains. All load cases are required to be controlled in order to determine the maximum structural response.



- (1) Power car (leading and trailing cars identical)
- (2) End coach (leading and trailing and coaches identical)
- (3) Intermediate coach

Figure 8.1 Load distribution of train model HSLM-A.

Table 8.1 Load model for HSLM-A.

Train model	Number of intermediate coaches N	Coach length D [m]	Bogie axle spacing d [m]	Point force P [kN]
A1	18	18	2.0	170
A2	17	19	3.5	200
A3	16	20	2.0	180
A4	15	21	3.0	190
A5	14	22	2.0	170
A6	13	23	2.0	180
A7	13	24	2.0	190
A8	12	25	2.5	190
A9	11	26	2.0	210
A10	11	27	2.0	210

The load model HSLM-B should only be applied on simple bridge structures, i.e. simply supported beam or slab bridges, with one span less than 7 m. HSLM-B consists of N point loads with a magnitude of 170 kN evenly spaced by the distance d according to Figure 8.2.

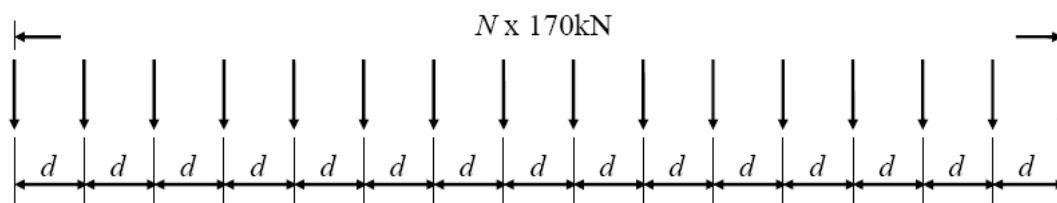


Figure 8.2 Load distribution of train model HSLM-B.

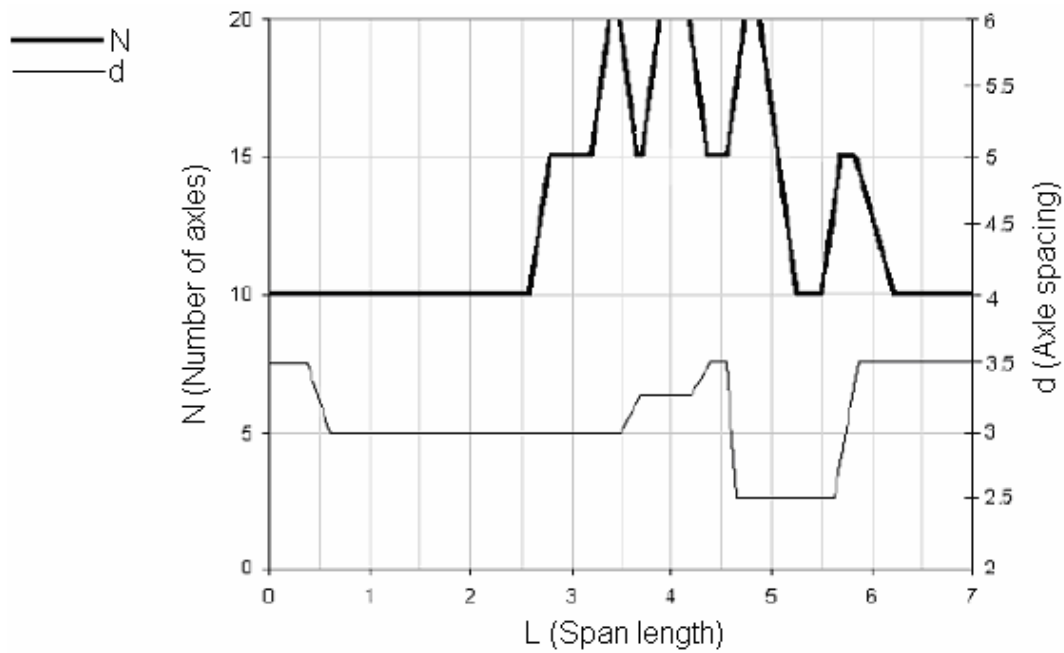


Figure 8.3 The spacing and number of loads for HSLM-B.

8.2 Damping

When dynamic analysis of a bridge structure is performed, a damping factor needs to be calculated. Appropriate values of the damping factors are suggested in Table 8.2, which should be applied unless more accurate values can describe the structural damping.

Table 8.2 Values of damping to be assumed for design purposes.

Bridge type	ξ Lower limit of damping [%]	
	Span $L < 20\text{m}$	Span $L \geq 20\text{m}$
Steel and composite	$\xi = 0,5 + 0,125(20-L)$	$\xi = 0,5$
Prestressed concrete	$\xi = 1,0 + 0,07(20-L)$	$\xi = 1,0$
Reinforced concrete	$\xi = 1,5 + 0,07(20-L)$	$\xi = 1,5$

8.3 Speed increment

The speed increment in the analysed velocity range cannot be greater than 5 km/h between each analysed velocity. If resonant effects are expected in the vicinity of a

specific velocity, the speed increments of the adjacent speed steps cannot exceed 2.5 km/h to ensure that the critical response is captured.

8.4 Vertical accelerations

To ensure the safety and comfort of the passengers travelling with trains passing the bridge, a maximum magnitude of the vertical acceleration is stated. If the track is placed on ballast, the maximum acceleration cannot exceed 3.5 m/s^2 within the ballast area. The maximum acceleration allowed for slabtrack or bridges with its track placed directly on top of the bridge deck is set to 5.0 m/s^2 . The vertical accelerations should at least be analysed for modes with natural frequencies up to 30 Hz.

8.5 Choice of model

The model should be created to reflect the structure's behaviour during the passage of a high-speed train. The soil conditions are, for most bridges, not required to be included in the model. The soil can therefore be considered as un-deformable.

9 The Norra Kungsvägen bridge

9.1 Bridge description

The Norra Kungsvägen bridge is situated 60 km south of Umeå, Sweden. The construction of the bridge was completed in August 2007 and is an essential element of the Bothnia line, which will span from Ångermanälven to Umeå. Figure 9.1 illustrates the elevation of the bridge.

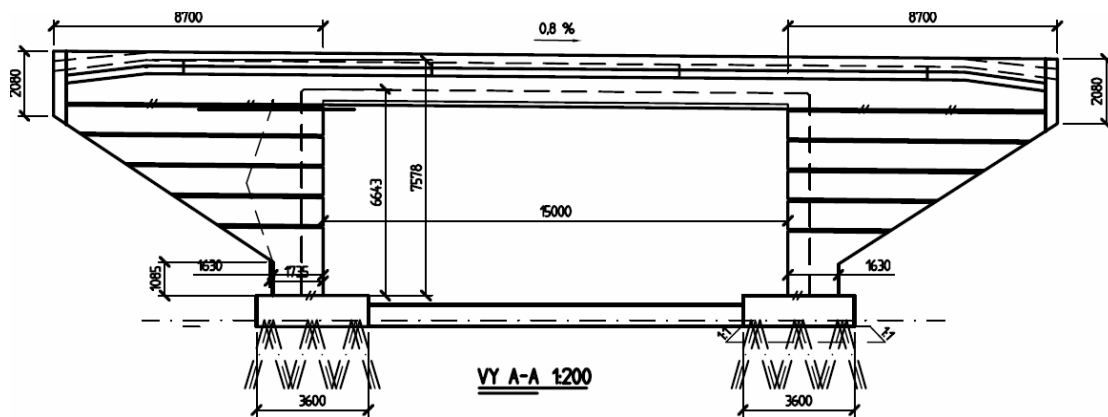


Figure 9.1 Elevation of the Norra Kungsvägen bridge, 1:200.

By studying Figure 9.2, illustrating the plan of the bridge, it should be noticed that the bridge is oriented perpendicular to the longitudinal direction of the bridge.

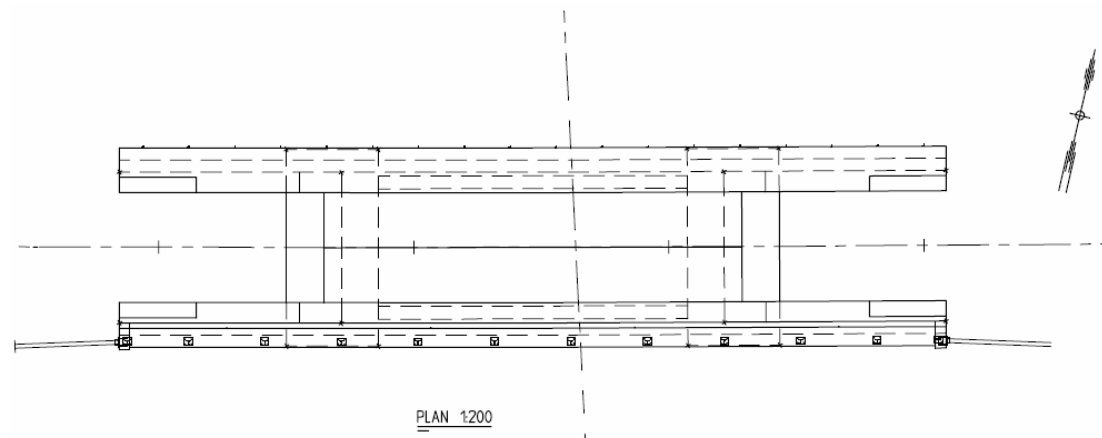


Figure 9.2 Plan of the Norra Kungsvägen bridge, 1:200.

The Swedish consultant company ELU Konsult was contracted to design the bridge structure. The bridge's structural system consists of a reinforced concrete frame with a trough constituting of a slab and two edge beams. The bridge is required to withstand the loads caused by high-speed trains according to BV BRO's guidelines. The use of dynamic amplification factors was therefore not sufficient to determine the dynamic effects and a detailed dynamic analysis was required.

9.2 Previous analyses

The dynamic analysis was performed using the finite element software LUSAS. To enable a reduction of the computational effort consumed by the dynamic analysis the mode superposition method was applied. This feature is available in the LUSAS application IMDPlus. To determine the required number of eigenmodes included in the analysis the SMPF, described in Section 6.2.3, was used as a cut-off criterion. LUSAS encourage its clients to include all significant modes so that $SMPF > 90 \%$, to ensure acceptable accuracy of the results.

The eigenvalue analysis produced the following results, with corresponding MPF and accumulated SMPF, for frequencies within the interval 0-35 Hz:

Table 9.1 Results from eigenvalue analysis of the Norra Kungsvägen bridge.

Mode	Eigenfrequency [Hz]	MPF [-]	SMPF [-]
1	1.49118	0.112681E-06	0.112681E-06
2	1.88860	0.170320E-10	0.112698E-06
3	1.90369	0.599213E-10	0.112758E-06
4	4.67282	0.526882E-10	0.112810E-06
5	5.12425	0.242511E-04	0.243639E-04
6	5.59383	0.117250E-07	0.243756E-04
7	6.62900	0.380217E-01	0.380461E-01
8	7.03100	0.248871E-08	0.380461E-01
9	7.89094	0.651799E-04	0.381112E-01
10	8.72788	0.557924	0.596036
11	10.8917	0.266391	0.862426
12	11.1584	0.171011E-04	0.862443
13	12.5246	0.937943E-08	0.862443
14	13.1837	0.513373E-05	0.862448
15	16.3357	0.133091	0.995539
16	20.6331	0.317391E-03	0.995857
17	22.2921	0.845095E-08	0.995857
18	23.1194	0.179468E-03	0.996036
19	23.2370	0.806814E-06	0.996037

20	23.3240	0.113182E-04	0.996048
21	25.3131	0.467518E-08	0.996048
22	25.6966	0.200645E-07	0.996048
23	26.3531	0.735210E-07	0.996049
24	28.0076	0.258756E-04	0.996074
25	29.1470	0.119101E-06	0.996074
26	29.4116	0.102497E-05	0.996076
27	29.8438	0.945006E-10	0.996076
28	32.9046	0.667766E-05	0.996082
29	32.9458	0.250655E-02	0.998589
30	34.1755	0.120306E-03	0.998709

Table 9.1 indicates that, in accordance with the criterion stated in equation (6.28), only the first 15 modes are needed to fulfil the requirement concerning SMPF. The maximum acceleration occurred at the quarter point ($X = 4.71$ m) of the bridge according to Figure 9.3.

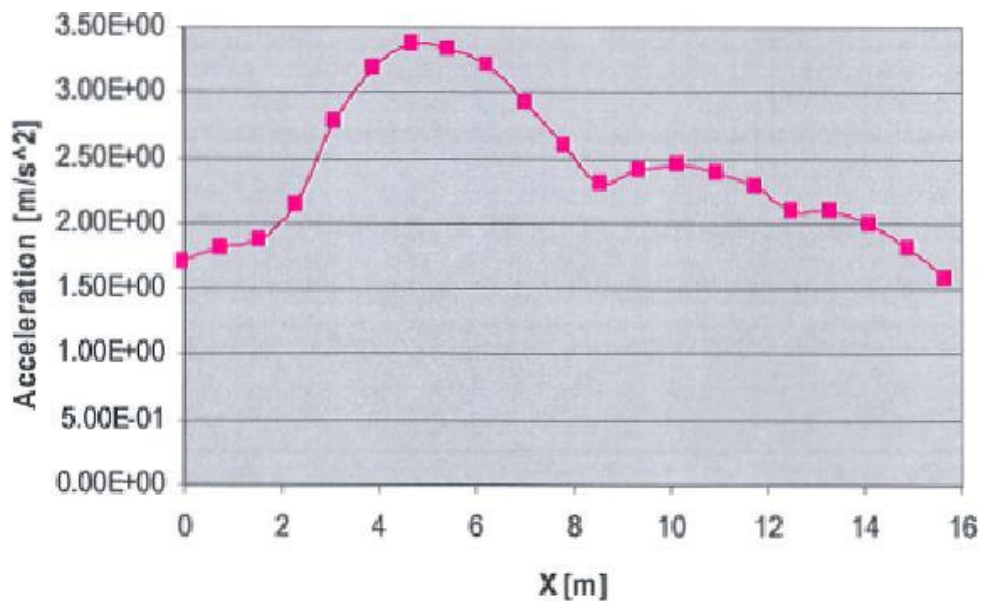


Figure 9.3 Maximal vertical acceleration of the bridge deck's middle section.

Figure 9.4 indicates that resonance appears at a speed of 79 m/s, or 285 km/h. The first dynamic analysis performed, included modes with corresponding eigenfrequencies belonging to the interval 0-30 Hz which generated a SMPF of 99.6 %, according to Table 9.1. In the second dynamic analysis only the 15 lowest eigenmodes were included, with a corresponding SMPF of 99.5 %. The 15 lowest modes' contribution to the SMPF is well above the suggested criterion. However, Figure 9.4 clearly indicates large deviations between the maximum vertical

accelerations calculated. This would indicate that MPF is not a reliable convergence criterion when determining the appropriate cut-off frequency. In a third analysis mode 16 and the asymmetric modes 21 and 25 were included, and the maximum peak accelerations were captured. The analyses are indicating that asymmetric modes indeed have an influence on the accelerational response of a structure. Table 9.1 shows that the additional modes do not have any significant contribution of the MPF. This would also indicate that MPF is not a sufficient parameter to study when determining a cut-off frequency.

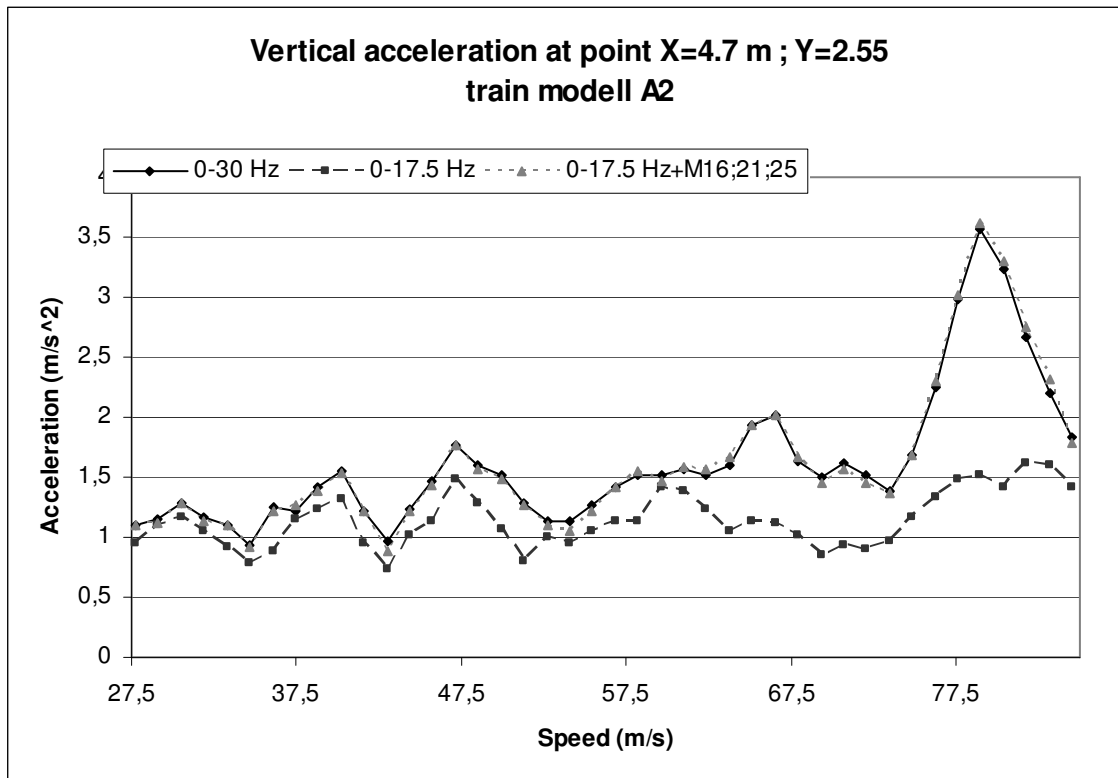


Figure 9.4 Vertical accelerational response for different cut-off frequencies.

The appearances of the critical eigenmodes are illustrated in Figure 9.5, 9.6 and 9.7.

Eigenvalue Analysis
Eigenvector: 16
Natural Frequency: 20.63

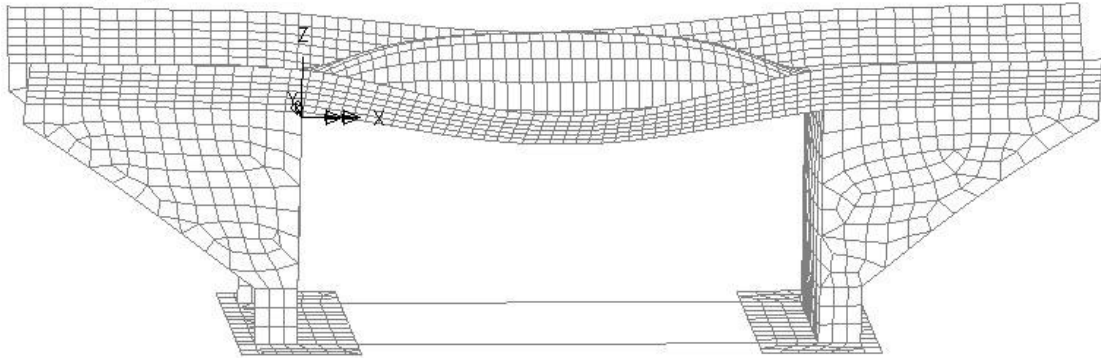


Figure 9.5 Eigenmode 16 with the natural frequency 20.63 Hz.

Eigenvalue Analysis
Eigenvector: 21
Natural Frequency: 25.31

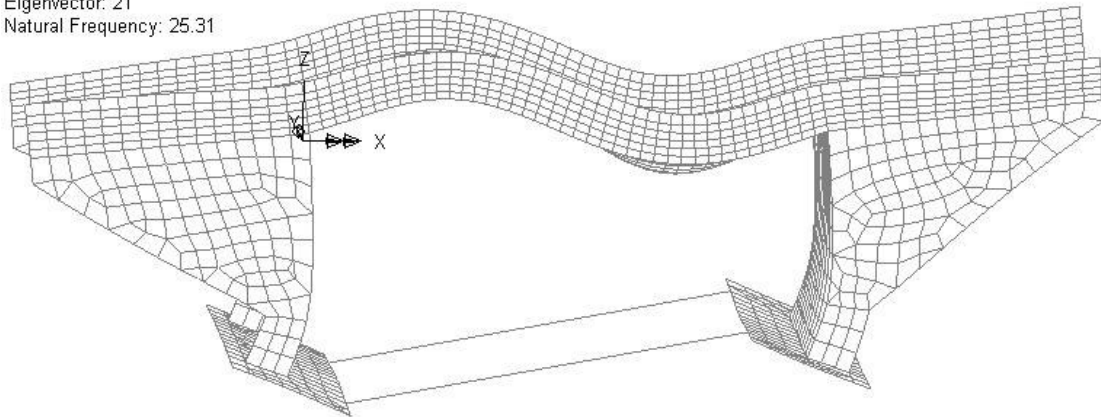


Figure 9.6 Eigenmode 21 with the natural frequency 25.31 Hz.

Eigenvalue Analysis
Eigenvector: 25
Natural Frequency: 29.15

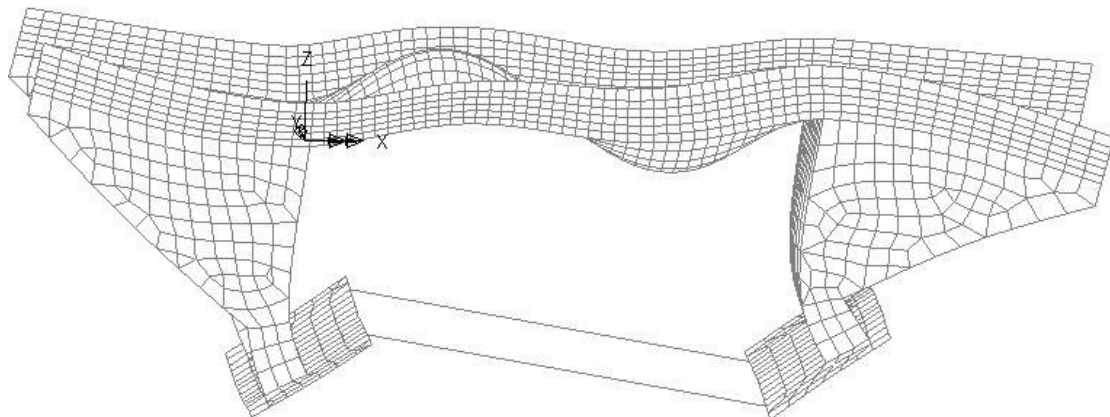


Figure 9.7 Eigenmode 25 with the natural frequency 29.15 Hz.

This specific error would never appear in a real design situation as the bridge code requires that at least the modes with a corresponding eigenfrequency less than 30 Hz are included in the modal superposition analysis.

9.3 Finite element model

To execute the dynamic analysis the constructural drawings were interpreted to represent the bridge's structural characteristics.

9.3.1 Geometry

The railway bridge was required to have a free opening of 15.0 m in longitudinal direction and a 4.7 m vertical opening. The free width of the bridge deck is 7.47 m. To connect the two footings, concrete truss elements were placed in between the fundaments. This makes the structure stiffer and enables the portal walls to act as one unit instead of two separate members. The modelling of the edge beams were of great importance since they contribute to much of the bridge's total stiffness. The Norra Kungsvägen bridge was designed to have two different edge beams with individually assigned cross-sections. The cross-sections of the edge beams were defined eccentrically with respect to their nodal lines. This eccentricity was necessary to obtain the correct geometrical positioning in the bridge's transversal direction. Figure 9.8 illustrates bridge model used for the dynamic analysis.

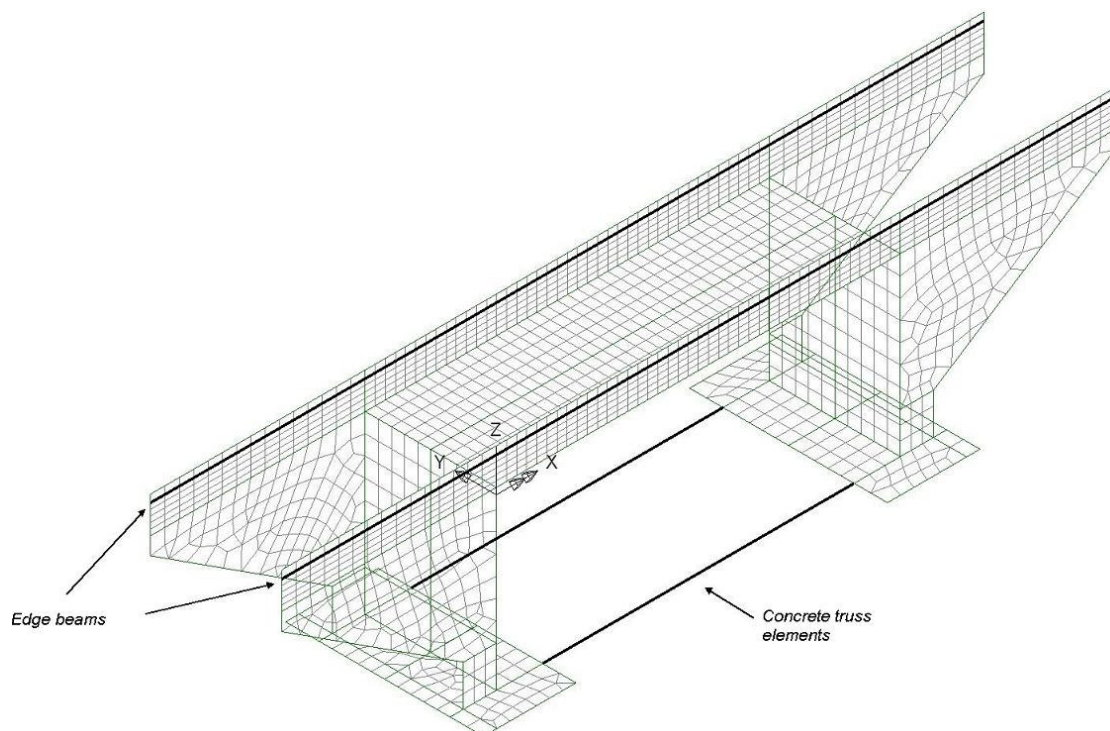


Figure 9.8 Finite element model of the Norra Kungsvägen bridge.

Figure 9.9 illustrates the north and the south edge beams of the bridge.

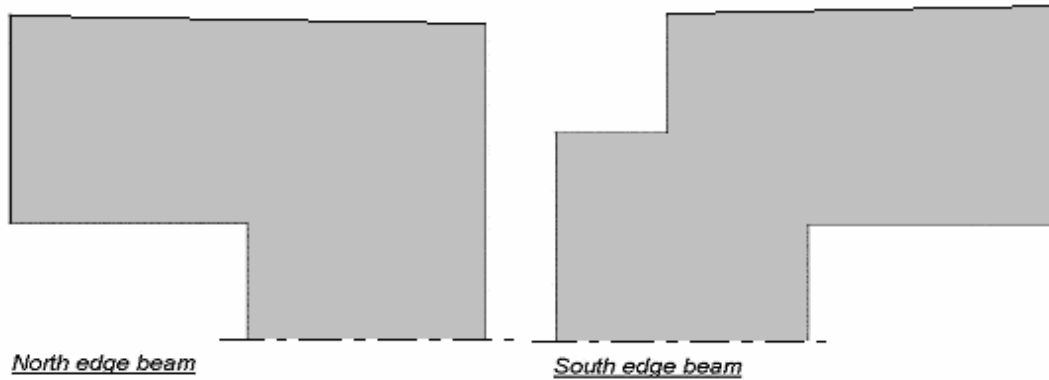


Figure 9.9 Geometry of the edge beams.

By utilising the section geometry of the edge beams the input parameters were calculated and are presented in Table 9.2.

Table 9.2 Cross-sectional constants of edge beams.

	North edge beam	South edge beam
Area [m ²]	0.537225	0.4861
Moment of inertia I _x [m ⁴]	0.018415	0.0165739
Moment of inertia I _y [m ⁴]	0.0390646	0.0331055
Torsional stiffness K _v [m ⁴]	0.0302085	0.0221848
Shear area A _{sx} [m ²]	0.431559	0.405273
Shear area A _{sy} [m ²]	0.459993	0.418893

9.3.2 Element types and mesh

The bridge was modelled with shell elements of Mindlin type (QTS4 thick shell elements) that are able to represent shear deformations. The edge beams were represented by Timoshenko beam elements (BRS2 thick beam 3D). Due to the bridge's geometry an irregular mesh was required on the wing walls and parts of the foundation. Figure 9.10 illustrates the mesh assignment selected for the bridge.

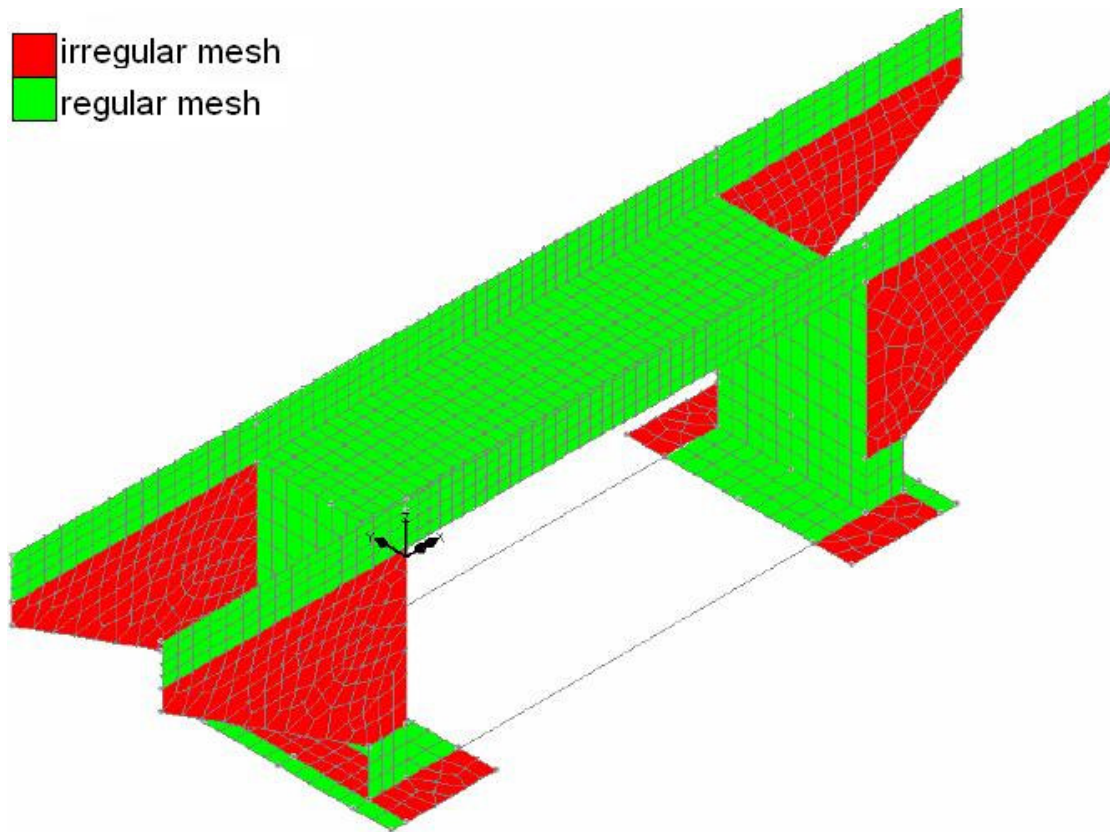


Figure 9.10 Element assignment.

The element assignment can be summarised as:

Trough

Bridge deck – regular mesh assembled of 10 x 40 shell elements with a thickness of 0.5 m.

South beam – regular mesh assembled of 4 x 40 shell elements with a thickness of 0.8 m.

North beam – regular mesh assembled of 4 x 40 shell elements with a thickness of 0.8 m.

Edge beams

15+40+15 Timoshenko beam elements with sectional constants according to Table 9.2.

Wing walls

Irregular mesh with a characteristic size of 0.5 m. Element thickness of 0.8 m.

Portal walls

Regular mesh assembled of 10 x 13 shell elements with a thickness of 0.7 m.

Footings

Regular and irregular mesh with a characteristic element size of 0.5 m. Constant element thickness of 1 m.

9.3.3 Boundary conditions

The soil condition present at the site of the bridge consists of a top layer of sand with an underlying layer of clay. To ensure the stability of the bridge structure, the concrete footings are placed on a layer of compacted filler material. The settlements of the bridge are minimised by supporting the fundamentals with concrete piles. The present soil conditions were modelled by inserting very stiff bar elements at the base of the portal walls. The stiff elements were forming a cross, which allowed the boundary conditions to be applied in the focal point. The stiff elements are, combined with appropriate boundary conditions, mimicking the actual structure's behaviour accurately. The footings will behave as stiff elements with translation and rotation only about their respective central points, where springs were applied. Figure 9.11 shows the stiff elements at the footings and the applied boundary conditions.

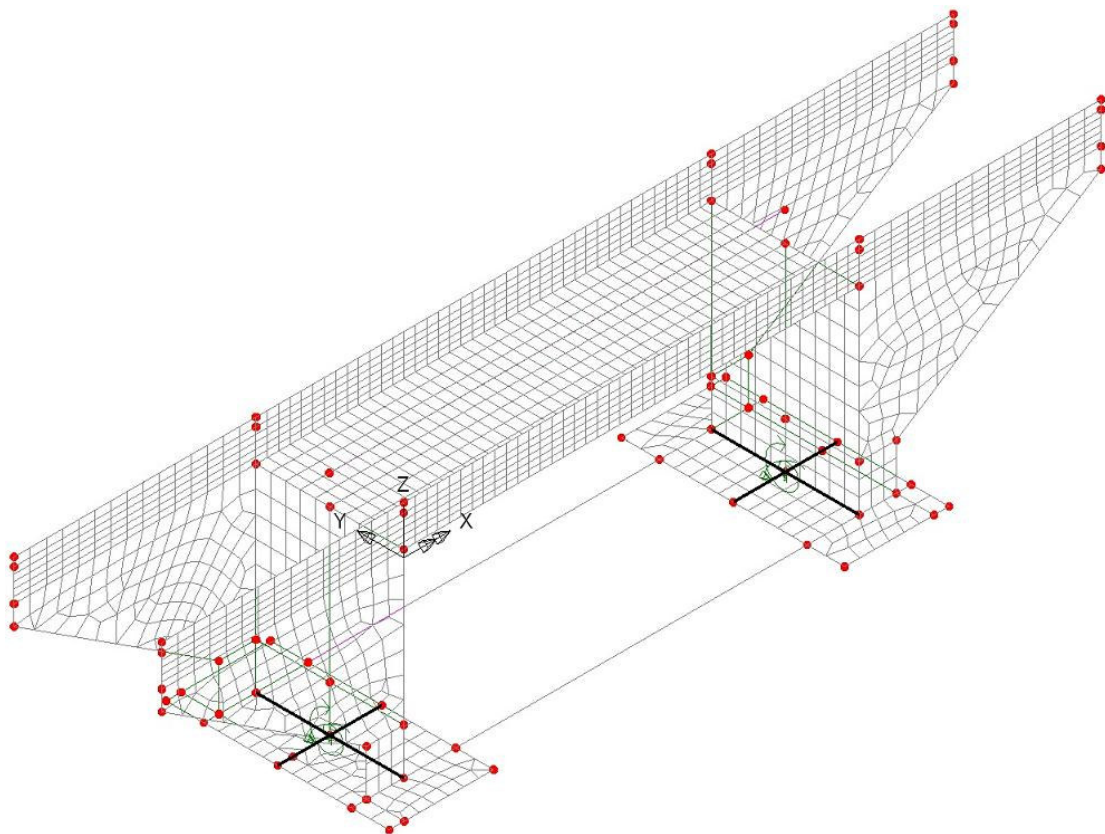


Figure 9.11 Boundary conditions.

The springs were assigned the following properties:

Translation

X-axis (longitudinal) – elastic springs placed in the centre of the forces acting on the fundament. Spring constant $k_x = 120.48$ MN/m.

Y-axis (transversal) – elastic springs placed in the centre of the acting on the fundament. Spring constant $k_y = 60.241$ MN/m.

Z-axis (vertical) – elastic springs placed in the centre of the forces acting on the fundament. Spring constant $k_z = 2.882$ GN/m.

Rotation

Rotation about X-axis (transversal to the bridge) – rotational elastic springs placed in the centre of the forces acting on the fundament. Spring constant $k_{rx} = 10.0$ MN/m.

Rotation about Y-axis (longitudinal to the bridge) – rotational elastic springs placed in the centre of the forces acting on the fundament. Spring constant $k_{ry} = 2.091$ MN/m.

Rotation about Z-axis (transversal to the bridge) – fixed torsional movement.

9.3.4 Loading

The train load, moving along the bridge structure, was modelled according to BV BRO's, Banverket (2006), 10 high-speed load models presented in Section 8.1.1. In order to capture the critical response of the bridge, each train model was analysed. The considered speed interval was ranging from 27.75 m/s (100 km/h) to 84.535 m/s (304 km/h) with a speed increment of 1.385 m/s (5 km/h). The train load was represented by point loads advancing along a path located 1 m above the bridge deck. The bridge deck is the primary member subjected to the load and was therefore selected as the load search area. Figure 9.12 illustrates the track search area and the train path.

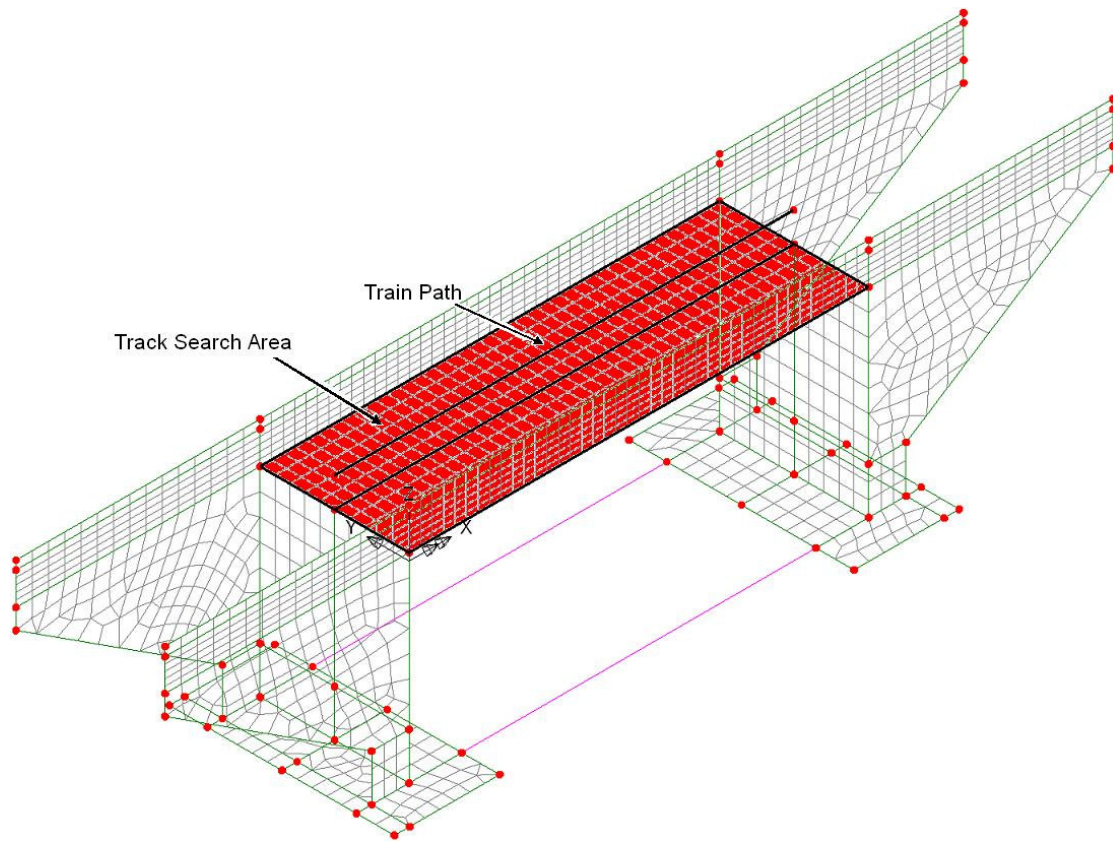


Figure 9.12 Train load definition.

The incremental distance, of which the discrete load progresses with, needs to be positive and sufficiently small to capture the movement of the load. Ideally, the distance increment used along the path should obey the following equation, LUSAS (2005):

$$\delta \text{Dist} \leq 3 \times \text{minimum speed} \times \delta t \quad (9.1)$$

If the condition stated in equation (9.1) is not fulfilled, the accuracy of the dynamic solution decreases with increasing oversampling ratio. The oversampling ratio decreases with increasing moving load speed and higher oversampling ratios are therefore allowed for lower speed where the dynamic amplification is reduced. As default values the incremental distance of the train load was set to 0.075 m and the time-step was set to 0.001 s.

The damping of the bridge was calculated according to Table 8.2 for reinforced concrete structures:

$$\left. \begin{array}{l} \xi = 1.5 + 0.07(20 - L) \\ L = 16 \text{ m} \end{array} \right\} \Rightarrow \xi = 1.78\%$$

9.3.5 Material properties

The bridge was constructed using C35/45 reinforced concrete. The material was assumed to be un-cracked during the analysis and elastic material behaviour was therefore applied. The effective modulus of elasticity was reduced by 40 % to account for the cracking of the concrete. The favourable dynamic effects allowing the Young's modulus to be increased were disregarded. The material parameters of the concrete are presented in Table 9.3.

Table 9.3 Material parameters C35/45.

Material parameters	C35/45
Young's modulus	20.4 GPa
Poisson's ratio	0.2
Mass density	2.5 kN/m ³
Thermal expansion coefficient	0.00001

Since the original model of the bridge was not containing any ballast, sleepers or rails the extra weight corresponding to the simplifications made was added as an increased density of the bridge deck. A similar procedure was utilised to account for the weight of the filler material on top of the footings. By increasing the density of the concrete, instead of altering the thickness, the correct mass of the bridge was obtained without adding stiffness. This assumption is un-favourable from a design perspective.

9.3.5.1 Calculation of equivalent densities

Bridge deck

$$q_{concrete} = 25 \frac{kN}{m^3}; \quad q_{ballast} = 20 \frac{kN}{m^3}; \quad q_{rail} = 2 \times 0.6 = 1.2 \frac{kN}{m}$$

$$q_{slipe} = 0.2^2 \times 2.5 \times 25 \times \frac{1}{0.65} = 3.85 \frac{kN}{m}$$

$$A_{concrete} = 0.5 \times 5.1 = 2.55 m^2; \quad A_{ballast} = 4.3 \times 0.75 = 3.225 m^2$$

Equivalent density:

$$Q_{tot} = A_{concrete} q_{concrete} + A_{ballast} q_{ballast} + q_{rail} + q_{slipe} = 133.2 \frac{kN}{m}$$

$$\rho_{eq,concrete} = \frac{Q_{tot}}{A_{concrete}} \frac{1}{g} = 5222 \frac{kg}{m^2}$$

Edge beams

The edge beams have a total cross-sectional area of 1.023 m^2 . The equivalent density of the beam elements was set to $\rho_{eq,concrete} = 2600 \text{ kg/m}^3$, which includes an additional mass of 102.3 kg/m corresponding to the weight of the parapets per metre.

Footings

The equivalent densities of the footings were not considered constant over the entire surface area. Therefore, two separate densities were assigned to the footings. The first density was equivalent to the weight of the concrete and the additional mass of the filler material between the wing walls. The height assumed was equal to the distance between the top of the footing to the top of the ballast material.

Equivalent density 1:

$$\left. \begin{aligned} M_{filler,1} &= 4.3 \times 1.45 \times 7.325 \times 1800 = 82208.5 \text{ kg} \\ \text{Corresponding volume in model: } V_1 &= 5.1 \times 1.8 \times 1 = 9.18 \text{ m}^3 \end{aligned} \right\} \Rightarrow$$
$$\Rightarrow \rho_{eq,1} = 2500 + \frac{M_{filler,1}}{V_1} = 11455.7 \frac{\text{kg}}{\text{m}^3}$$

The second density was equivalent to the remaining part of the footings. The footings were assumed to be covered by 1 m of filler material.

Equivalent density 2:

$$\left. \begin{aligned} M_{filler,2} &= (7.7 \times 3.6 - 5.9 \times 2.15) \times 1 \times 1800 = 27063.5 \text{ kg} \\ \text{Corresponding volume in model: } V_2 &= (7.7 \times 3.6 - 5.1 \times 1.8) \times 1 = 18.54 \text{ m}^3 \end{aligned} \right\} \Rightarrow$$
$$\Rightarrow \rho_{eq,2} = 2500 + \frac{M_{filler,2}}{V_2} = 3959.71 \frac{\text{kg}}{\text{m}^3}$$

The concrete density assignments are illustrated in Figure 9.13.

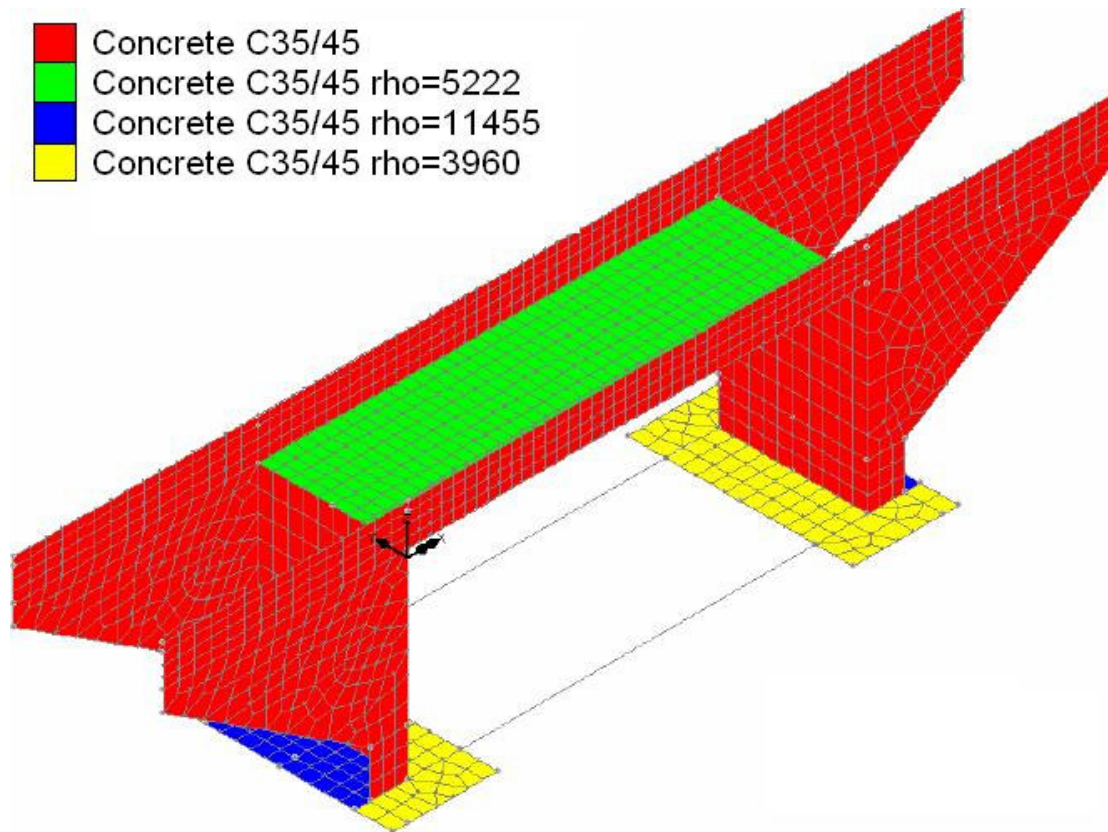


Figure 9.13 Concrete density assignments.

10 Result of analyses

10.1 Static analysis

To determine the consistency of the model, a static analysis of the bridge was performed. The static analysis only considered the bridge's self weight which should correspond to the material and geometrical properties assigned to the model.

Expected mass of the bridge:

Trough, bridge deck	$5.8162 \cdot 15 \cdot 2500 = 218107.5$ kg
Ballast material	$4.3 \cdot 0.75 \cdot 15.7 \cdot 2000 = 101265$ kg
Rails, sleepers and parapets	$(385 + 120) 15.7 + 100 \cdot 34.6 = 11388.5$ kg
Edge beams	$1.023325 \cdot 2 \cdot 8.7 \cdot 2500 = 44515$ kg
Portal walls	$6.075 \cdot 0.7 \cdot 5.9 \cdot 2500 \cdot 2 = 125449$ kg
Wing walls	$(2.08 \cdot 8.7 + 5.165 \cdot 4.56 + 1.085 \cdot 1.63) 0.8 \cdot 4 \cdot 2500 = 347335$ kg
Footings	$2 \cdot 7.7 \cdot 3.6 \cdot 1 \cdot 2500 = 138600$ kg
Filler material	$2 \cdot 82208 + 2 \cdot 27063 = 218542$ kg
Concrete truss elements	$2 \cdot 0.25 \cdot 12.1 \cdot 2500 = 15125$ kg
Total mass	1220327 kg

When the expected mass was compared to the static analysis performed in LUSAS (1208335.8 kg), the deviation was about 1 %. The difference is acceptable as it can be considered an error due to the numerical simplifications made.

The static deformations were analysed and compared to the expected response. Figure 10.1 indicates that the static deflections were reasonable. The consistency of the model was therefore assumed.

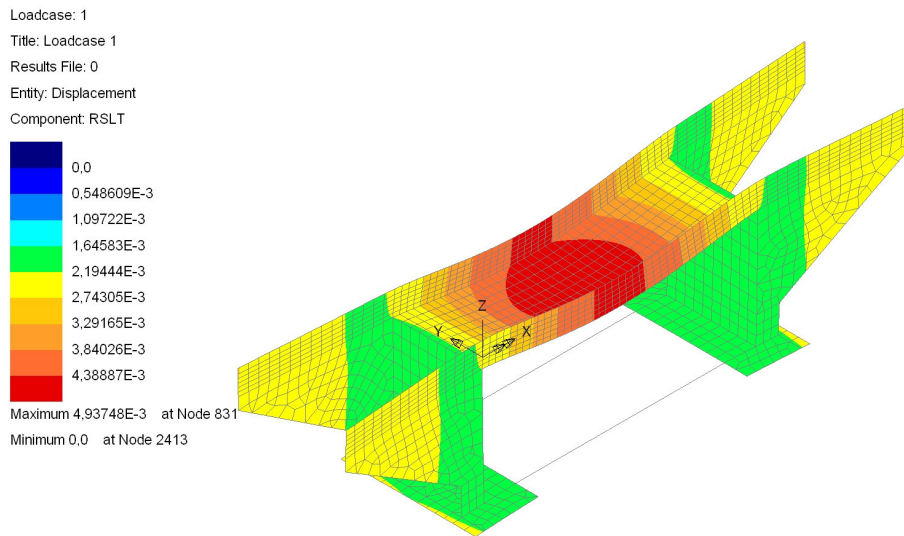


Figure 10.1 Static deflection of the bridge due to gravity load.

10.2 Parameter study

To find the optimum parameters for the dynamic analyses, a parameter study was performed. This procedure is very important as a too refined model will lead to prolonged analyses, while a too simplified model will produce great discretisation and integration errors.

The parameter study was only considering the influence of the HSLM-A2 high-speed train model, as additional models should generate similar behaviour. The displacements of the bridge are proportional to a cosine function containing the natural frequency, similarly to equation (2.12):

$$Displacement = U_0 \cos(\omega_n t) \quad (10.1)$$

However, the accelerations of the bridge are defined by the second time derivative of the displacements, and are therefore proportional to the natural frequency squared:

$$Acceleration = -U_0 \omega_n^2 \cos(\omega_n t) \quad (10.2)$$

Due to the relations presented in equations (10.1) and (10.2) the response of the accelerations will be more sensitive to the changes made in the parameter study. Therefore, the acceleration was the main parameter studied.

10.2.1 Load step increment

To ensure that the default load step increment was sufficiently small, the acceleration of the critical node was examined for different lengths. In the analyses all modes in the interval 0-30 Hz were considered. Figure 10.2 show that even sparse increments of 0.1 m produce acceptable results.

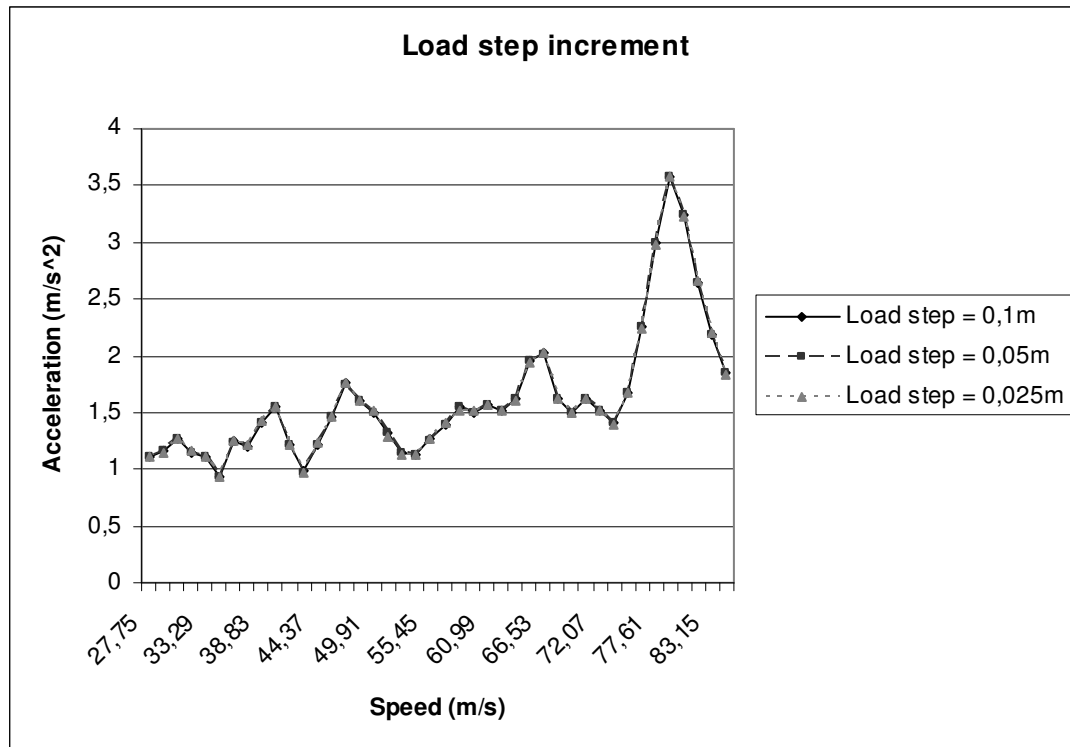


Figure 10.2 Parameter study of the load step increment.

Due to the risk of oversampling, the shorter load step increment of 0.025 m was used for further analyses.

10.2.2 Time-step increment

The influence of the time increment, separating the time instances on which the structural response is calculated, was studied to determine whether it had any substantial effect on the accelerational response. The moving load analyses were performed for different magnitudes of time-step increments with the remaining parameters kept constant. All modes in the interval 0-30 Hz were considered in the analyses. Figure 10.3 indicates that the accelerations are converging for a time-step increment of 0.001 s. This increment was therefore used for further analyses.

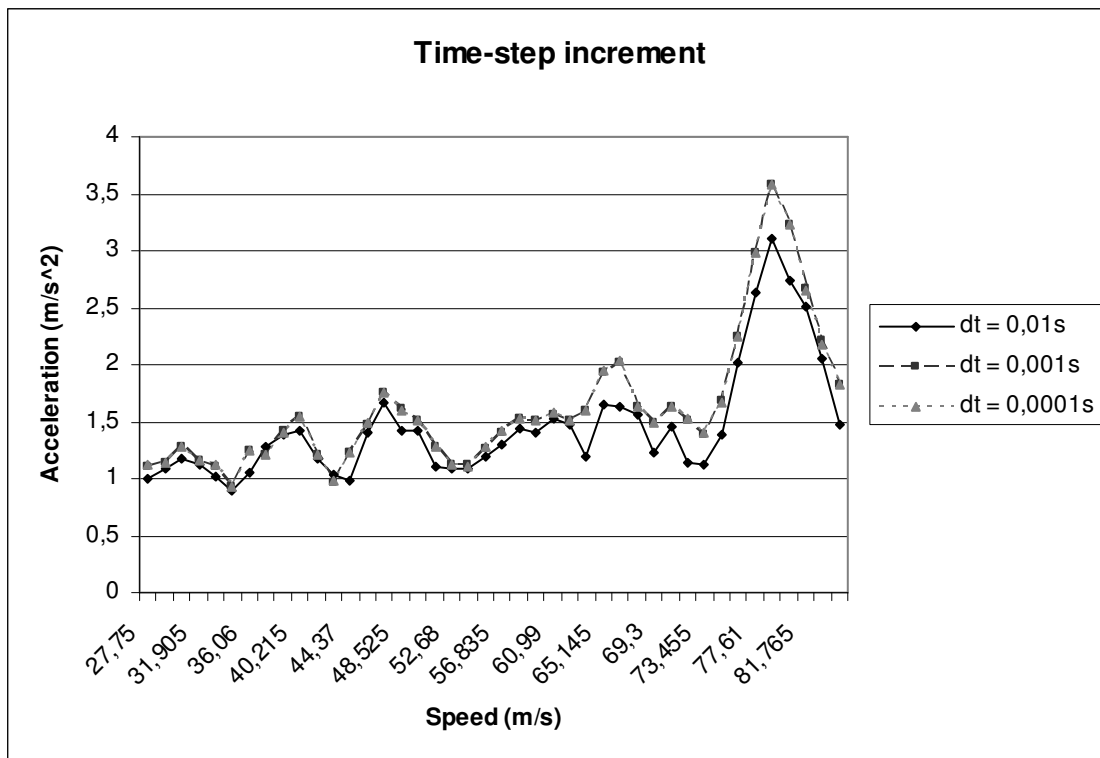


Figure 10.3 Parameter study of the time step duration.

10.2.3 Mesh density

An important procedure included in the convergence study of a finite element model is to determine the optimal mesh density. If a dense mesh is applied to the model, the representation of the actual structural behaviour is of higher accuracy. Since linear variation between the nodal points of intersecting mesh elements generally is assumed, it is of great importance to provide enough points on which the structural response is calculated. Three different mesh densities were analysed, using the original parameter values, to determine which mesh provided an result with acceptable accuracy. The negative aspect of using a too dense mesh is the amount of computer capacity required to solve the system of equations generated by the model. The objective was therefore to find an optimum mesh density. Figure 10.4 shows the absolute peak accelerations of point for different meshes; the original, a finer mesh (0.5 x element size) and a coarser mesh (2 x element size).

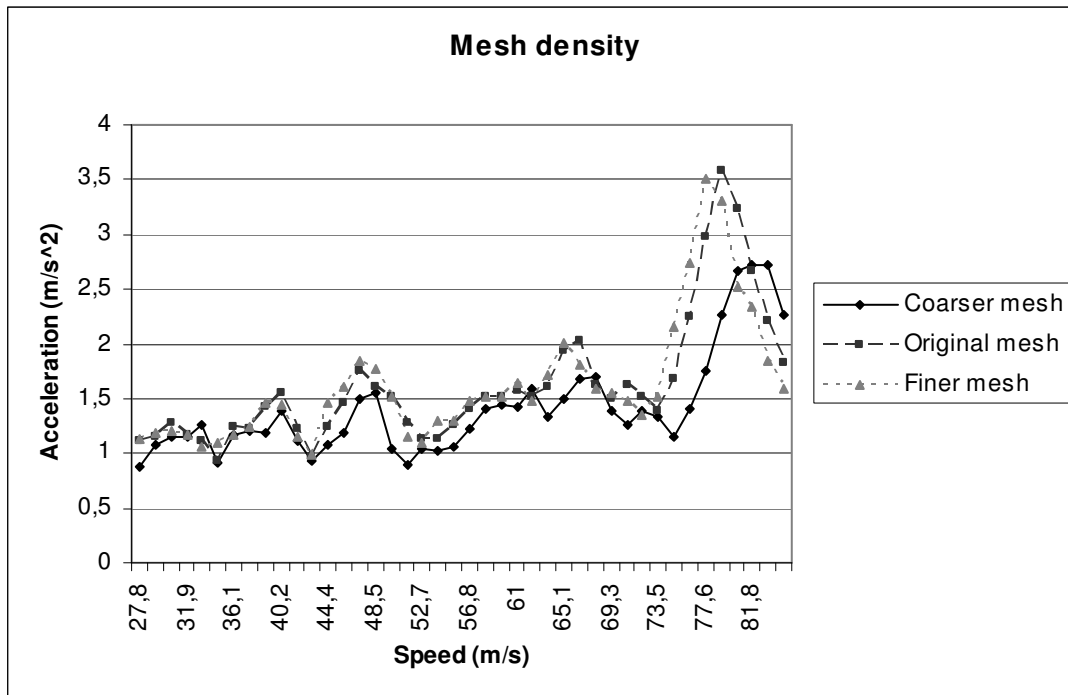


Figure 10.4 Parameter study of the mesh density.

The figure indicates that the original mesh provides results that capture the highest resonance peaks while limiting the usage of computer capacity.

10.2.4 Truncation of modes

The benefit of truncating the number of modes, included in the modal analysis, is obvious. By reducing the number of modes the amount of computer capacity required can be limited. To obtain results that are accurate enough while minimising the amount of time needed to perform the analysis is therefore highly desirable in today's increasingly competitive industry.

Figure 10.5 illustrates the maximum accelerations obtained by including different frequency ranges in the modal analysis.

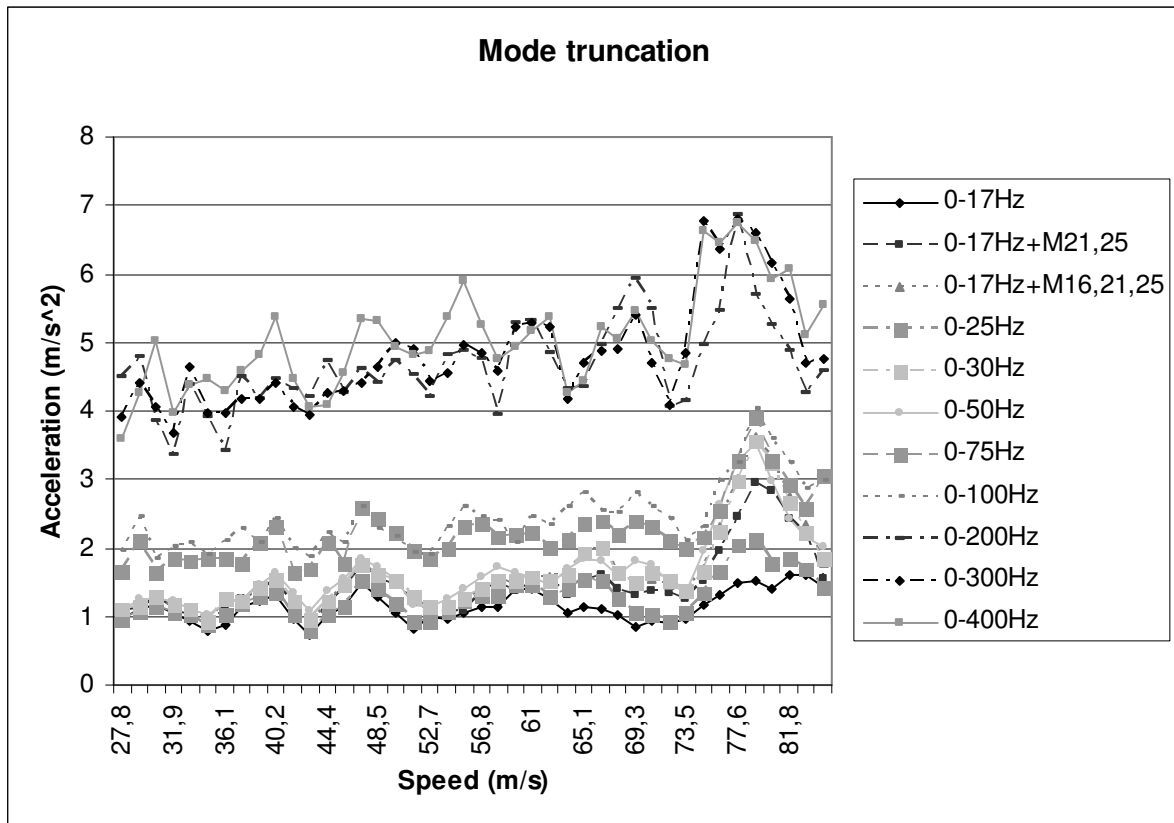


Figure 10.5 Parameter study of mode truncation.

The figure indicates that the maximum accelerations are successively increasing as more modes are accounted for in the analysis. Convergence to a stable solution cannot be assumed until all eigenmodes in the frequency range 0-200 Hz are considered. Even though the train load is clearly capable of exciting the higher frequency modes, the mode's actual influence on the performance of the bridge, i.e. ballast stability and comfort conditions, is questionable. The maximum driving frequency of the train can roughly be estimated by:

$$f_{train,max} = \frac{\text{Maximum train speed [m/s]}}{\text{Minimum axle spacing [m]}} = \frac{84.535}{2} = 42.27 \text{ Hz} \quad (10.3)$$

indicating that the driving frequency of train load is probably coinciding with multiples of the high frequency modes, Frýba (1996).

10.3 Patch load

The reason for the model's sensitivity to higher frequencies may be that neither the actual track nor the ballast were modelled. This could result in a discontinuous load transfer to the structure as the train moves onto the bridge and might cause higher frequency modes to be excited. In the original analysis, which had sustained convergence issues, unit point loads were utilised to represent the train load. The unit

point loads were representing an axle of the moving train. Since the bank was not modelled the loads will be projected on the bridge deck in the two progressing points. In reality, the load will be transferred through the rail, via the sleepers, into the ballast and finally subjecting the bridge deck to a uniform pressure. The most simplified procedure to model this phenomenon is to represent the train by a unit patch load, designed to mimic the actual load distribution. Figure 10.6 illustrates how the load distribution was assumed. The total patch area is 3 x 0.95 m.

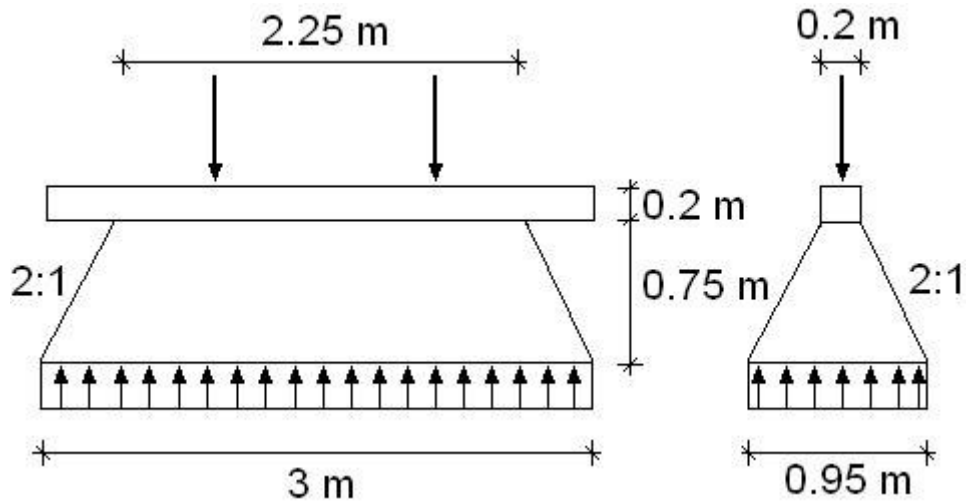


Figure 10.6 Assumed load distribution of patch load.

The parameter study indicates that applying patch loads are generating lower accelerations making the utilisation of point loads the more conservative method. Figure 10.7 illustrates the results from the sensitivity analysis performed.

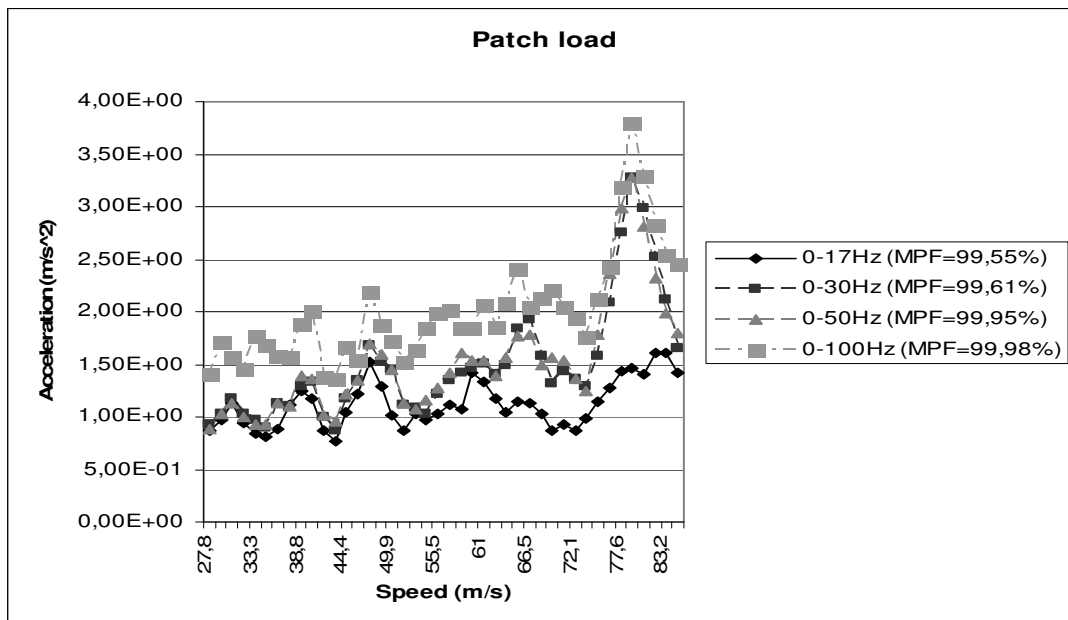


Figure 10.7 Sensitivity analysis of patch load.

Though modelling the train load as distributed patch loads may be a more accurate representation, the stability of the analysis was not increased.

10.4 Modelling of ballast and track

As explained in Section 10.3, the discontinuous load transfer occurring when the train model is initially introduced to the bridge may explain the structure's sensitivity to high frequency modes. In an attempt to resolve this issue, the bank on the bridge was modelled and added to the original model configuration. The bank segment was connected to the bridge deck using slidelines, with the bank assigned as the slave feature and the bridge deck designated as the master. The bank was modelled using weightless volume and beam elements to represent the ballast material, rails and sleepers. The reason for this choice was to maintain the appearance of the original model as constant as possible. The increased density of the bridge deck was thus preserved, with the bank only contributing with stiffness able to transfer the induced train loads. The sleepers were equally spaced with a distance of 0.65 m along the bridge, according to the bridge code specifications. To ensure that the load was acting on the rail, and not directly on the bridge deck, the load search area was assigned to thin weightless shell elements located between the rails. The partitions of the bank which were not in contact with the bridge deck were assumed to have fixed translational and rotational degrees-of-freedom. Figure 10.8 illustrates the bridge with the modelled the ballast and track included.

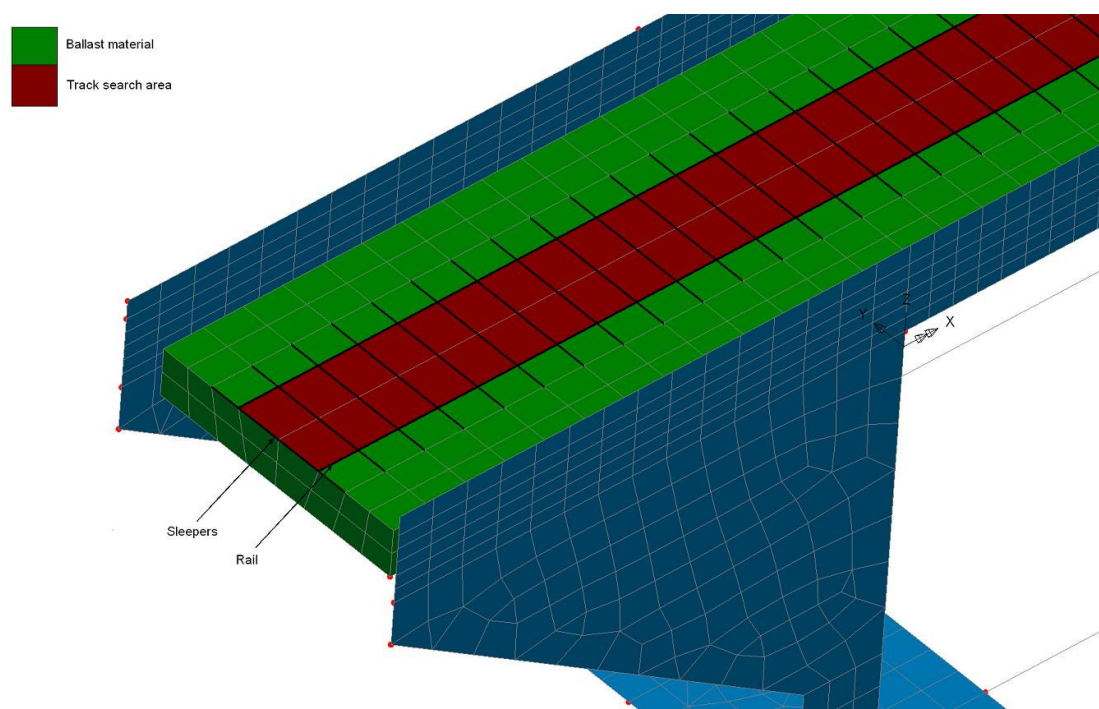


Figure 10.8 Model of the bridge with included bank representation.

An eigenvalue analysis was performed to determine the un-coupled eigenmodes in the interval 0-100 Hz. Figure 10.9 shows the variation of peak accelerations obtained when different intervals were considered.

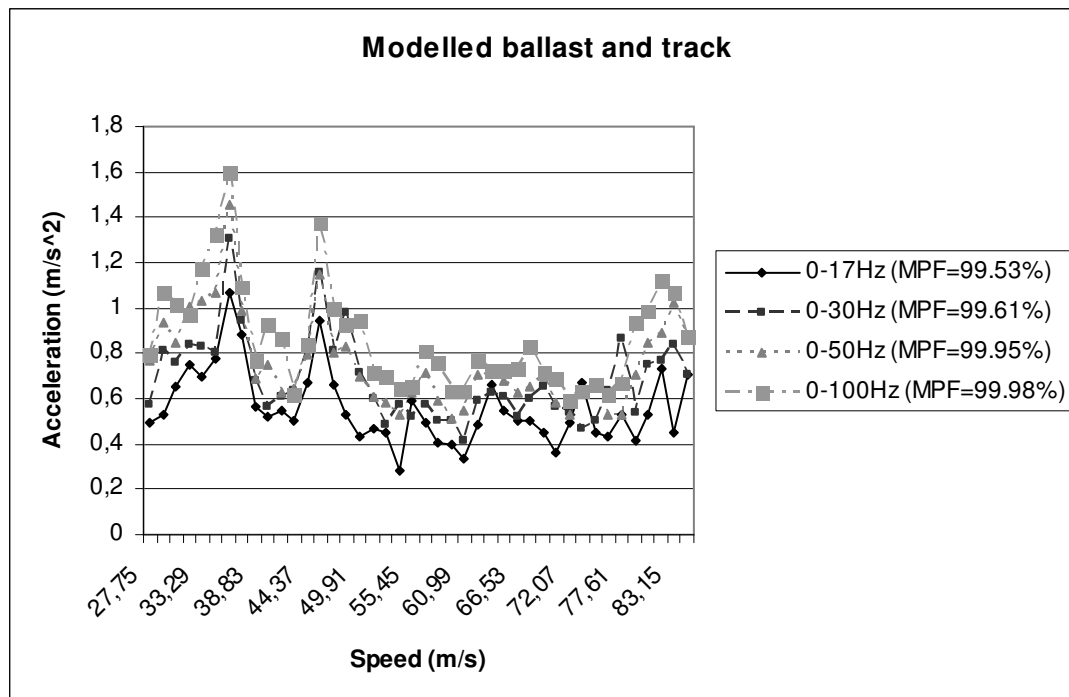


Figure 10.9 Vertical acceleration with ballast and track included in the model.

Figure 10.9 indicates that the model's behaviour is completely different from the previous performed analyses. The resonance peaks are located at considerably lower speeds and the maximum accelerations are of lower magnitudes. This behaviour can be explained by major differences in the boundary conditions introduced to the model. The result from this analysis is therefore not comparable to the other analyses performed and should be studied separately.

By studying Figure 10.9 it was noticed that the model showcase similar behaviour for all the studied intervals. However, the maximum peak accelerations were not captured in the analysis including eigenmodes in the interval 0-17 Hz, even though the MPF was well above 90 % at 99.53 %. With the soil, in contact with the bridge foundation, modelled as deformable, the bridge is allowed to have modes with a significant rigid body component with a great contribution to the total MPF. The rigid body modes (RBM) are allowing the whole structure to translate in a principle direction without deforming its members. Using MPF as a cut-off criterion may therefore be highly unsuitable for this configuration of boundary conditions. The maximum vertical acceleration is considerably lower than for previously performed analyses, indicating that the modelling of the ballast and track is an even less conservative choice if compared to patch loads.

10.5 Modelled soil pressure

A common simplification made while modelling bridge structures is to exclude the pressure acting on the portal walls due to movement of the bridge relative the adjacent filler material. This pressure can be modelled by inserting springs with varying

stiffnesses on the shell elements representing the portal walls highlighted in Figure 10.10.

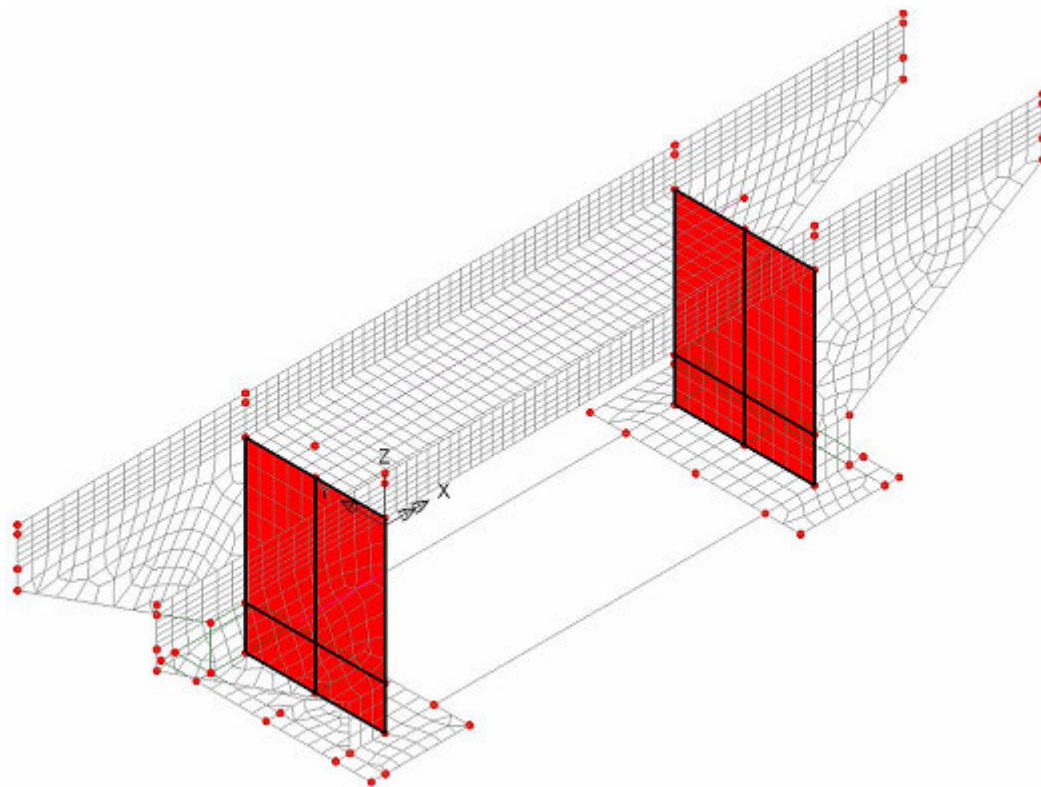


Figure 10.10 Soil pressure representation.

Due to temperature movements and vibrations, the bridge was assumed to always be in contact with the filler material and the presence of the additional pressure is therefore constant. This assumption is only valid when the portal walls have similar geometry and the eigenfrequencies are only effected by the change of the loads acting on the structure, and are not influenced by the introduction of a static load.

The pressure variation is defined by the bridge code as:

$$\Delta p = c \cdot \gamma \cdot z \cdot \beta = \frac{c \cdot \gamma \cdot z}{h} \cdot \delta \left[\frac{N}{m^2} \right] \Rightarrow k_{spring} = \frac{c \cdot \gamma \cdot z}{h} \quad (10.4)$$

where $\gamma = 18 \text{ kN/m}^3$ is the density of the filler material, $c = 300$ or 600 is a case specific constant and $\beta = \frac{\delta}{h}$ where δ is the relative displacement and h is the height of the portal wall. The spring stiffness k_{spring} is determined as a linear function of the depth z , defined according to Figure 10.11.

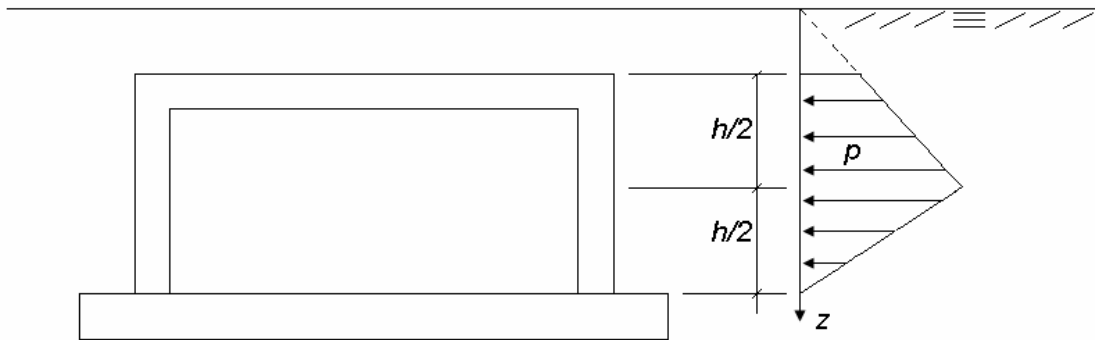


Figure 10.11 Soil pressure variation according to Bro 2004.

Figure 10.12 is illustrating the vertical acceleration when the soil pressure was incorporated into the model.

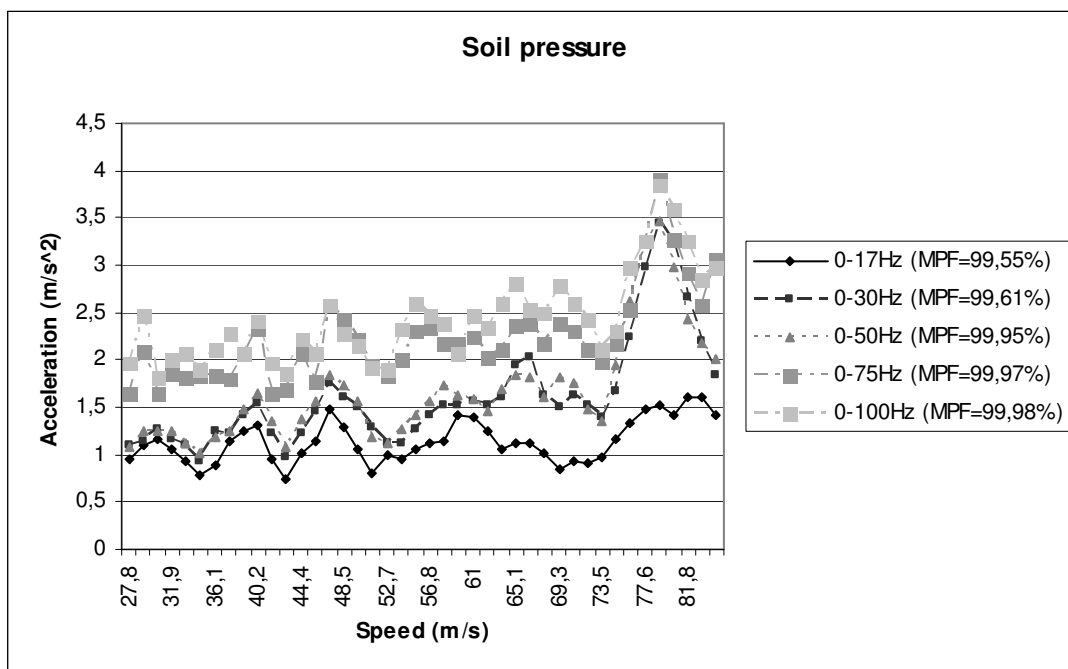


Figure 10.12 Vertical accelerations with modelled soil pressure.

The figure is indicating that the modelling of the soil pressure has a minor effect of the total structural response. The maximum accelerations are almost identical to the response of the original model. Additionally, it was noticed that convergence is not obtained even though $SMPF > 90\%$.

Figure 10.13 is illustrating the displacements obtained from the analysis.

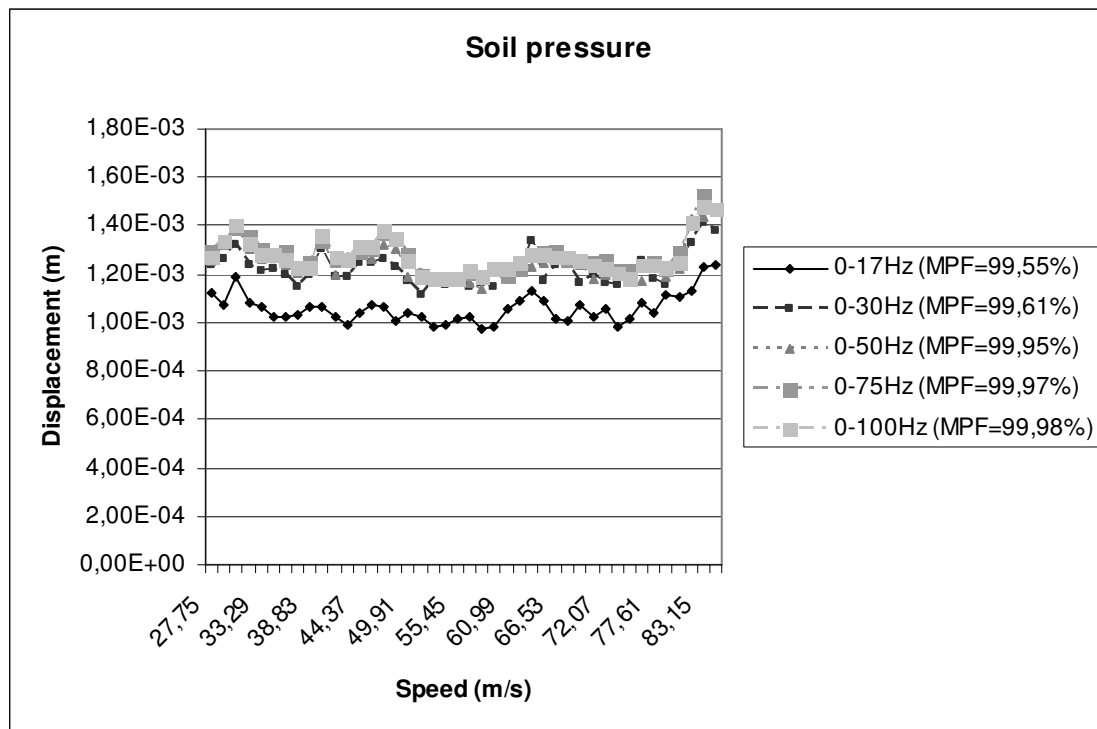


Figure 10.13 Vertical displacements with modelled soil pressure.

The maximum displacements obtained were providing non-converging results for frequency intervals with SMPF > 90 %. This is indicating that MPF not always is an appropriate convergence criterion when calculating displacements, and should perhaps be accompanied with requirements on the assignment of boundary conditions.

10.6 Different boundary conditions

To determine the effects on the structural response caused by the selected boundary conditions, modal analyses were performed with various configurations. By increasing the stiffness of the support, the speeds at which resonance peaks occur, will move up in the frequency spectrum and possibly be situated outside of the speed range expected on the bridge. This behaviour can be explained by studying the definition of the natural frequency presented in equation (2.10).

10.6.1 Fixed vertical translation

By not allowing the footings to move vertically, rigid body modes were prevented in the prescribed direction. The prevented translation, forces a wider frequency range to be analysed in order to obtain SMPF > 90 %. The remaining spring stiffnesses were assigned values consistent with the original model. Figure 10.14 illustrates the vertical accelerations calculated with the specific boundary conditions.

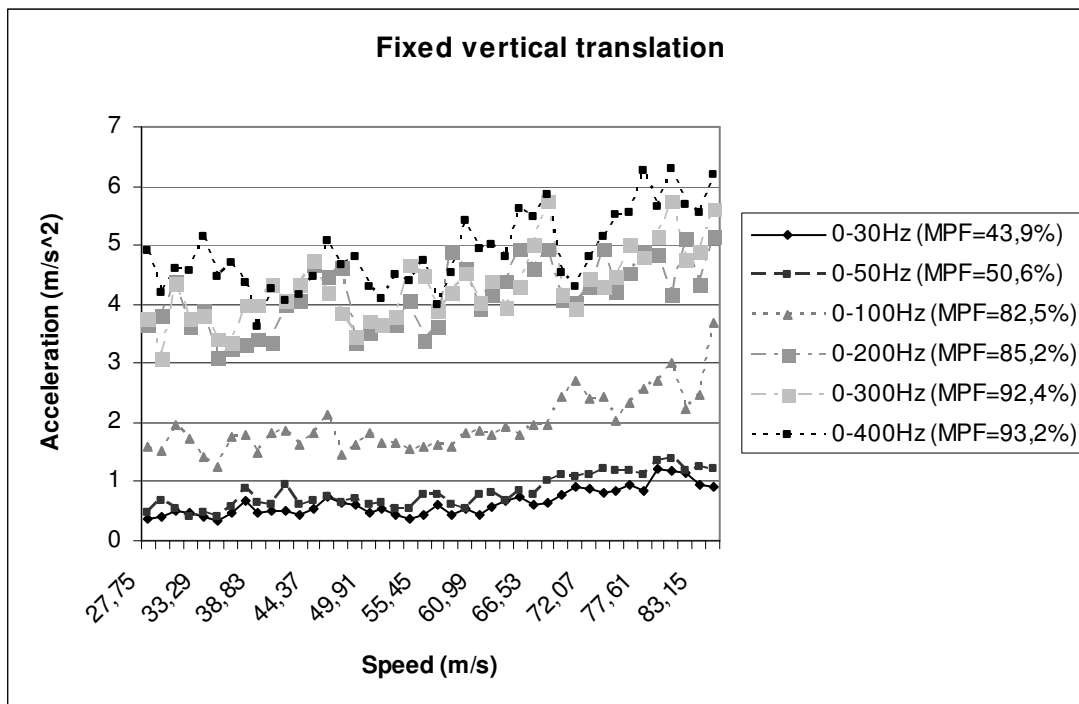


Figure 10.14 Vertical acceleration when translation in z -direction is prevented.

The increased vertical stiffness caused the maximum vertical accelerations to decrease, possibly underestimating the response. By studying the figure, one can assume that a resonant peak is located just outside the analysed speed interval.

The figure also indicates that MPF may be unsuitable as a convergence criterion since the maximum accelerations for the intervals with a SMPF $> 90\%$ were not converging. Due to the relation between acceleration and eigenfrequency, presented in equation (10.2), the accelerations are possibly overestimated for the frequency ranges required to generate high SMPF.

10.6.2 Increased spring stiffness

The spring stiffnesses used, were derived from calculations of the level of support provided statically by the piles. A common assumption made is that springs are stiffer when subjected to dynamic loading, compared to static loading. To obtain intermediate boundary conditions, the spring stiffnesses were multiplied with constant factors with the objective to locate the critical point where the spring stiffnesses are large enough to resist excessive translations. To illustrate that the convergence of displacements is less sensitive to the number of included eigenmodes, presented in equation (10.1), the maximum displacements are also presented for the following analyses. The maximum accelerational response will, according to Tavares (2007), decrease with increased vertical stiffness and underestimate the actual response.

10.6.2.1 Original stiffness x 3

Figure 10.15 illustrates the vertical acceleration when the spring stiffnesses were multiplied by 3.

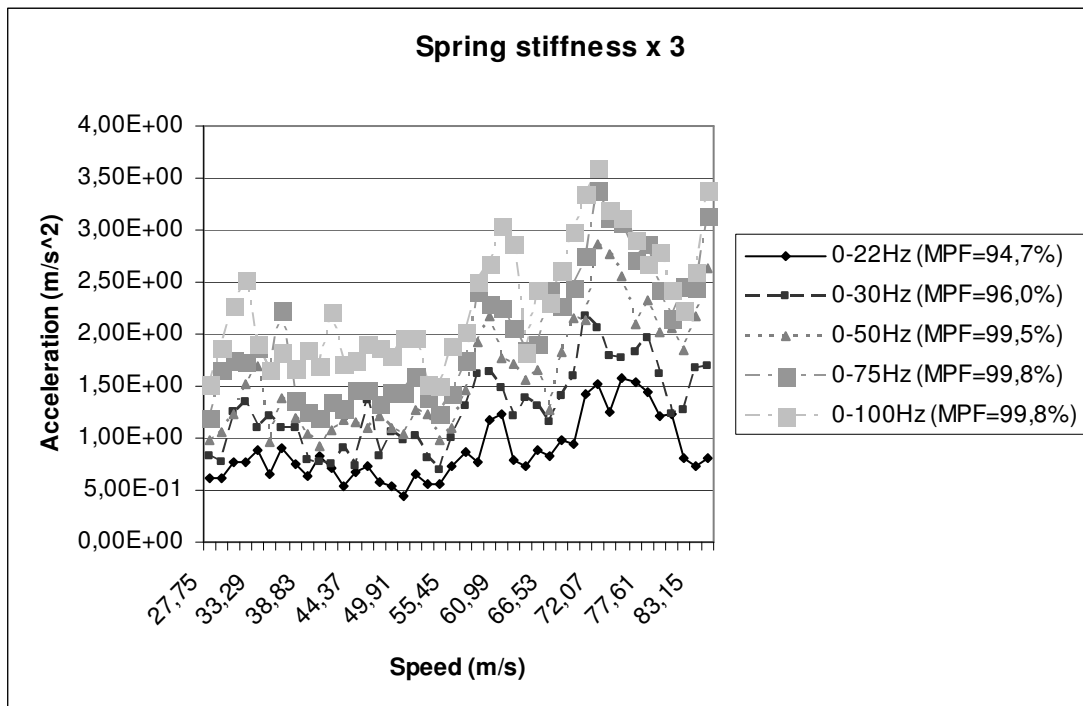


Figure 10.15 Vertical acceleration with spring stiffness multiplied by 3.

By studying the figure, it is clear that the MPF does not provide any indication of convergence as there is a wide scatter of accelerational response. Figure 10.16 shows the variation of the displacements for different intervals of eigenmodes.

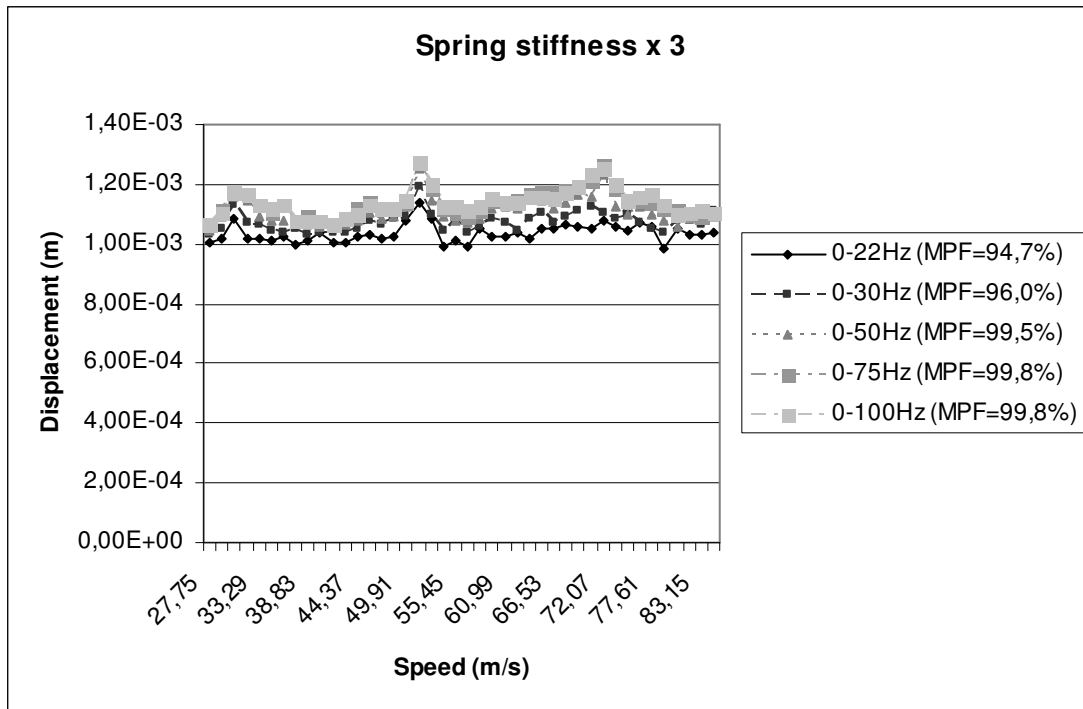


Figure 10.16 Vertical displacement with spring stiffness multiplied by 3.

Figure 10.16 indicates that the accuracy of the results produced was substantially better for the displacements when compared to the accelerations. The results are consistent with the assumption that MPF is a useful convergence criterion when calculating the deformations, if accompanied with boundary conditions that are minimising the influence of the RBM.

10.6.2.2 Original stiffness x 5

Figure 10.17 indicates that the magnitude of the accelerations decreases as the stiffnesses increase. This behaviour was expected as a stiffer structure is more difficult to excite.

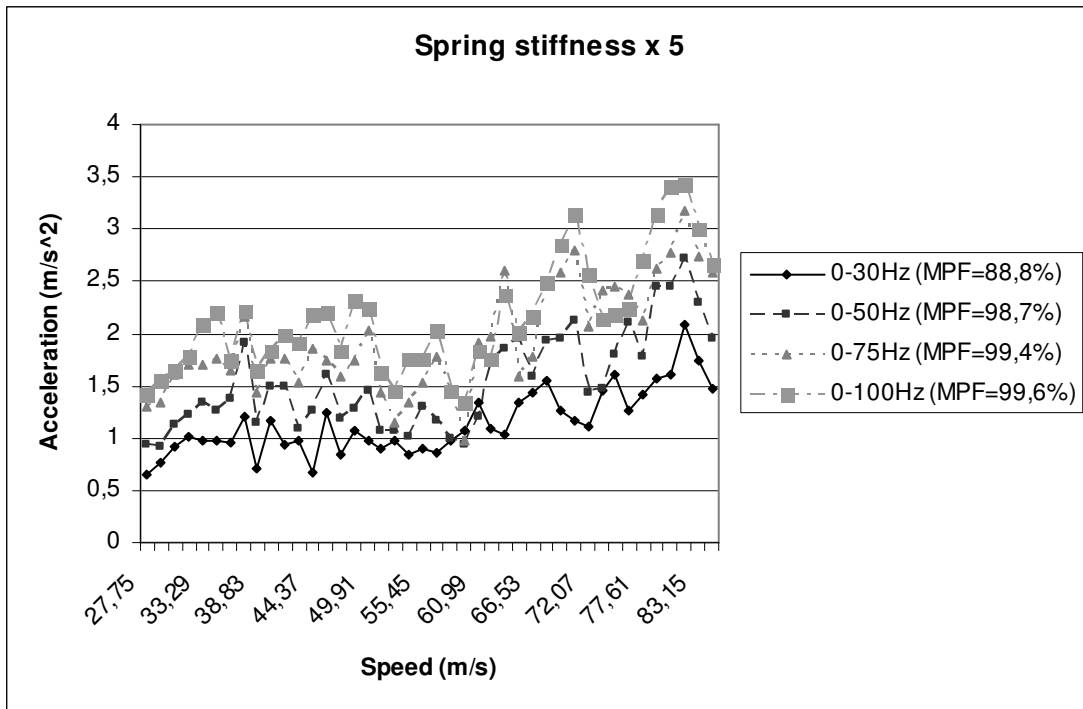


Figure 10.17 Vertical acceleration with spring stiffness multiplied by 5.

Similarly to the analysis where the spring stiffnesses were multiplied by a factor of 3, it is impossible to notice any correlation between convergence and SMPF > 90 % by studying the maximum accelerations.

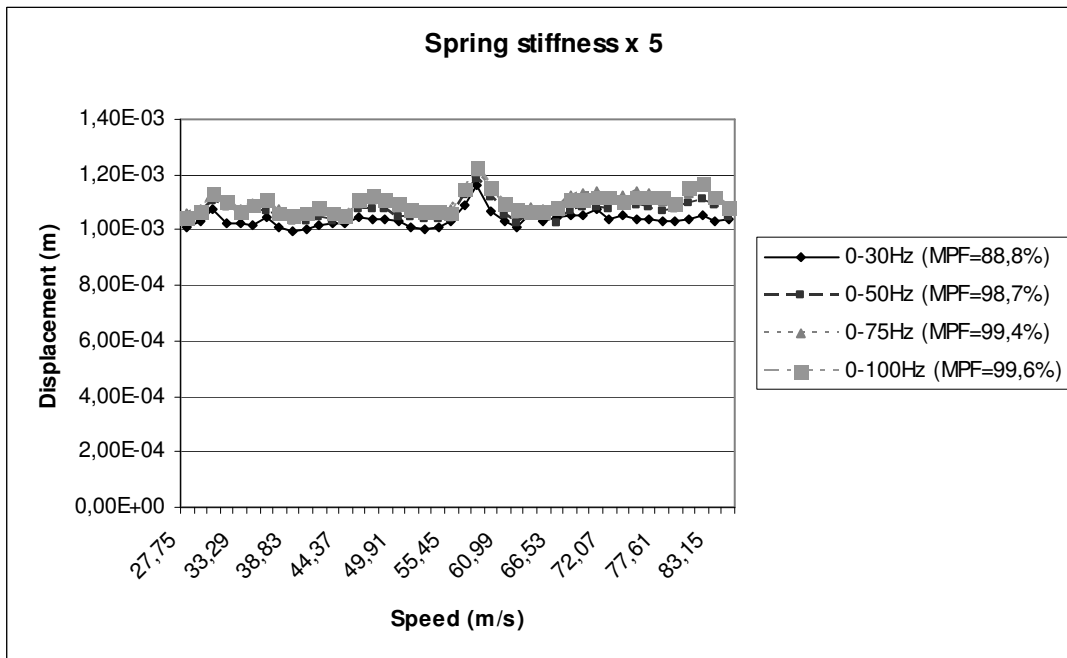


Figure 10.18 Vertical displacement with spring stiffness multiplied by 5.

Figure 10.18 indicates that the use of MPF as a convergence criterion to determine the maximum displacements for this configuration is conservative, as acceptable accuracy

is obtained prior to $SMPF = 90\%$. As expected, the resonance peaks occurred at higher speeds when the stiffness was increased.

10.6.2.3 Original stiffness x 10

Figure 10.19 illustrates the vertical acceleration when spring stiffnesses were increased by a factor of 10.

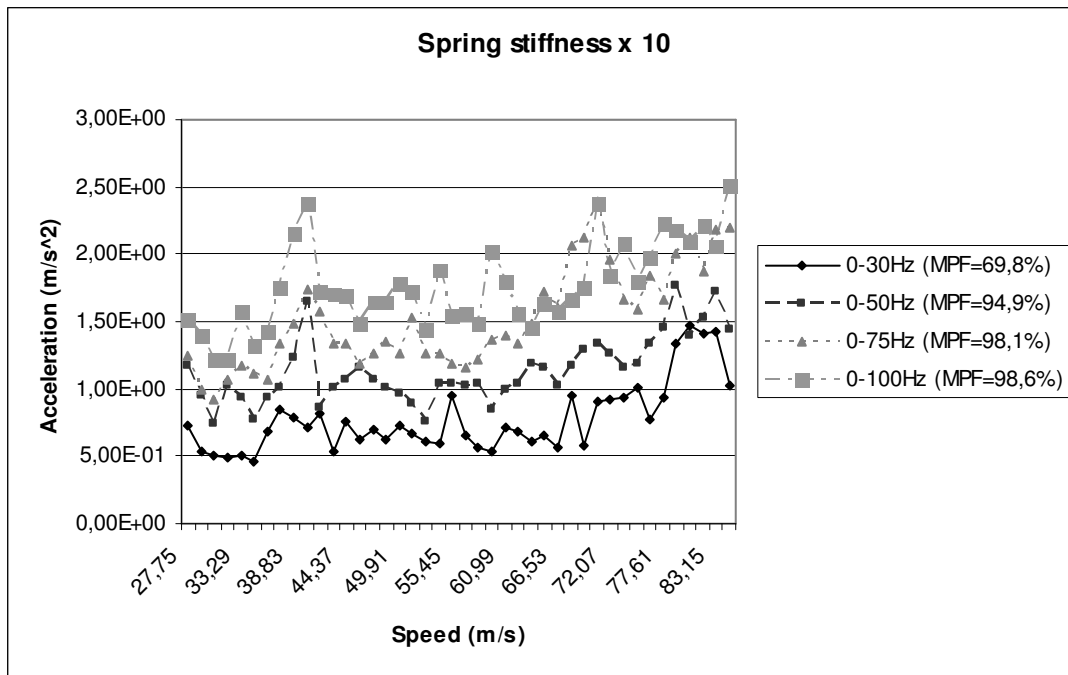


Figure 10.19 Vertical acceleration with spring stiffness multiplied by 10.

The results are indicating that the increased stiffness does not improve the usage of MPF as a convergence criterion when determining the maximum accelerations.

The assumption regarding improved accuracy of the result, produced by the modal analysis when increasing the frequency range, can be proven theoretically. However, to include more modes might not be an appropriate procedure when determining the maximum acceleration in a design situation.

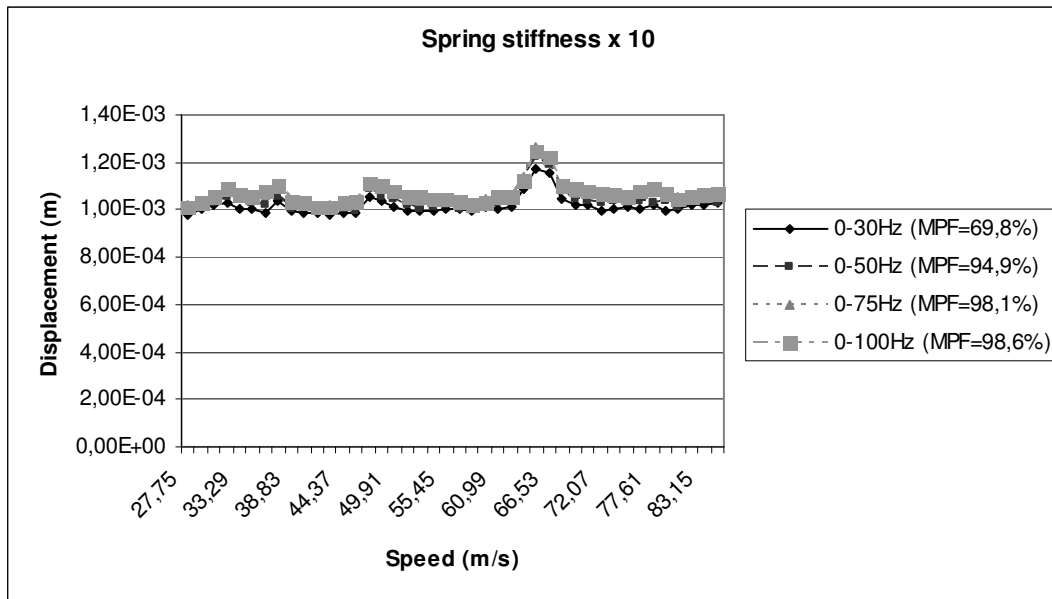


Figure 10.20 Vertical displacement with spring stiffness multiplied by 10.

Figure 10.20 indicates good accuracy of the displacements when the SMPF is greater than 90 %. The displacements stands in direct relation to the section forces and MPF might therefore be a useful criterion when determining forces present in the structure.

10.6.3 Fixed translations

According to the code requirements, Banverket (2006), the soil in contact with the foundation of the bridge is allowed to be modelled as un-deformable. However, this might not be the most accurate representation of the actual soil conditions. The structure will most likely sustain rotational and translational movement during its service life. By providing the boundary conditions with fixed translations and rotational springs around the x-axis and y-axis, the desired model was obtained. The maximum accelerational response for the different speed increments are presented in Figure 10.21.

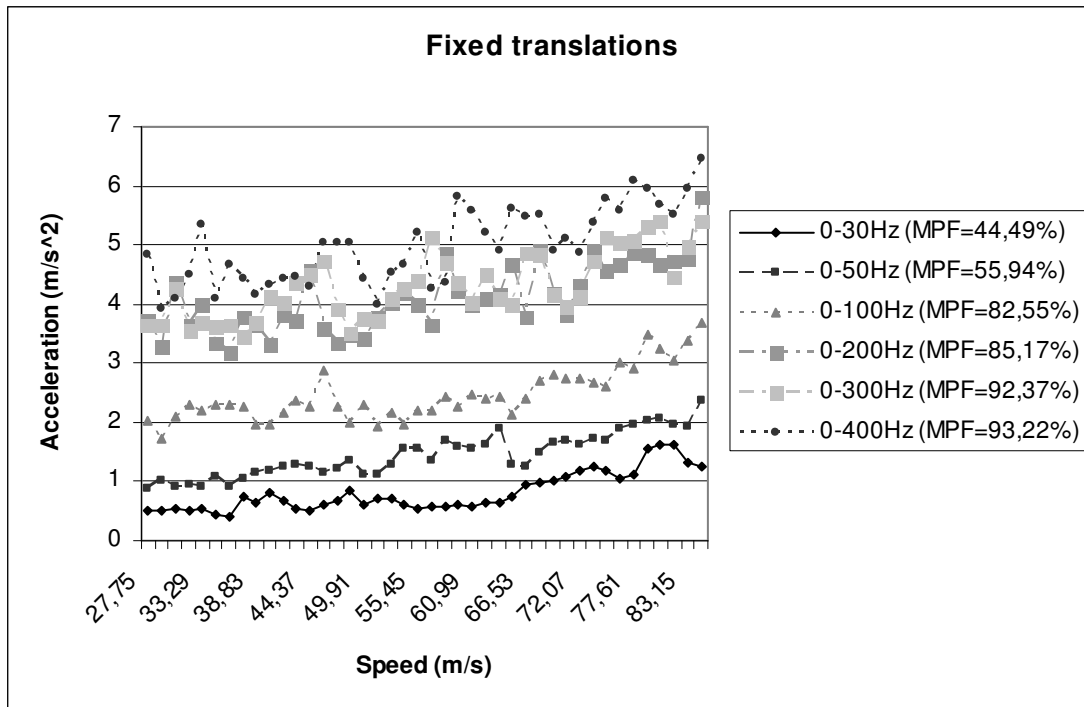


Figure 10.21 Vertical acceleration with fixed translations.

Figure 10.21 indicates, in accordance with previous analyses, that the maximum accelerations are increasing when wider ranges of natural frequencies are considered. It should be noticed that the frequency range 0-300 Hz, which generates SMPF = 92.37 %, is not converging to the more accurate solution provided by the wider frequency range of 0-400 Hz. The time required to calculate and analyse eigenmodes generating SMPF > 90 % is for this configuration of boundary conditions very extensive. It is therefore not advantageous nor time efficient to perform analyses including a too wide frequency range to determine the accelerational response.

11 Conclusions

11.1 General

The accelerational response of a bridge structure subjected to a dynamic loading is greatly influenced by the soil conditions present at the location of the bridge. The modelling of the boundary conditions in a finite element model is therefore extremely important as the magnitude of the response will be greatly effected. When the vertical stiffnesses of the supports, dictated in the boundary conditions, are increased the resonance peaks are moved to higher speeds, and may occur outside of the speed range expected on the bridge. The analyses performed indicate that the maximum accelerations are underestimated by stiff support conditions. However, if the assumed supports are flexible the resonance peaks are captured but the SMPF is allowed to increase rapidly, due to eigenmodes with a significant rigid body component. The RBM are allowing the whole structure to translate in a principle direction without deforming its members. The RBM will maximise the mass participation for the effected modes and will thus undermine the usage of MPF as a convergence criterion.

Another disadvantage of MPF is that the parameter does not provide any indication of how many asymmetric modes that are required in the analysis. Due to the definition of MPF, the contribution to the total fraction of mass active in the asymmetric modes is cancelled out by the equal deformations in positive and negative direction.

The main objective of the project has been to conclude whether the MPF is a reliable criterion to determine a cut-off frequency when analysing the accelerational response of a bridge. Due to the relation between the acceleration and the structure's eigenfrequency, presented in equation (10.2), the accelerational response is amplified by the magnitude of the eigenfrequencies included in the modal analysis. The total response is contained by the decreased magnitude of the initial amplitudes corresponding to the higher frequency eigenmodes. The results of the analyses are indicating that the high frequency modes are greatly contributing to the total accelerations of the bridge structure. In reality the higher order acceleration components are not of any significance for the bridge performance i.e. ballast instability, comfort conditions etc. This property prevents the use of MPF as a convergence criterion for bridges with stiff support conditions, where the maximum accelerations are analysed, as higher frequency modes are required to obtain the suggested value of 90 %. The usage of MPF as a cut-off criterion in a modal analysis is therefore not applicable for some structures:

- Bridges with flexible support conditions.
- Any bridge where the maximum accelerations are analysed.

However, the MPF is a useful parameter when analysing the sectional forces. The section forces are proportional to the deformations which have been proven to converge for rather narrow frequency ranges. The MPF should when utilised be accompanied with appropriate boundary conditions that prevents rigid body modes. The suggested cut-off criterion of $MPF > 90 \%$ may, if used properly, be considered as conservative when determining deformations as convergence often is achieved for lower values.

As a final conclusion, the proposed procedure to calculate the accelerational response is to determine at which frequency range the deformations are converging and thereafter apply the same cut-off frequency to the analysis of the accelerations, regardless of the MPF. The accelerations obtained from the analysis will theoretically possess sufficient accuracy as the deformations are converging, and an overestimation of the maximum accelerations is thus prevented.

11.2 Further investigations

The influence of the modelled soil conditions has often proved to dictate the structural response. A study investigating possible methods of how the soil can be represented and incorporated into a finite element model is therefore a natural continuation to this project. A comparison between recorded acceleration data of real bridge structures and the modelled response would be interesting in order to determine the correlation between the results.

Another interesting aspect would be to compare the results from dynamic analyses performed using the mode superposition method to the exact solution obtained using a direct transient integration scheme. The comparison could determine the relation between the computational time gained and accuracy lost, and thus conclude whether the mode superposition method is the optimal analysis method.

To confirm our conclusions the research can be extended to include more bridges, of various types. It would be interesting to include for example a multi span bridge or a frame bridge with a shorter span. Furthermore, analyses including additional train vehicles should be performed to investigate the effects that different types of load models have on the structural response.

12 References

- Banverket, (2006): BV BRO – Banverkets ändringar och tillägg till Vägverkets Bro2004, (Revision and additions by the Swedish Railway Administration to the Swedish Bridge code, Bro 2004. In Swedish), inklusive supplement nr 1, Utgåva 8, BVS 583.10.
- Bathe K.-J. (1996): *Finite Element Procedures*. Prentice Hall, Englewood Cliffs, New Jersey, USA.
- Björklund, L. (2005): *Dynamic Analysis of a Railway Bridge*. Master of Science Thesis. Department of Civil and Architectural Structural Engineering, Royal Institute of Technology, Publication no. 05:218, Stockholm, Sweden, 2005.
- Craig Jr. R.R., Kurdila A.J. (2006): *Fundamentals of Structural Dynamics*., Wiley, Hoboken, New Jersey, USA.
- Dutta A., Ramakrishnan C.V. (1997): Error estimation in finite element transient dynamic analysis using modal superposition. *International journal for Computer-Aided Engineering*, Vol. 14, No. 1, 1997, pp. 135-158.
- Fryba L. (1996): *Dynamics of Railway Bridges*. Thomas Telford Services Ltd, Prague, Czech Republic.
- Hilber H.M., Hughes T.J.R., Taylor R.L. (1977): Improved numerical dissipation for time integration algorithms in structural dynamics. *Earthquake engineering and structural dynamics*, Vol. 5, No. 1, 1977, pp. 283-292.
- López O.A., Cruz M. (1996): Number of modes for the seismic design of building. *Earthquake Engineering and Structural Dynamics*, Vol. 25, No. 8, 1996, pp. 837-855.
- Lundin, B., Mårtensson P. (2006): *Finding general guidelines for choosing appropriate cut-off frequencies for modal analyses of railway bridges trafficked by high-speed trains*. Master's dissertation. Division of solid mechanics, Lund University, Publication no. TFHF-5127, Lund, Sweden, 2006.
- LUSAS (2006): *Modeller Reference Manual Version 14*. LUSAS, Issue 1, Kingston upon Thames, Surrey, United Kingdom
- LUSAS (2005): *IMDPlus User Manual Version 13.8*. LUSAS, Issue 1, Kingston upon Thames, Surrey, United Kingdom
- LUSAS (2005): *Theory Manual 1 & 2 Version 13.8*. LUSAS, Issue 1, Kingston upon Thames, Surrey, United Kingdom
- Ottosen, N., Petersson, H. (1992): *Introduction to the Finite Element Method*. Prentice Hall, New York, New York, USA.

Tavares R.A. (2007): Influence of the Vertical Support Stiffness on the Dynamic Behavior of High-Speed Railway Bridges. Master of Science Thesis. Department of Civil and Architectural Structural Engineering, Royal Institute of Technology, Publication no. 255, Stockholm, Sweden, 2007.

UIC (2007): *Guidelines for Railway Bridges: Dynamic Measurements and Calculations*, Bridgecap project Team G776x-2006.